Modeling Supermassive Black Holes in Cosmological Simulations

Michael Tremmel

A dissertation
submitted in partial fulfillment of the
requirements for the degree of

Doctor of Philosophy

University of Washington

2017

Reading Committee:

Fabio Governato, Chair

Thomas R. Quinn

Marta Volonteri

Program Authorized to Offer Degree:
Astronomy

University of Washington

Abstract

Modeling Supermassive Black Holes in Cosmological Simulations

Michael Tremmel

Chair of the Supervisory Committee:
Professor Fabio Governato
Department of Astronomy

My thesis work has focused on improving the implementation of supermassive black hole (SMBH) physics in cosmological hydrodynamic simulations. SMBHs are ubiquitous in massive galaxies, as well as bulge-less galaxies and dwarfs, and are thought to be a critical component to massive galaxy evolution. Still, much is unknown about how SMBHs form, grow, and affect their host galaxies. Cosmological simulations are an invaluable tool for understanding the formation of galaxies, self-consistently tracking their evolution with realistic merger and gas accretion histories. SMBHs are often modeled in these simulations (generally as a necessity to produce realistic massive galaxies), but their implementations are commonly simplified in ways that can limit what can be learned. Current and future observations are opening new windows into the lifecycle of SMBHs and their host galaxies, but require more detailed, physically motivated simulations. Within the novel framework I have developed, SMBHs 1) are seeded at early times without *a priori* assumptions of galaxy occupation, 2) grow in a way that accounts for the angular momentum of gas, and 3) experience realistic orbital evolution. I show how this model, properly tuned with a novel parameter optimization technique, results in realistic galaxies and SMBHs. Utilizing the unique ability of these simulations to capture the dynamical evolution of SMBHs, I present the first self-consistent prediction for the formation timescales of close SMBH pairs, precursors to SMBH binaries and merger events potentially detected by future gravitational wave experiments.

TABLE OF CONTENTS

LIST OF FIGURES

Figure Number Page

ACKNOWLEDGMENTS

This accumulation of the work I've done over the course of my time as a graduate student would not have been possible had I not had the tremendous support academically, professionally, and personally from a great number of people.

My work and academic growth has benefitted greatly from the advice and knowledge gathered from members, past and present, of the UW N-Body Shop. I am grateful to have been a part of such a supportive group and am indebted to many for helping me these past several years in one way or another. As I'm sure someone has said before, the N-Body Shop always pays their debts.

I want to thank in particular my adviser, Fabio Governato, for putting maximum effort into guiding me both scientifically and professionally. I am grateful that Fabio would often treat me more like a colleague than a student, even if he was (allegedly) right $\sim$75% of the time. Thanks also to Tom Quinn, whose wizard-like wisdom of physics, code development, and computers was critical to my success in developing, debugging, running, and analyzing complicated and intimidatingly large simulations.

Thanks to Marta Volonteri and Andrew Pontzen who, despite being all the way across an ocean, have been very influential to my scientific development and have never failed to be incredibly supportive.

Thanks to my very first officemate, Ferah Munshi, who made me feel welcome in a brand new place. She was incredibly supportive and continues to be a great resource for advice related to both science and life. Most importantly, she would not hesitate to call me out on self-deprecation. Hopefully those tally marks remain on the white board for future generations to ponder!

A big ‘thank you’ to the entire graduate student body in the UW Astronomy Department. The culture here is very positive and makes for a great work place environment, with foosball and karaoke aggressively encouraged. In particular, I want to thank Nell, Russell, Ben, Phoebe, Kristen, Rodrigo, Ethan, Grace, and John L for being amazing classmates, officemates, cat sitters, and some of the best friends I could have asked for. I’ll always cherish those strange hours in the department playing Anomia and watching Arrested Development instead of working on homework or research. Leaving the great friends I’ve made at UW is probably the hardest part of moving on, but I wouldn’t trade it for anything.

Thanks to my parents, Lynn and Fred Tremmel, for their unwavering support, for teaching me to always ask a lot of myself, and for encouraging me to find and achieve things that are personally fulfilling. I wouldn’t be the person I am today, doing what I am doing, had it not been for them and the loving environment in which I was raised.

Finally, I want to thank my amazing wife, Carrie Templeton, for loving me unconditionally despite all of the stress I tend to bring home with me. Carrie, with some help from our cat, Banjo, made Seattle truly home for me. She makes me a better person and always reminds me to be positive and enjoy life. Most of all, she is my home no matter where we live. We are Groot.

DEDICATION

To my wife, Carrie, and my parents, Lynn and Fred.

To the anonymous little girl I overheard on the bus one day reciting this poem that has since become a family motto for Carrie and I.

Be a dragon

Find a way

Be a dragon

Have a great day

Chapter 1

INTRODUCTION

For a few decades it has been understood that a supermassive black hole (SMBH) resides within the center of the Milky Way and, in fact, the centers of most massive galaxies (e.g. Gehren et al., 1984; Kormendy & Richstone, 1995; Kormendy & Ho, 2013) . It has also been discovered that such objects are responsible for some of the most energetic events in the Universe, with the ability to out-shine entire galaxies. How these objects form, grow, and affect their host galaxies has become a crucial part of galaxy formation theory and a major question presented to both observers and theorists. While cosmological simulations have already proven to be a useful tool to understand these processes (e.g. Di Matteo et al., 2008; Sijacki et al., 2009; Dubois et al., 2014a; Sijacki et al., 2015), SMBHs present a unique challenge. In this chapter, I outline various areas of research on SMBHs and their connection to galaxy evolution, as well as some of the current and future observations that will potentially aid our understanding, if coupled with sophisticated enough simulations. Finally, I summarize the role of cosmological simulations and the challenges presented by SMBHs.

1.1 The Co-Evolution of Galaxies and Supermassive Black Holes

SMBHs are ubiquitous not only in massive galaxies (e.g. Gehren et al., 1984; Kormendy & Richstone, 1995; Kormendy & Ho, 2013) but also in small, bulge-less disk galaxies (Shields et al., 2008; Filippenko & Ho, 2003) and dwarfs (Reines et al., 2011; Reines & Deller, 2012; Reines et al., 2013; Moran et al., 2014). Our current understanding of SMBHs is that they grow with their host galaxies. Processes dictating the evolution of a galaxy (mergers, star formation, accretion and depletion of gas) are also thought to drive and regulate the growth of SMBHs. Conversely, energy emitted from growing SMBHs is likely a crucial feedback

process affecting the star formation and gas content of galaxies, particularly at high masses. A major goal of modern galaxy evolution theory is to explain this co-evolution and how it shapes the observed population of galaxies and SMBHs.

1.1.1 Empirical Scaling Relations

Observations correlating the mass of SMBHs and the mass and morphology of their host galaxies is indicative of co-eval growth (Häring & Rix, 2004; Gültekin & et al., 2009; Volonteri & Bellovary, 2012; Schramm & Silverman, 2013; Kormendy & Ho, 2013). The picture that arises is that SMBHs grow primarily by accreting gas from their surrounding galaxy. Massive galaxies within larger dark matter halos have more gas with which to fuel both star formation and black hole growth. In turn, energy released by SMBHs during this period of grown can regulate star formation within the host galaxy. In accordance with this picture, AGN undergo cosmic downsizing, where more massive black holes grow slower at later times (Ueda et al., 2003), as do galaxies (Cowie et al., 1996; Treu et al., 2005).

Modern techniques for measuring black hole masses are revealing new aspects to this relationship. Analysis of broad-line AGN allows the estimation of SMBH masses from actively growing SMBHs, revealing that the relationship between SMBH and host galaxy may depend on both the mass and evolutionary state of the galaxy and SMBH (Reines & Volonteri, 2015). This has important consequences for our understanding of the SMBH and AGN population over cosmic time and the mechanisms that connect SMBHs to their host galaxy (Volonteri & Reines, 2016). *How does the relationship between SMBH and host galaxy change over cosmic time as well as over the history of an individual galaxy?*

1.1.2 SMBHs and the Quenching of Star Formation

Through abundance matching, it can be shown that both low and high mass halos are inefficient at producing stars in their central galaxies, with peak efficiency occurring approximately at the luminosity function turnover $L_\star$ (Bower et al., 2006; Guo et al., 2010; Moster et al., 2013; Behroozi et al., 2013b). At the low mass end, star formation is regulated by

the ultraviolet background radiation slowing the accretion of gas (Efstathiou, 1992; Bullock et al., 2000; Somerville, 2002) and energy input due to supernovae and UV emission from young stars (e.g. Efstathiou, 2000; Governato et al., 2007; Pontzen et al., 2008). These processes, however, become unable to properly regulate star formation beyond $M_{vir} \approx 10^{12}$ $M_{\odot}$ (Keller et al., 2016).

A number of processes have been considered to explain the decrease in star formation efficiency in higher mass halos, including gas shock heating (e.g. Binney, 1977; Somerville & Primack, 1999) and starvation due to a decreasing gas supply (Feldmann & Mayer, 2015). Still, semi-analytic models regularly find that an additional physical mechanism is necessary to explain the division between star forming disk galaxies and quenched elliptical galaxies (Bower et al., 2006), a division that is in place even at high redshift (Ilbert et al., 2010). This additional mechanism is often invoked as feedback from growing SMBHs. Many works have shown that this energy input from SMBHs is able to regulate star formation in massive galaxies using both cosmological simulations (e.g. Di Matteo et al., 2005; Sijacki et al., 2007; Di Matteo et al., 2008; Dubois et al., 2013, 2016) and semi-analytic models (e.g. Bower et al., 2006; Croton et al., 2006), but reproducing the population of quenched galaxies as they are observed remains a challenge (Bluck et al., 2016). *How does SMBH feedback interact with the gas accretion and merger histories of galaxies to regulate and, in some cases, extinguish star formation? How do SMBHs influence the morphological evolution of galaxies?*

1.1.3 Drivers of SMBH Growth: Mergers vs. Secular Processes

While SMBHs exist within most massive galaxies, they are not always actively growing and the ones that are can be growing at starkly different rates, from modest AGN in the local Universe to bright quasars detectable and more common at high redshift (Hopkins et al., 2006). A simple picture that has developed is that galaxy mergers drive the strongest accretion episodes (e.g. Hopkins et al., 2005, 2006). There is also evidence for this effect at lower redshift using dual and offset AGN (Comerford et al., 2015; Barrows et al., 2017).

As observations improve, allowing us to probe down to lower luminosity AGN and ex-

amine the properties of AGN host galaxies, the picture becomes more complicated. Recent studies have found little dependence of the AGN population on the morphology of their host galaxies, indicating that the AGN population is similar between star forming, bulge dominated, or interacting galaxies out to $z \sim 3$ (Rosario et al., 2015; Bruce et al., 2016). X-ray stacking analysis shows a relatively constant relationship between SMBH accretion rate and star formation rate in star forming galaxies (Mullaney et al., 2012), though more recent analysis indicates that SMBH growth may be a stronger function of galaxy stellar mass (Yang et al., 2017). Understanding how secular processes within the galactic disk may drive SMBH growth, how this is similar or different from growth driven by galaxy mergers, and how both of these processes are reflected upon the population of AGN observed across cosmic time still remains an important open question. *What processes drive SMBH growth and different times and how does this inform SMBH-galaxy co-evolution?*

1.2 New Insights with Current and Future Observations

Current observational projects are already examining galaxies in fine detail at a variety of scales and epochs. Integral field unit (IFU) spectroscopy surveys such as SAMI, MANGA, and MASSIVE are probing the detailed structure of galaxies. IFU spectroscopy can also study the winds driven by active SMBHs in order to better understand the nature of AGN feedback (Wylezalek et al., 2017). The COS-Halos survey uses quasar sight lines to examine galaxies at larger scales, studying the structure of the circum-galactic medium (CGM) and providing new insight into the merger, accretion, and feedback histories of galaxies (Werk et al., 2014, 2016). Deeper, more detailed multi-wavelength surveys are examining new, lower luminosity populations of AGN and their host galaxies over cosmic time (Bruce et al., 2016). Recent progress has also been made on detecting dual and offset AGN (Barrows et al., 2016, 2017). As these observations are pushed to higher redshift and brighter AGN, more constraints on how and when SMBHs grow as a result of galaxy mergers will be possible.

SMBH science is at the center of many future projects as well. The James Web Space Telescope (JWST) will probe early epochs of star formation in galaxies and may even be

able to provide constrains on the very first SMBHs and their high redshift growth (Natarajan et al., 2017; Volonteri et al., 2017). The planned LISA mission, as well as current pulsar timing array efforts, seek to detect gravitational waves emitted by merging and/or binary SMBHs (Sesana, 2013; Klein et al., 2016). Such observations will be critical for better constraining the formation of SMBH seeds and the evolution of the SMBH mass and luminosity function over cosmic time (e.g. Volonteri et al., 2008b).

While these current and future observational endeavors have the potential to broaden our understanding of SMBHs and their relationship with their host galaxies, insight from simulations remains a critical component. As the observations and scientific questions become more detailed, so too must simulations. Both high resolution and more careful implementation of SMBH physics are necessary.

1.3 Cosmological Simulations

Simulations are crucial tools for understanding the physical processes surrounding galaxy formation and evolution. Coming in different flavors of complexity, each type of simulation contributes uniquely to our ability to understand these processes. Semi-analytic models examine how different processes interact with dark matter halo formation histories using phenomenological prescriptions. Their simplicity allows for many different realizations of the models without much computational cost, but they lack the ability to resolve the internal structures of galaxies. Hydrodynamic simulations of isolated galaxies or merging pairs of galaxies allow for high resolution due to their relative simplicity and are useful tools for exploring specific physical processes, but they lack a cosmologically evolving environment and so cannot effectively explore a galaxy's evolutionary history.

Cosmological simulations are the most complex and costly type of simulation, following the formation of galaxies and large-scale structure within a fully cosmological environment. The internal structures of galaxies and their detailed evolution is followed throughout cosmic time and as a self-consistent prediction derived from each galaxy's unique gas accretion and merger history. Large volume simulations have been useful in exploring the evolution of the

population of SMBHs over cosmic time (e.g. Sijacki et al., 2015; Volonteri et al., 2016b) while also retaining the ability to follow individual galaxies to understand how SMBH feedback can shape galaxy evolution (e.g. Di Matteo et al., 2008; Dubois et al., 2013, 2016). Smaller, 'zoom-in' cosmological simulations are useful for examining the evolution of individual galaxies in finer detail but still within a cosmologically evolving environment (e.g. Bellovary et al., 2013; Sanchez et al., 2016). The new 'Genetic Modification' technique (Roth et al., 2016) is a particularly useful tool for 'zoomed-in' simulations and allows for controlled experiments on how specific aspects of a galaxy's assembly history inform the evolution of the galaxy and its SMBH (Pontzen et al., 2017).

SMBHs present a unique challenge to cosmological simulations. The resolution is, by necessity, relatively low due to the scales they achieve. Even the highest resolution, 'zoomed-in' simulations do not model individual stars and attain at best 10s of pc spatial resolution. SMBHs, on the other hand, are single objects whose size and relevant physical processes occur well below 1 pc. To make things more complicated, these single objects have the potential, as we've seen in the previous section, to influence the structure and evolution of entire galaxies (10s-100s kpc). This dynamic range present in SMBH physics makes them challenging and their importance means that simulators must carefully account for their effects using sub-grid models. These parameterizations map the state of gas, stars, and SMBHs at the smallest resolved scales to physical processes occurring well below the resolution limit of the simulation. While much progress has been made in these efforts (e.g. Di Matteo et al., 2008; Sijacki et al., 2009; Booth & Schaye, 2009; Rosas-Guevara et al., 2015; Anglés-Alcázar et al., 2017), there is still much room for improvement.

As observations become more advanced, so too must cosmological simulations and the 'sub-grid' models that they entail. Relating the growth of SMBHs to the morphology of their host galaxies and their CGM requires simulations able to resolve those structures. To differentiate between mechanisms driving SMBH growth and galaxy quenching requires SMBH dynamics and accretion algorithms that respond to the evolving kinematics of their host galaxy. Predicting AGN activity during the earliest epochs requires that SMBHs are

included in the simulation at early times and within realistic environments. Providing predictions and context to current and future observations of SMBH mergers and dual/offset AGN requires SMBHs to experience realistic orbital evolution within galaxies. These are all aspects of SMBH physics that most modern cosmological simulations miss. The goal of my thesis has been to develop and implement a model for SMBHs for large scale cosmological simulations in order to improve upon these limitations and allow these simulations to remain relevant for current and next generation observations of SMBHs and AGN. The model that I have developed is a marked improvement over how SMBHs are seeded, grow, and evolve dynamically within their host galaxy. In the following chapters I will describe in detail each aspect of the model I've developed and compare it to more common approaches while outlining some important scientific applications that such a detailed model allows.

Chapter 2

SUPERMASSIVE BLACK HOLE DYNAMICS IN COSMOLOGICAL SIMULATIONS

In this chapter, I explain a novel approach I have developed for accurately tracking the orbits of SMBHs within galaxies in cosmological simulations. The resolution in these simulations makes tracking of single objects especially challenging, but in order to correctly model SMBH activity during and following galaxy mergers, the formation of SMBH binaries and merging pairs, and the prevalence and evolutionary context of dual and/or offset AGN, such detail is needed.

First, I describe in more detail the need for a new method, highlighting the shortcomings of current approaches. Then I describe the model I have developed, accounting for unresolved dynamical friction acting on SMBHs in simulations. In the following sections I explain our isolated collapsing halo test simulations and the results, showing how my method is a stark improvement over more common approaches. Finally, I show an example cosmological simulation examining how SMBHs can have a variety of different orbits after they are deposited within a galaxy through merger events. I conclude with a summary and discussion about the implications of SMBH orbital evolution and why it is necessary to include physical prescriptions such as the one I have developed in cosmological simulations.

Material from this chapter was previously published in collaboration with Fabio Governato, Marta Volonteri, and Tom Quinn in the August 2015 edition of Monthly Notices of the Royal Astronomical Society (Tremmel et al., 2015), and has been reproduced here with permission of the Royal Astronomical Society.

2.1 The Need for a New Model

Dynamical friction, the force exerted by the gravitational wake caused by a massive object moving in an extended medium (Chandrasekhar, 1943; Binney & Tremaine, 2008) causes the orbits of SMBHs to decay towards the center of massive galaxies (Governato et al., 1994; Kazantzidis et al., 2005). In cosmological simulations, modeling DF is particulary challenging, as the particle representing a SMBH is often only a few times the mass of the background particles. In this case SMBH orbits can become dynamically heated due to the limited mass resolution and the resulting spurious collisionality from a noisy gravitational potential (Hernquist & Barnes, 1990). This numerical heating can cause the black holes to gain/lose energy and be unrealistically perturbed away from the center of its host halo. In order to lessen collisionality and improve performance, N-body simulations employ a gravitational softening length, a characteristic scale below which the gravitational force between two particles becomes damped. This mechanism, while necessary numerically, hinders DF by preventing the close interactions that are necessary to form a wake in the vicinity of the SMBH.

To account for the unrealistic dynamics of SMBHs in cosmological simulations, many groups employ artificial advection schemes that change the motion of SMBHs. Each method comes with its own drawbacks. For example, placing the SMBH at the position of the lowest potential gas particle around it (e.g. Springel et al., 2005; Booth & Schaye, 2009) causes chaotic motions, especially when relative velocity constraints are put on the gas particles (Wurster & Thacker, 2013). Utilizing a large 'tracer mass' with which the SMBH gravitationally interacts with its surroundings (Debuhr et al., 2011) affects the morphology in the galactic center as well as the accretion history of the SMBH (Wurster & Thacker, 2013). Pushing the SMBH a certain distance in the direction of either the local stellar density gradient (Okamoto et al., 2008) or the local center of mass (Wurster & Thacker, 2013) can avoid chaotic motions but adds an additional free parameter, the distance the SMBH is pushed each step. Even disregarding their individual drawbacks, none of these

solutions are ideal, as they all require the explicit assumption that SMBHs rapidly decay into and remain stable at the center of their host galaxies , which is often not accurate (Bellovary et al., 2010).

In strongly interacting systems, where SMBHs are thought to go through much of their growth and possibly their formation (Mayer et al., 2007), the inner regions of a galaxy are likely to experience strong potential fluctuations, affecting the dynamics of the SMBH. This could be especially evident in dwarf galaxies, where black holes exist (Reines et al., 2013; Moran et al., 2014) within a shallow potential with a cored density profile (Oh et al., 2011; Teyssier et al., 2013), making perturbations to their orbits more likely. Additionally, SMBHs accreted during both major and minor mergers, especially dry mergers (Kazantzidis et al., 2005), do not immediately sink to the center of the galaxy, creating a population of small 'wandering' SMBHs (Islam et al., 2003; Volonteri & Perna, 2005; Bellovary et al., 2010). Advection, by assuming that orbital decay timescales are always short, could then artificially increase the mass of central SMBHs, through inflated merger and accretion rates.

More advanced approaches have been explored. For example, Dubois et al. (2013) include a sub-grid prescription for gas dynamical friction acting on the SMBH. While this is a promising method, it requires assumptions about the multiphase nature and equation of state of the gas far below the resolution limit of any cosmological simulation ($\sim 1-5$ pc). Lupi et al. (2015) increase the resolution around SMBHs to attain very accurate dynamics, but their method is applicable only for very high resolution simulations meant to closely follow BH-BH mergers, not cosmological simulations.

The method I have developed during the course of my thesis is a simple solution to correcting SMBH dynamics in cosmological simulations, which is to estimate the unresolved dynamical friction felt by the SMBH and apply the appropriate force to the SMBH particle. This is a significant improvement over artificial advection, as it makes no assumption about where the SMBHs should be located in a galaxy at a given time and it has no explicit effect on the SMBH surroundings. In addition, it requires minimal assumptions about the state of the simulation below the resolution limit and it naturally converges with increasing resolution.

2.2 The Dynamical Friction Prescription

Dynamical friction occurs due to both large (Colpi et al., 1999) and small scale perturbations to the black hole's surroundings. We consider perturbations on scales larger than the gravitational softening length, ϵ_g, to be well resolved. On these scales the potential should be smooth, so long as enough particles are used so that dynamical heating is minimized.

The acceleration a black hole of mass M_{BH} feels from DF due to particles of mass $\mathrm{m}_a \ll \mathrm{M}_{BH}$ is given by the following formula:

$$\mathbf{a}_{DF} = -4\pi \mathrm{G}^2 \mathrm{M}_{BH} \mathrm{m}_a \ln\Lambda \int d^3\mathbf{v}_a f(\mathbf{v}_a) \frac{\mathbf{v}_{BH} - \mathbf{v}_a}{|\mathbf{v}_{BH} - \mathbf{v}_a|^3} \tag{2.1}$$

Where $f()$ is the velocity distribution function, $\ln\Lambda$ is the Coulomb logarithm, $\mathbf{v}_a$ is the velocity of the surrounding background objects relative to the local center of mass (COM) velocity, and $\mathbf{v}_{BH}$ is the relative velocity of the black hole. We assume that within ϵ_g from the black hole the velocity distribution is isotropic, giving Chandrasekhar's Dynamical Friction Formula (Chandrasekhar, 1943).

$$\mathbf{a}_{DF} = -4\pi \mathrm{G}^2 \mathrm{M} \mathrm{m}_a \ln\Lambda \frac{\mathbf{v}_{BH}}{\mathrm{v}_{BH}^3} \int_0^{\mathrm{vBH}} d\mathrm{v}_a \mathrm{v}_a^2 f(\mathbf{v}_a) \tag{2.2}$$

This can be further simplified by substituting the integral for $\rho(< \mathrm{v}_{BH})$, which is the density of particles moving slower than the black hole.

$$\mathbf{a}_{DF} = -4\pi \mathrm{G}^2 \mathrm{M} \rho(< \mathrm{v}_{BH}) \ln\Lambda \frac{\mathbf{v}_{BH}}{\mathrm{v}_{BH}^3} \tag{2.3}$$

The Coulomb logarithm depends on the maximum and minimum impact parameters, b_{max} and b_{min}, such that $\ln\Lambda \sim \ln(\frac{\mathrm{b}_{max}}{\mathrm{b}_{min}})$. Because DF is well resolved at scales greater than the softening length, we set $\mathrm{b}_{max} = \epsilon_g$ to avoid double counting frictional forces that are already occurring. For the minimum impact parameter, we take it to be the minimum 90° deflection radius, with a lower limit set to the Schwarzschild Radius, R_{Sch}.

$$\mathrm{b}_{min} = max(\mathrm{b}_{90}, \mathrm{R}_{Sch}); \mathrm{b}_{90} = \frac{\mathrm{GM}_{BH}}{\mathrm{v}_{BH}^2} \tag{2.4}$$

For the calculation, we use 64 collisionless particles (i.e. dark matter and star particles, if present) closest to the black hole. We calculate the velocity of each particle relative to the COM velocity of those 64 particles. We verified that our results do not depend strongly on the number of neighbors used, although using too few particles could result in numerical noise in the calculation of this force. Since we are explicitly assuming the velocity distribution is isotropic, the following must be true.

$$\rho(< \mathrm{v}_{BH}) = \frac{\mathrm{M}(< \mathrm{v}_{BH})}{\mathrm{M}_{\mathrm{total}}}\rho \tag{2.5}$$

Where ρ, the total density around the black hole, is calculated by smoothing over the chosen 64 particles, i.e. $\rho = \sum_i^{64} m_i W(\mathbf{r}_{BH} - \mathbf{r}_i, h)$. $\mathrm{M}(< \mathrm{v}_{BH})$ is the total mass of the chosen particles that are moving slower than the black hole relative to the local center of mass velocity and $\mathrm{M}_{\mathrm{total}}$ is the summed mass of all 64 particles.

The resulting acceleration (from eq. 3) is added to the black hole's current acceleration, to be integrated the following time step. As the spatial resolution or black hole mass increases (or the velocity of the black hole decreases) b_{min} will become greater than b_{max}, in which case we claim DF is being fully resolved and therefore the correction is not needed.

This method is not accounting for DF from gas, which can have important effects for supersonic black holes in regions where gas density dominates stars and dark matter (Ostriker, 1999; Chapon et al., 2013). This should not occur often on the scales relevant in these simulations. The center of larger galaxies are dominated by stars and smaller galaxies have significant star and dark matter fractions within the central regions (Oh et al., 2008, 2011), so this effect will only be a minor correction in most cases. DF may be overestimated within resonant DM cores where DF can become much less efficient (Read et al., 2006). This effect is secondary and mainly important when the gravitational softening length is appreciable compared to the size of the core structure. Often the orbital differences should be smaller

than or similar to the resolution limit and therefore unimportant. Additionally, interactions with clumpy gas has been shown to significantly increase the timescale for the orbital decay of SMBH binaries below $\sim 100pc$ (Fiacconi et al., 2013; Roškar et al., 2015). However, this effect would not be well resolved by even high resolution 'zoomed-in' cosmological simulations.

2.3 Test Simulations

*2.3.1 **I**solated **C**ollapsing **In**itial Conditions **G**enerator (ICInG)*

To test the dynamics of black holes in a realistic DM halo, we generate initial conditions for a collapsing overdensity following the procedure of Evrard (1988), approximating an isolated, cosmologically collapsing region with a single radial cosine wave.

$$\delta(r_0) = \frac{\delta_0}{2}[1 + cos(r_0/r_f)] \tag{2.6}$$

The size of the spherical region is defined as r_f. We start by defining the over density based on 1) the initial redshift we want the simulation to begin with, z_{start}, 2) the total virtualized mass, M_{vir}, at a later redshift, z_{end}, and 3) the radius within the isolated spherical region that should be virtualized at z_{end}, r_c. The aim is to create a realistic environment for a SMBH to evolve dynamically within, i.e. one that is still actively collapsing at any given time. Using these constraints, we are able to define a unique δ_0 by solving the following integral equality.

$$\frac{3}{4\pi r_c^3}\int_0^{r_c} \delta(r) 4\pi r^2 dr = 1.7\frac{z_{end}}{z_{start}} \tag{2.7}$$

Once δ_0 is derived given the input constraints, the particles are perturbed starting from an isotropic sphere of radius r_f, with the following radial position and peculiar velocity perturbations, as calculated in Evrard (1988), where r_p and r_0 are respectively the perturbed and initial radial positions of the particles.

$$r_p = r_0[1 - \frac{\delta(x_0)}{3}]v = -\frac{2}{3}Hx_0\delta(x_0) \tag{2.8}$$

The initial isotropic sphere of particles are created from a gravitational glass particle distribution using the publicly available code provided with *Gadget-2*. Such a distribution is less prone to noisy instabilities which can artificially create substructure within our sphere. Once the perturbations have been created, a bulk spin is imparted to approximate the angular momentum a halo should have, given by $L = \lambda * M_{vir} * *(5./2.)/E^{1/2}$, where E is the total internal energy of the halo. Tangential velocities are imparted assuming solid body rotation and a mass distribution that is nearly a uniform sphere (not a bad approximation for the initially small perturbations). The canonical value of 0.05 is used for λ.

Finally, in order to avoid radial instabilities, random tangential motions are added to the particles as a constant fraction of their infall velocities. After many tests, it was found that imparting random motions with half the energy of the infall was able to wash out much of the radial instabilities while minimizing the formation of unusual, non-spherical structures within the halo. The resulting halo density profile is found to be approximately that found by Navarro et al. (1996).

The code to generate the initial conditions, called ICInG, including the gravitational glass particle distribution hdf5 file is located on my github page (https://github.com/mtremmel/ICInG) and is publicly available.

2.3.2 Setting Up the Test Simulations

We begin each simulation by approximating the state of a halo beginning to collapse at high redshift. We then allow the halo to collapse before implanting a black hole of mass 10^6 $M_\odot$. We run a suite of simulations at different mass and spatial resolutions (see Table 2.1) with a massive 'black hole' particle initially 1) at the center while the halo is still actively collapsing or 2) on an eccentric orbit after the halo has mostly relaxed. The resolution of the 'Low Res' and 'Oversampled' runs are comparable to current uniform volume simulations (Kereš

Table 2.1: Information about the resolution of each isolated dark matter halo test simulation.

Name	Number of Particles	Dark Matter Mass ($M^*_\odot$	Softening length, ϵ_g (pc)†
Low Res	1.05×10^6	9.78×10^5	311
Oversampled	8.39×10^6	1.22×10^5	311
High Res	6.71×10^7	1.53×10^4	77
Small Soft	6.71×10^7	1.53×10^4	10

$*$ Mass of the dark matter particles in the simulation

† spline kernel gravitational softening

et al., 2012; Sijacki et al., 2015; Schaye et al., 2015; Dubois et al., 2014a), while the 'High Res' simulation is representative of high resolution 'zoomed-in' simulations (Governato et al., 2012; Christensen et al., 2014; Hopkins et al., 2014). The force softening lengths adopted are typical of cosmological runs, while in 'Small Soft', a variant of the 'High Res' simulations, the force resolution is only 10pc, typical of simulations of isolated binary mergers (Capelo et al., 2015) or very high-res cosmological zoomed-in simulations (e.g. Dubois et al., 2014b).

The halo we use here has (after a time consistent with z $\sim$ 0) $M_{vir} \sim 2 \times 10^{11}$ $M_\odot$, $R_{vir} \sim 115$ kpc, and a concentration $c \sim 4.5$. An analytic expression of the approximate timescale for a rigid object to sink to the center of a DM halo was calculated by Taffoni et al. (2003). Given these conditions and the mass of the test black hole, the estimated DF timescale (τ_{DF}) for an eccentric (v= $0.1v_{circ}$) orbit at an initial distance of 2 kpc from the halo center is approximately 1.8 Gyr. This initial orbit was chosen as typical of a SMBH after its parent satellite has been tidally disrupted. It has a non-negligible τ_{DF}, but still much less than a Hubble time.

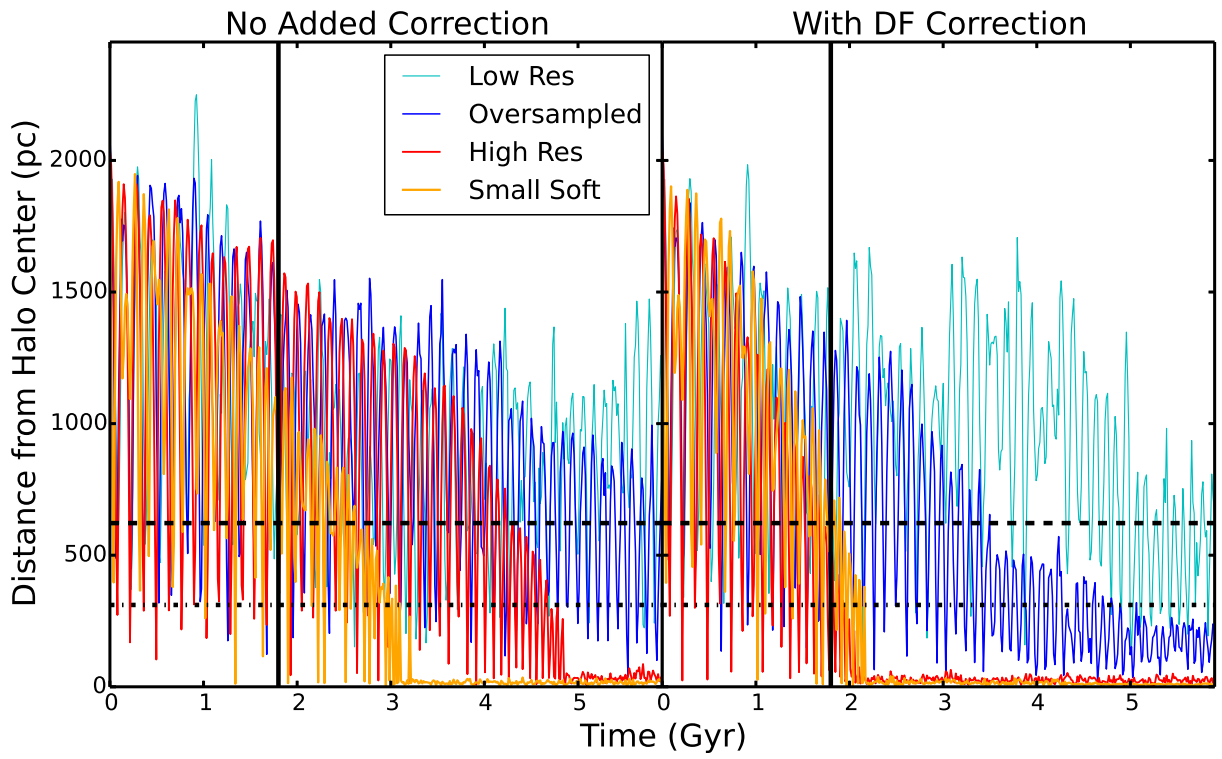

Figure 2.1: Effects of the DF correction: Distance of a test 10^6 $M_\odot$ black hole from halo center as a function of time at different resolutions. Dashed-dot and dashed lines indicate ϵ_g and $2\epsilon_g$ respectively for both the Low Res and Oversampled models. The black hole starts on an eccentric (v= 0.1 v_{circ}) orbit with apocenter of 2 kpc. The vertical solid line represents the analytically derived timescale for orbital decay. When the DF correction is applied, marked improvement is seen for all models except 'Low Res', which experiences too much dynamical heating due to the lower mass resolution. The orbits of 'High Res' and 'Small Soft' are very nearly the same once the correction is implemented, indicating numerical convergence when the DM particle mass is $\sim 10^4$ $M_\odot$. Figure from Tremmel et al. (2015), © RAS. Reproduced with permission.

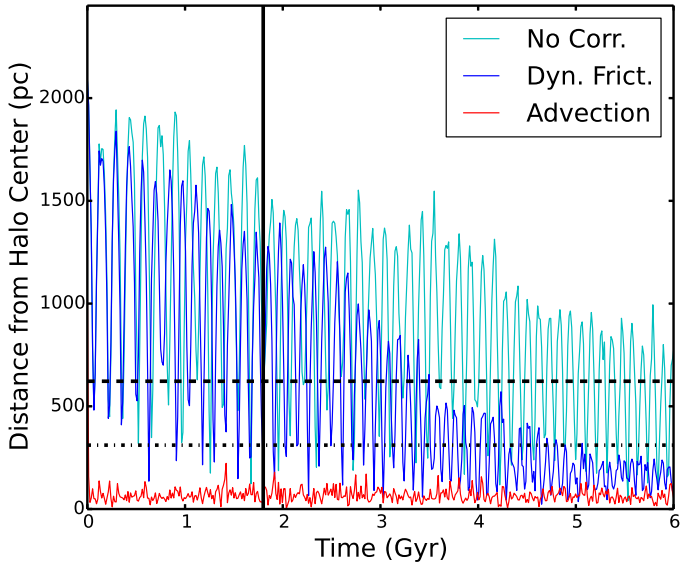

Figure 2.2: DF CORRECTION VS ADVECTION: Results from the 'Oversampled/ model when implementing our DF correction (blue) compared with a commonly used advection routine (red) and no correction to dynamics (cyan). Dashed-dot and dashed lines indicate ϵ_g and $2\epsilon_g$ respectively.The black hole starts on an eccentric (v= 0.1 v_{circ}) orbit with apocenter of 2 kpc. Advection immediately pushes the off-center black hole to the center, missing the orbital decay that our method captures well. Without any correction, the orbit decays far too slowly, remaining far ($> 2\epsilon_g$) from halo center even after 6 Gyr. Figure from Tremmel et al. (2015), © RAS. Reproduced with permission.

2.4 Results

2.4.1 Isolated Dark Matter Halo

We find that, for SMBHs placed in the center of a collapsing halo, only the Low Res simulation experiences significant dynamical heating, causing the BH to be unrealistically perturbed away far from halo center. In the rest of the runs the BH remains within one softening length from halo center for 6 Gyrs and shows no sign of heating. This is due to the higher mass resolution present in those runs. Simulations including either our DF correction or an advection correction (see below) have the same results, showing little difference from simulations with no correction at all for this scenario.

Figure 2.1 shows the orbital evolution of a black hole initially on an eccentric (v= 0.1 v_{circ}) orbit with apocenter of 2 kpc, placed in the halo after it has finished most of its collapse. The center of the halo is defined at each step using the shrinking spheres method (Power et al., 2003). We verified that the density maximum and potential minimum coincide within much less than the force resolution. The vertical line represents the dynamical friction timescale for the orbit derived from the analytic model of Taffoni et al. (2003) and the horizontal lines represent ϵ_g and $2\epsilon_g$. Without the DF correction, only the 'Small Soft' model, with 10 pc spatial resolution and DM particle mass almost 100 times smaller than the BH, is able to show substantial orbital decay within $2\tau_{DF}$. Implementing our DF correction results in a noticeable improvement for the orbital decay, even at the relatively modest resolution of the Oversampled model, where it falls to within $2\epsilon_g$ of the center before $2\tau_{DF}$. At higher resolution, the dynamics converge to closely match with the analytical approximation. Note that even for our highest resolution simulation, Small Soft, the DF correction causes the SMBH to sink almost 1 Gyr sooner. These are very encouraging results, as they indicate that this correction results in realistic black hole orbital evolution even at resolutions attainable in large volume simulations and it has important consequences even at the highest resolutions tested here.

Figure 2.2 compares the performance of our DF prescription to that of a commonly

used advection scheme used in Sijacki et al. (2007) and various other simulations. The test is done using the Oversampled run, as this most closely resembles the resolution of a cosmological volume simulation. The BH is placed on an eccentric orbit, as in Figure 2.1. The advection scheme adopted repositions the black hole each time step to the position of the lowest potential particle within its 32 nearest neighbors while keeping the velocity unchanged. Not surprisingly, this results in the black hole staying very close to the center of the halo even when initially set on an off-center orbit. The DF correction captures the more gradual orbital decay that the advection scheme completely misses. The run with no dynamical correction fails to have the BH sink within $2\epsilon_g$ even after 6 Gyr.

This is an important conclusion because these different orbital evolutions would result in drastically different accretion histories for the black hole. Off center BHs should accrete less due to lower gas densities. Additionally, simulations that utilize advection would have black holes merge much sooner than what is predicted by their orbital decay timescale. Our improved method should then have important implications for the growth and merger rate of SMBHs in cosmological simulations of galaxy formation.

2.4.2 Cosmological Dwarf Galaxy Simulation

As a first test of the dynamics of SMBHs in a fully cosmological setting, we run a high resolution 'zoomed-in' simulation that results in two dwarf galaxies with masses $\sim 10^{10}$ $M_\odot$ at z = 0. The simulation has a resolution similar to our High Res isolated halo model, with dark matter particle mass 1.6×10^4 $M_\odot$, gas particle mass 3.3×10^3 $M_\odot$, and gravitational softening of only 87 pc. We showed in the previous section that at this resolution our DF prescription gives results that match analytic models. We chose a dwarf galaxy for this test because SMBHs are more likely to become perturbed away from galactic center, given their shallow gravitational potential and actively evolving, cored DM profile (Governato et al., 2012; Pontzen & Governato, 2012). This will guarantee a useful test environment for exploring the differences between out method and advection.

This test is also topical, as there is a growing sample of dwarf galaxies with detected

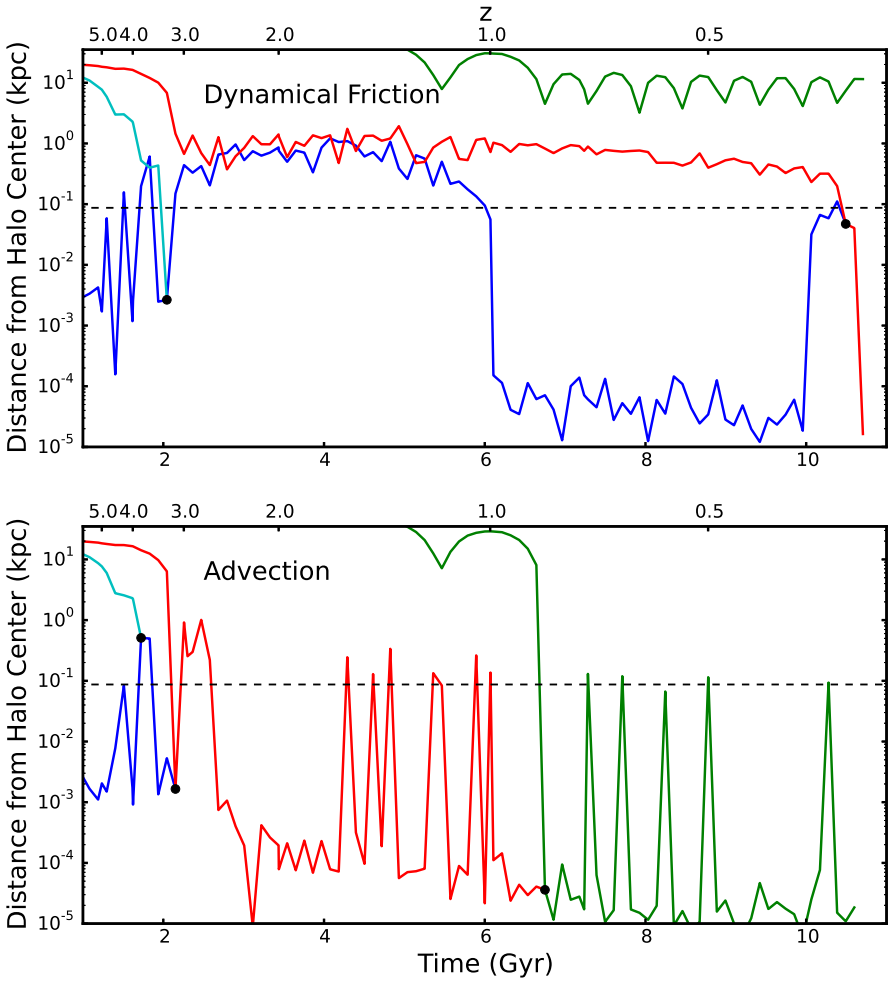

Figure 2.3: DF correction in a cosmological dwarf simulation:The dynamics of four black holes in the cosmological zoomed-in dwarf galaxy simulation with DF (top) and advection (bottom). These are the black holes that end up in the most massive system by the end of the simulation. Each colored line traces the distance of a black hole from the center of the most massive halo. Black dots mark merger events and the dashed lines mark the gravitational softening length of the simulation (87 pc). Which of the two black holes emerges from a merger event and which is 'eaten' is unimportant. DF is able to sustain a long-lived dual black hole system (blue and red) while the advection scheme causes them to quickly merge. The green black hole remains on a very wide orbit in the DF run, but is quickly and unrealistically pulled to the center with advection. Figure from Tremmel et al. (2015), © RAS. Reproduced with permission.

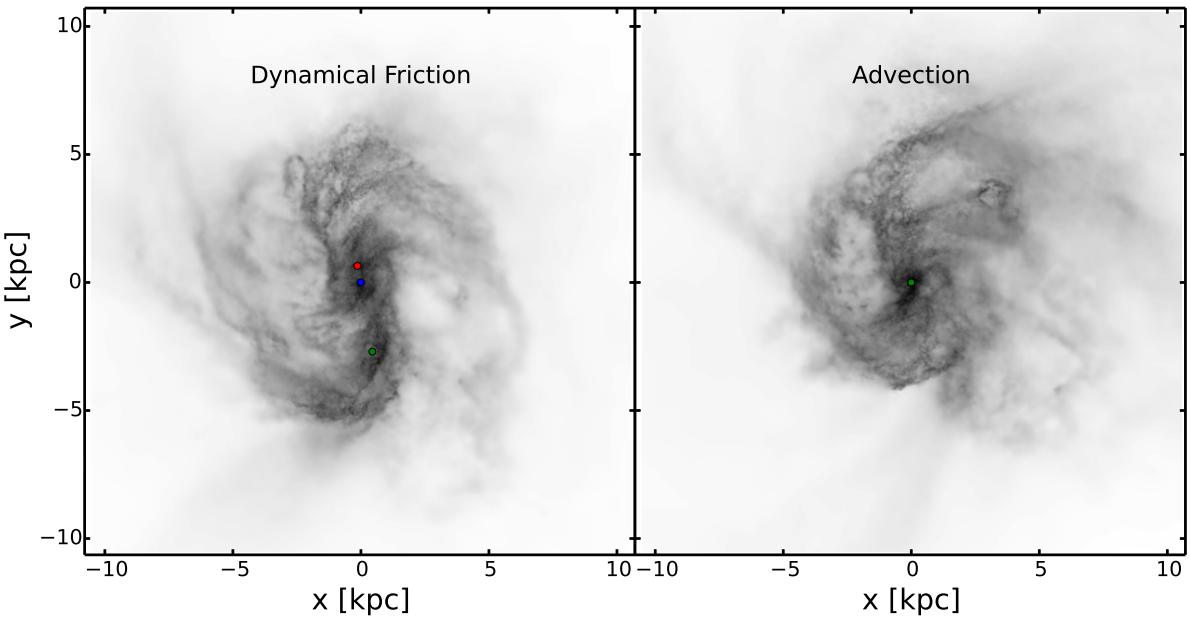

Figure 2.4: BHs in a Cosmological Dwarf: A snapshot of a zoomed-in cosmological simulation of a forming dwarf galaxy at z = 0.846. The gas density integrated along the line of sight is shown with darker colors indicating higher densities. In the dynamical friction simulation, a previous merger has created a central binary BH system (red and blue, see Figure 2.3). The separation of ~ 1 kpc is well resolved by the simulation, which has a force resolution of 87 pc. A more recent merger has set a third BH (in green) on a wide orbit (see Figure 2.3). In the image, the green BH is at its closest approach to galactic center. In the advection simulation, all BHs are quickly pushed to the center, where they merge, causing the simulation to miss these more realistic BH orbits. Figure from Tremmel et al. (2015), © RAS. Reproduced with permission.

SMBHs (Reines et al., 2013; Moran et al., 2014). Realistic numerical studies of BH formation and growth in these small galaxies, focusing on their occupation fraction and how they and their host galaxies evolve toward the correlation with the stellar velocity dispersion, would provide vital constraints on BH seed masses and early growth mechanisms (Volonteri et al., 2008b; Volonteri & Gnedin, 2009; Volonteri, 2010a).

We use the new N-body + SPH code ChaNGa (Menon et al., 2015), which includes all of the physics modules previously implemented in Gasoline (Wadsley et al., 2004) such as hydrodynamics, gas cooling, a cosmic UV background, star formation and SNe feedback. The 'zoomed-in' approach preserves the large scale tidal field while allowing us to model a small region at high resolution. This is similar to the simulation described in Governato et al. (2010) and in Shen et al. (2014). In this particular simulation, stars and DM densities dominate that of gas within the inner regions by more than a factor of 10. Examining other dwarf galaxy simulations (e.g. Governato et al., 2010), we find that gas densities can often reach similar values to DM and stars. In either case the contribution from gas to DF is only a minor correction, at most a factor of a few, and negligible in our current example.

By z <1 these systems are a good representation of real dwarf galaxies, with an extended stellar disk, no bulge, a high gas fraction and a cored DM profile. We first run the simulation until z = 6, when we insert five black holes of mass 5×10^5 $M_\odot$ in the centers of the five most massive halos at the time, which all have a mass of 2×10^8 $M_\odot$ or higher. In these simulations black holes do not accrete or produce feedback, as we are only interested in following their dynamics. From z=6 we run two simulations to $z < 1$, one with our DF routine and the other with advection. By the end of the simulation, there are only two major star forming galaxies with masses $\sim 10^{10}$ $M_\odot$.

We then run the Amiga Halo Finder (AHF) (Knollmann & Knebe, 2009) for all the saved snapshots and calculate the center of the main halo at each step using the shrinking spheres approach. In Figure 2.3 we follow the trajectories of four black holes with respect to the center of this halo (which originally just has the blue BH at its center). Each color represents a different black hole. Black dots indicate a black hole merger, which happens when two

BHs come within two ϵ_g of one another at relative speeds low enough to be gravitationally bound. The dashed black lines indicate the gravitational softening length of 87 pc.

The black holes become perturbed as the red, cyan, and blue host galaxies interact between $z = 3$ and 4. In the advection case the black holes are driven quickly toward the center where they all merge, leaving only one black hole (labeled as red). With the DF correction, only the cyan and blue BHs merge. After the red and blue galaxy hosts merge with DF, the blue and red BHs remain orbiting around the center of the merger remnant. The blue BH comes back to the center only after 4 Gyr and the red BH remains orbiting at around 1 kpc (11 times the force resolution) for another 4 Gyr before sinking and merging with the blue BH.

The more striking difference between the DF and the advection run involves the green black hole. When the much smaller green host galaxy merges with the blue/red host at $z \sim 1$, it is initially far from halo center ($\sim$ 30 kpc) and is quickly disrupted by the main galaxy. With DF, the BH stays on a wide orbit, never coming much closer than a few kpc from halo center. In the advection case, however, the green black hole is quickly pushed to the center where it merges with the central red BH (see Figures 2.3 and 2.4). This is an unrealistic result, as the DF timescale of a 5×10^5 $M_\odot$ black hole that far away from the center of such a small galaxy would be longer than a Hubble time.

With this simulation we can clearly see how the choice of dynamical correction can affect the ability of SMBHs to become perturbed during mergers. In the DF simulation, BHs are able to remain off-center for many Gyr while with advection they are quickly driven to the center. Additionally, the DF simulation allows for sustained wide orbits resulting from minor mergers. Such dynamics can have an important impact on interpreting the connection between the initial occupation probability of SMBH seeds in dwarf galaxy progenitors and the observed occupation at low redshift. Methods such as the advection scheme presented here would predict a more direct connection, while the simulation with DF indicates that the nature of the mergers (i.e. mass ratio and orientation) can have an impact on which dwarf galaxies have observable SMBH activity and when that activity occurs. The DF correction

could also have important implications for BH merger rates, allowing them to become more decoupled from galaxy merger rates than advection simulations. This will affect predictions of gravitational wave detections as well as estimates for recoiling BHs, which can have an important effect on observability (e.g. Madau & Quataert, 2004).

This simulation is a useful illustration of the variety of different, realistic BH orbits our method allows compared to commonly used advection schemes. In future work, we will explore the dynamics of BHs in a variety of different merger events within a cosmological context.

2.5 Discussion and Summary

We have introduced a sub-grid force correction term for SMBH motion based on dynamical friction. This correction allows us to better model the orbital decay of SMBHs in numerical simulations. We have shown using controlled experiments of isolated DM halos that this addition matches analytic predictions of the orbital decay in DM halos with resolutions attainable by large-volume cosmological simulations. We have also demonstrated that our prescription naturally converges with resolution.

This method is a significant improvement over existing 'advection' methods that force a short orbital decay timescale regardless of the dynamical state of the system. When applied to a cosmological dwarf galaxy simulation, our method results in noticeably different black hole dynamics compared with the advection scheme. In particular, our prescription:

- Models perturbations and orbital decay of BHs during and following galaxy mergers
- Allows for long-lived dual BH systems with close (< 1 kpc) orbits.
- Maintains a stable central BH when appropriate.
- Allows for sustained wide (> 5 kpc) orbit BHs.

Correctly modeling the orbital dynamics of a black hole within its host galaxy can have important consequences for its accretion history, duty cycle, and observability that was previously neglected in simplified 'advection' schemes. The dynamically complex and more realistic orbits allowed by our method will have crucial implications for the early growth of

SMBHs, which takes place in small, rapidly growing galaxies at high redshift (Aykutalp et al., 2014). Additionally, understanding the relative importance of different accretion mechanisms throughout a SMBH's lifetime requires the ability to accurately model its dynamics during all phases of galaxy evolution, including mergers. Implementation of the method presented here will allow cosmological simulations to better model SMBH accretion, growth and energy deposition in the IGM and, therefore, increase the ability of simulations to interpret and predict observational results.

Chapter 3

SMBH FORMATION IN COSMOLOGICAL SIMULATIONS

In this chapter, I explain my model for the formation of early SMBHs in cosmological simulations, called SMBH seeds. I first summarize the main theories of SMBH seed formation, then current approaches to seeding SMBHs in cosmological simulations. Finally, I explain the method I have developed and show how it results in the early formation of SMBHs and occupation fractions that place a SMBH in all massive galaxies while maintaining predictive power at lower masses where observations are lacking.

Material from this chapter has been previously published in collaboration with Michael Karcher, Fabio Governato, Marta Volonteri, Tom Quinn, Andrew Pontzen, Lauren Anderson, and Jillian Bellovary in the September 2017 edition of Monthly Notices of the Royal Astronomical Society (Tremmel et al., 2017), and has been reproduced here with permission of the Royal Astronomical Society.

3.1 Current Theories of SMBH Seed Formation

There are three prevailing theories for how SMBH seeds may have formed: 1) Population III stars, 2) runaway collapse of nuclear star clusters, and 3) the direct collapse of gas into a supermassive object. All require slightly different conditions for the seeds to form and predict different initial masses and prevalence within early galaxies. Further probing the high redshift mass function and halo occupation of SMBHs with future observations of gravitational waves as well as higher redshift observations from future observatories like the James Webb Space Telescope could help constrain which formation channel (or combination thereof) is correct (Natarajan et al., 2017; Volonteri et al., 2017).

Population III stars are the first population of stars to form in the Universe from pristine

gas that has not yet been enriched by previous episodes of star formation. Because they form from low metalicity gas, which can have large fragmentation scales, these stars can potentially reach a few hundred solar masses (Carr et al., 1984; Omukai & Nishi, 1998; Tan & McKee, 2004) though the exact mass function is highly uncertain (e.g. Turk et al., 2009). For seeds massive enough to be able to grow into the behemoth objects we observe across cosmic time, they must come from stars with mass greater than ≈ 260 $M_\odot$. Above this limit, the star does not explode and is able to create a black hole on the order of 100 $M_\odot$ (Bond et al., 1984). This formation scenario would be relatively common and should form a SMBH in nearly all small halos that form population III stars.

Nuclear star clusters can form during the first phases of efficient star formation in gas that has been enriched by the first supernovae (SN) explosions. While still at relatively low metallicity and with the UV field by nearby stars to limit the amount of molecular hydrogen, the density of fragmentation for gas is very large. Nuclear star clusters that form from such gas are very dense (Schneider et al., 2006), such that they will begin to collapse before the most massive stars explode as SN, forming a very massive star at the center and resulting in a black hole of mass on the order $10^2 - 10^4$ $M_\odot$ (Devecchi & Volonteri, 2009)

The direct collapse of gas into a supermassive black hole can be achieved in a scenario where gas is able to avoid fragmentation into stars (e.g. Haehnelt & Rees, 1993; Bromm & Loeb, 2003; Lodato & Natarajan, 2006). This requires the gas to be pristine, without any enrichment from previous star formation episodes, and with molecular hydrogen formation suppressed. H_2 will naturally form in a collapsing cloud of hydrogen gas as densities increase and is a powerful coolant. The presence of H_2 decreases the local Jeans length and causes fragmentation. However, if the formation of H_2 can be avoided, the cloud could cool more gradually and collapse into a single supermassive object, resulting in a black hole of mass $10^4 - 10^6$ $M_\odot$ (Volonteri, 2010b), assuming that the gas can also efficiently lose angular momentum (Begelman et al., 2006a; Begelman & Shlosman, 2009; Begelman et al., 2006b). Different mechanisms have been proposed to suppress H_2 formation, such as the UV field from nearby stellar populations (e.g. Agarwal et al., 2014) and Lyman α trapping (Spaans

& Silk, 2006).

Despite their clear differences, all of the scenarios share common traits, namely that SMBH seeds form from dense, relatively low metalicity environments in the early Universe. The main differences between the models are in the details: what is the initial occupation fraction for SMBH seeds, when precisely do they form, and what are their initial masses.

3.2 Common Approaches to SMBH Seeding

Like most aspects of SMBH physics, the process of black hole seed formation occurs far below the resolution limits of even the highest resolution cosmological simulations. A technique often used is to place a seed black hole in the center of halos as they cross a given mass threshold. (e.g. Di Matteo et al., 2003; Sijacki et al., 2015; Schaye et al., 2015), This often requires an 'on the fly' halo finder that is able to continuously identify dark matter halos so that, once a halo crosses this threshold, it is given a black hole seed if it does not already have one. The initial black hole mass and halo threshold are chosen so that 1) all massive halos have a SMBH and 2) the galaxy initially is likely to lie on the observed scaling relations for SMBH mass and galaxy mass.

The problem with this approach is that it assumes a step function in the SMBH occupation function. Halos below the threshold will never have SMBHs and those above will always have one, while in reality is likely a smoother transition, as more low mass galaxies are observed to host AGN (e.g. Reines et al., 2013). Perhaps more serious is the time of the seeding. A common halo mass threshold is generally between 10^{10} and 10^{11} $M_{\odot}$. In contrast, the theories described in the previous section will result in halos of mass 10^{6-8} $M_{\odot}$ being seeded with black holes, depending on the formation scenario. By seeding at higher mass, the black holes are place in the simulation at much later times and aspects of their evolution, and the effect they have have on their host galaxies, is lost.

To counteract the problems inherent to this approach, Bellovary et al. (2011) seed black holes at high redshift by selecting a random sample of star forming gas particles that have low metallicity. Star formation in simulations only occurs in high density gas. At low metallicity,

one would be sampling the first stars to form in the simulation and, therefore, the first regions to form stars at high redshift. This results in higher redshift formation times, as would be expected by all of the seed formation theories presented in the previous section. However, in practice, this resembles most closely the Pop. III stars scenario. While SMBH seeds should certainly be common in this formation mechanism, not all of them should necessarily be able to grow to high masses that they are seeded with (in this case, they are seeded as the same mass as an entire star particle, which itself is meant to represent star clusters).

3.3 A New Implementation of SMBH Seed Formation in Cosmological Simulations

Similar to the implementation by Bellovary et al. (2011), our simulations form SMBH seeds based on the physical state of the gas particle, choosing a subset of gas parties that would, based on the star formation prescription of the simulation, be forming stars (i.e. they have crossed both the density and temperature thresholds required by the star formation prescription). However, rather than choose a random sub-set of these star-forming gas particles, we deterministically choose which should form SMBH seeds based on their detailed properties.

A would-be star particle just forming out of pristine gas in the early Universe is turned into a SMBH particle instead using the following criteria:

- Low mass fraction of metals ($Z < 3 \times 10^{-4}$)
- Density 15 times that of the SF threshold (3 m_p/cc)
- Temperature between 9500 K and 10000 K

These criteria ensure that black holes form only from gas that a) is collapsing quickly (i.e. faster than the star formation timescale as it has not been turned into a star already) while b) cooling relatively slowly, approximating formation cites predicted for SMBH seed formation (Begelman et al., 2006a; Volonteri, 2012).

The criteria above were not chosen via an extensive parameter search. Rather, they were empirically derived via analysis of star forming gas particles in high redshift volume simulations. The model limits SMBH growth to the highest density peaks in the early Universe with high Jeans mass. This is a marked improvement over stochastic formation from star forming gas, resulting in seed formation that occurs in environments that are different than the average unenriched star forming region, as seen in higher resolution tests of SMBH formation sites (Agarwal et al., 2014; Habouzit et al., 2017). Because we are following conditions of gas at resolved scales (i.e. hundreds of pc), these criteria are designed to capture the regions where SMBH seeds should exist and grow quickly to large masses, regardless of the specifics of the true formation mechanism at unresolved scales.

The metallicity threshold of 3×10^{-4} was chosen to select gas that had seen very little chemical evolution. We found that choosing more strict (lower) metallicity criteria or colder gas, biases SMBH formation *away* from the densest regions of the early Universe, an undesired outcome due to the finite resolution of our runs, that we specifically decided to avoid. SF will often form stars nearly simultaneously with SMBH particles. As stars form and massive stars give off stellar winds and SNe explode, metal rich gas permeates throughout the halo and beyond, effectively shutting down any potential seed formation within the parent halo as well as nearby halos. Metal diffusion in SPH codes is explicitly regulated by a diffusion equation; here we follow the implementation in Shen et al. (2010) with coefficients for both metal and thermal diffusion both set to 0.03, which give realistic values for galaxy metallicity gradients in high resolution dwarfs (Brooks et al 2017 in prep.).

Once formed, the SMBH seed mass is set to 10^6 $M_\odot$. To attain this mass, the newly formed SMBH accretes as much mass as it needs from surrounding gas particles (total mass is then explicitly conserved), representing rapid, unresolved growth. The initial mass, while somewhat higher than most theoretical estimates (Johnson et al., 2012; Volonteri, 2012), is motivated by the fact that much of the early growth onto SMBH seeds, or the exotic objects that may proceed them, can exceed 0.1 $M_\odot$ yr^{-1} and be governed by the environment and physical processes well below the resolution limit of our simulations (e.g. Hosokawa et al.,

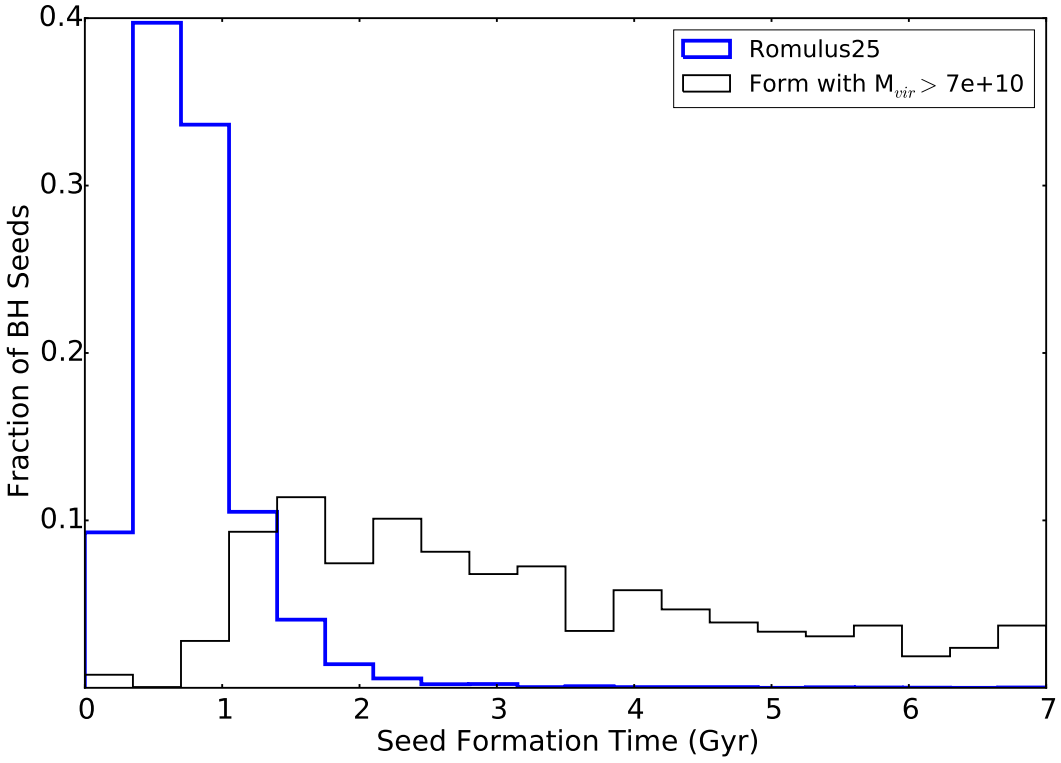

Figure 3.1: Seed Formation Times. The distribution of black hole seed formation times using our approach applied to a 25 Mpc run (Romulus25; blue line) compared to the seed formation if we applied a threshold halo mass criterion similar to other common approaches to seed formation in large simulation of this type (Di Matteo et al., 2003; Sijacki et al., 2015; Schaye et al., 2015). Using our scheme, black hole seeds form much earlier, the vast majority forming within the first Gyr of the simulation, similar to the expected formation epoch for SMBHs (Volonteri, 2012). We compare to the halo threshold scheme, meant to approximate that used in Sijacki et al. (2015), where halos are seeded once a halo reaches a critical mass of $7 \times 10^{10} M_{\odot}$. Using this, black holes are seeded at much later times, even in the most massive halos, which would cause the earliest periods of SMBH growth to be missed. Figure from Tremmel et al. (2017), © RAS. Reproduced with permission.

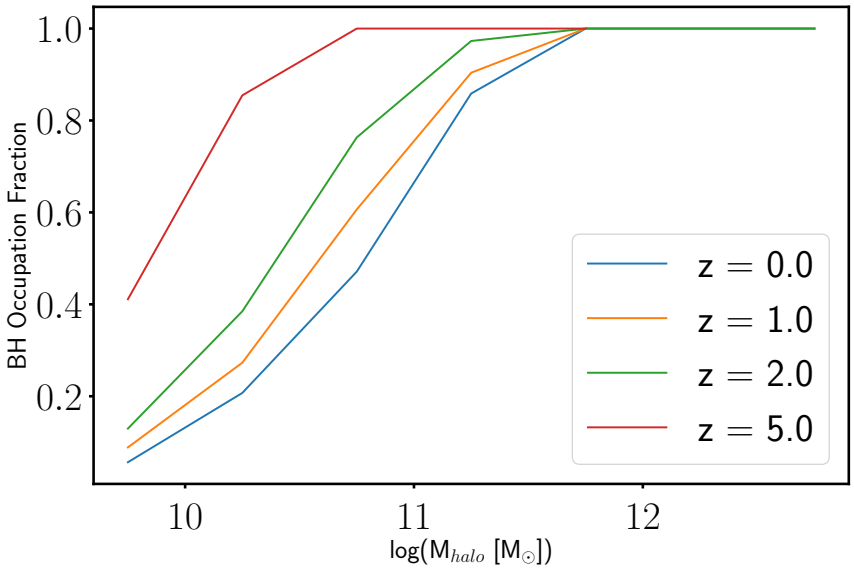

Figure 3.2: SMBH Occupation Fraction. The fraction of halos hosting at least one SMBH in its central galaxy as a function of the total Virial mass of the halo at different redshifts. By $z = 5$, $\approx 95\%$ of SMBHs that will form have been formed in the simulation. As halos merge over time, the occupation fraction evolves accordingly.

2013; Schleicher et al., 2013). In reality, SMBH seeds would likely attain a spectrum of masses early on, but since such processes are unresolved, we cannot differentiate between where a larger SMBH seed should grow. This mass is also sufficiently large compared to our DM and gas particle masses that the dynamics of all SMBHs will be well resolved (Tremmel et al., 2015). We verified that even with this initial mass, SMBH seeds that exist in unfavorable environments (i.e. dwarf galaxies) naturally have limited growth, with about 50% of SMBH seeds having less than 10% mass growth over a Hubble time. We also verify that SMBHs that grow to more than 10^7 $M_\odot$ have grown enough through accretion to be insensitive to initial conditions.

Figure 3.2 shows the resulting occupation fraction as a function of halo mass and redshift for the Romulus25 Simulation (see chapter 5). All massive halos have SMBHs and galaxies in

lower density environments, such as field dwarf galaxies, are likely to never form SMBHs. It should be noted that observational estimates for the occupation fractions are often based on AGN which itself is a lower limit to the overall occupation fraction and are highly uncertain at lower masses (Miller et al., 2015)

3.4 Summary

In this chapter, I summarized the prevailing theories of SMBH seed formation and presented a new approach to modeling this process within cosmological simulations. The model presented forms seeds based on the properties of gas such that SMBHs form in the high density, collapsing, metal poor environments in the early Universe. Once formed, the SMBHs gain mass from the surrounding gas particles to attain a user-defined initial mass. This has several advantages over more common approaches. SMBH seeds form at more realistic times (in the first ~ 1 Gyr) and are allowed to form in lower mass galaxies, maintaining predictive power for AGN and SMBH occupation in dwarf galaxies.

Chapter 4

SMBH ACCRETION IN COSMOLOGICAL SIMULATIONS

In this chapter, I briefly describe Bondi-Hoyle accretion, the basis behind accretion algorithms for SMBHs in most simulations modeling galaxy-scale or larger systems. I will present a short derivation of the Bondi-Hoyle formalism and describe its short comings with regard to cosmological simulations. Finally, I will outline a new approach that I have developed for accounting for angular momentum supported gas when estimating accretion rates onto SMBHs, a crucial addition in order to properly model accretion from gaseous disks common in star forming galaxies. I will then outline the numerical approach to both accretion and feedback and how many potential pitfalls, such as overeaten gas particles and overcooling, are avoided.

Material from this chapter has been previously published in collaboration with Michael Karcher, Fabio Governato, Marta Volonteri, Tom Quinn, Andrew Pontzen, Lauren Anderson, and Jillian Bellovary in the September 2017 edition of Monthly Notices of the Royal Astronomical Society (Tremmel et al., 2017), and has been reproduced here with permission of the Royal Astronomical Society..

4.1 Bondi-Hoyle Accretion and Its Limitations

The standard approach to estimating the accretion of gas onto SMBHs in large scale simulations is Bondi-Hoyle accretion. The overarching assumption with this formalism is that the physical state of the gas far from the SMBH dictates the rate of accretion on smaller scales. Because the very issue that we are dealing with in cosmological simulations is one of connecting the smallest resolved scales to processes occurring far below the resolution limit, this approach is clearly very attractive. In this section I briefly visit the derivation of Bondy-

Hoyle accretion and then discuss its short comings with respect to current simulations.

4.1.1 A Brief Derivation of Bondi-Hoyle Accretion

This process of accretion was studied first with respect to accretion of hydrogen gas by stars as a way of understanding their formation. This process was first explored in the regime of an object of mass M moving through a static cloud of gas at equilibrium (Hoyle & Lyttleton, 1941; Bondi & Hoyle, 1944). The crucial assumption taken is that the internal energy of the gas is negligible compared to the bulk relative motion to the massive object and gravity.The authors show that, assuming mass and momentum conservations, the flow of material onto the massive object is proportional to the amount of material entering the sphere of influence of the SMBH.

$$\dot{M} \propto 2\pi(\frac{GM}{V^2})^2\rho_\infty V = 2\pi\frac{G^2M^2\rho_\infty}{v^3}, \tag{4.1}$$

where ρ_∞ is the density of the gas far from the object and V is the velocity of the relative velocity of the object at the cloud. They go on to show that pressure from density gradients that develop in the gas through this process are negligible compared to the gravitational force. The proportionality factor is found to be of order unity.

Bondi (1952) presents the case for accretion in a different regime, where the massive object is embedded in a static cloud with no relative motion. In this scenario, the internal energy of the gas becomes the determining factor, rather than the bulk motion. The Bernoulli equation gives the following relation at all radii from the massive object.

$$\frac{v^2}{2} + \int_{p_\infty}^{p}\frac{dp}{\rho} - \frac{GM}{r} = 0 \tag{4.2}$$

By assuming the gas behaves adiabatically ($P/P_\infty = (\rho/\rho_{infty})^\gamma$; $1 < \gamma < 5/3$) and that $v \sim c_s$, where c_s is the sound speed far from the massive object, defined such that $c^2 = \gamma p_\infty/\rho_\infty$, one arrives at $r \propto \frac{GM}{c_s^2}$. Assuming that the mass flowing through this radius will make its way onto the massive object, the accretion rate is simply given by the continuity equation, $\dot{M} \propto 4\pi r^2\rho v$. Plugging in the appropriate values for r and v as described, we arrive

at an approximation for the accretion rate onto the massive object.

$$\dot{M} \propto \frac{4\pi\rho_\infty (GM)^2}{c_s^3} \tag{4.3}$$

Once again, the constant of proportionality is found to be on the order of 1. The similarity between equation 4.3 and 4.1 means that it is simple to combine the two for an order of magnitude calculation for the accretion rate in intermediate regimes (Bondi, 1952). It is this formula that represents Bondi-Hoyle accretion.

$$\dot{M} \propto \frac{\pi\rho_\infty (GM)^2}{(c_s^2 + V^2)^{3/2}} \tag{4.4}$$

In practice, this result can be derived by defining an 'accretion radius' around the SMBH, within which gas becomes bound, R_{acc}. Assuming mass continuity the accretion rate becomes $\dot{M} \approx 4\pi R_{acc}^2 \rho v$, where ρ and v are the density and radial velocity of the gas relative to the central object. R_{acc} is defined then simply by setting the gravitational potential equal to the sum of internal and bulk energies of the surrounding medium at large scales.

4.1.2 Limitations of Using Bondi-Hoyle in Simulations

The first, most obvious limitations to utilizing Bondi-Hoyle in lower resolution simulations is that, for cold, dense gas, the ISM of a galaxy is likely to be multiphase, with density structures well below the resolution limit of the simulation. In, for example, a smoothed-particle hydrodynamics simulation like ChaNGa, the density of each gas particle should be taken as the average density over that region. This effectively smooths out all of this structure and can lead to underestimates in the accretion rate given by equation 4.4 (Booth & Schaye, 2009). This often compels simulators to invoke a 'boost factor' to their calculated accretion rates to account for this underestimation.

The second, less obvious limitation deals with the symmetries assumed by, in particular, the calculation by Bondi (1952), where accretion on to the SMBH is assumed to be spherically symmetric. In realistic scenarios, SMBHs are likely to grow in star forming, disk dominated

galaxies (Mullaney et al., 2012; Yang et al., 2017). Thus, they receive their accreted gas from a disk that is at least partially supported by angular momentum in addition to gas pressure. The gas must first lose this angular momentum in order to make its way onto the SMBH.

Hopkins & Quataert (2010) run a detailed simulation of an isolated disk galaxy with adaptive resolution reaching sub pc scales within the central regions near the accreting SMBH. They find that gas inflow is driven less by the gas thermodynamics and more by the large scale torques imparted from an asymmetric distribution of stars within the disk. This torque drives gas inward, determining the accretion rate of the SMBH. The prediction from these simulations is that the true accretion rate should in fact be much lower than that predicted by the Bondi-Hoyle formalism by several orders of magnitude (Hopkins & Quataert, 2011a).

4.2 Accounting for Angular Momentum Support and Limited Resolution

I will present in this section an overview of the accretion algorithm I have implemented into ChaNGa. The accretion rate, $\dot{M}$, is estimated via a modified Bondi-Hoyle prescription applied to the smoothed properties of the 32 nearest gas particles. The initial derivation of our approach is exactly the same as Bondi accretion. If we define some accretion radius, R, relative to the SMBH beyond which gas is bound to the black hole, and assume that mass continuity is roughly upheld on long time scales, the accretion rate onto the SMBH should be similar to the rate of mass flowing through a spherical surface of that radius:

$$\dot{M} \sim \pi R^2 \rho v. \tag{4.5}$$

Here v is the characteristic velocity of gas through the surface and ρ is the density of the ambient gas. In Bondi-Hoyle accretion, the calculation of the accretion radius, R, balances the SMBH's gravitational potential and both the internal and bulk kinetic energies of the gas. In order to avoid underestimating the accretion rate due to resolution effects when calculating the density and temperature of nearby gas, we apply a density dependent boost factor to this accretion rate, following the prescription of (Booth & Schaye, 2009) where the

standard Bondi rate is multiplied by a density dependent factor, $\left(\frac{\rho_{gas}}{\rho_*}\right)^{\beta}$, where β is a free parameter and ρ_* is the star formation density threshold.

However, even with a well motivated (but often poorly constrained) density boost, Bondi-Hoyle accretion is unable to account for angular momentum support, which often dominates the dynamics of cold gas at resolved scales, as in the disks of star forming galaxies (Hopkins & Quataert, 2010, 2011b). Past efforts have focused on sub-grid models for angular momentum transport on sub-galactic scales (Anglés-Alcázar et al., 2017) or within the SMBH's accretion torus (Rosas-Guevara et al., 2015).

To take advantage of the improved spatial resolution of modern simulations, we implement an accretion algorithm that accounts for the angular momentum of gas *at resolved scales*. Our approach avoids any additional assumptions of sub-grid physics or free parameters beyond those required by the conventional Bondi-Hoyle prescription, namely that the accretion rate, averaged over timescales relevant to the simulation, is a direct consequence of mass flux across the accretion radius, defined as the scale at which the gravitational potential of the SMBH balances the internal and bulk energetics of the gas, as measured at the smallest resolved scales of the simulation.

In the reference frame of rotating gas, angular momentum provides an effectively lower gravitational potential such that $U_{eff}(\mathbf{r}) \sim -\frac{GM}{r} + \frac{j(r)^2}{2r^2}$, where $j(r)$ is the angular momentum per unit mass of the gas at distance r from the SMBH. We can replace $j(r)^2/r^2$ with v_θ^2, the rotational velocity of the surrounding gas. It is important to note that v_θ is distinct from the bulk velocity, which we will refer to as v_{bulk}, in the Bondi-Hoyle formula, which accounts for a flow of gas, not a coherent rotational motion.

If the dominant motion of the gas is rotational rather than a bulk flow, we can use the effective potential above and solve for R, ignoring order unity terms, such that the effective potential balances with the thermal energy of the gas, i.e $U_{eff} \sim c_s^2$. By definition the tangential motion must not contribute to the mass flux through our area. Returning to the simple equation for $\dot{M}$ above we get the following relation.

$$\dot{M} \propto \frac{\pi (GM)^2 \rho c_s}{(v_\theta^2 + c_s^2)^2}. \tag{4.6}$$

Note that we do not assume v_θ is constant on unresolved scales, only that its value should inform the radius, R, at which the gravity of the SMBH dominates the gas dynamics. This is similar to the original Bondi-Hoyle formalism, where the energetics of gas far from the black hole are used to approximate the accretion radius. In this case, v_θ encapsulates the amount of angular momentum support the gas has on the smallest resolved scales, translating to a smaller accretion radius and therefore lower accretion rate.

To avoid uncertainties in particle dynamics below the force softening scale, we calculate the specific angular momentum, j, relative to a target black hole for gas particles that are between 3 and 4 softening lengths away (with our spline kernel softening, Newtonian forces are followed exactly at 2 ϵ_g). We then calculate the tangential velocity that gas one softening length,ϵ_g, away from the SMBH would have if the angular momentum on the larger scales was conserved, $v_\theta(\epsilon_g) \sim j/\epsilon_g$. The smallest relative velocity of the 32 gas particles closest to the SMBH, which we take as a proxy to $v_{\rm bulk}$, is compared to v_θ. If $v_\theta > v_{bulk}$ we use equation (6) to calculate $\dot{M}$. Otherwise, we use the normal Bondi rate. Both calculations include the density-dependent boost factor, resulting in:

$$\dot{M} = \alpha \times \begin{cases} \frac{\pi (GM)^2 \rho}{(v_{\rm bulk}^2 + c_s^2)^{3/2}} & \text{if } v_{\rm bulk} > v_\theta \\ \\ \frac{\pi (GM)^2 \rho c_s}{(v_\theta^2 + c_s^2)^2} & \text{if } v_{\rm bulk} < v_\theta \end{cases} ; \alpha = \begin{cases} \left(\frac{\rho}{\rho_*}\right)^\beta & \text{if } \rho \geq \rho_{th,*} \\ \\ 1 & \text{if } \rho < \rho_\star \end{cases} . \tag{4.7}$$

Unlike Rosas-Guevara et al. (2015), we do not implement a viscosity parameter in our accretion rate calculation. This was an explicit choice made to avoid the inclusion of an additional free parameter and is justified by the fact that we are not attempting to approximate the behavior of an accretion torus, as in Rosas-Guevara et al. (2015), where viscous timescales can be more critical. Still, there is uncertainty in the normalization of equation (7) when $v_\theta >> c_s$, which will be explored in future work. It should also be noted that

equation (7) is not continuous at $v_{\rm bulk} = v_\theta$. We find this effect is sub-dominant compared to variations in density and velocity inherent to discreet calculations. This is shown in practice in figure 14, where our approach produces a less bursty accretion history in MW-mass halos compared to normal Bondi accretion.

For the density dependent boost factor, we compare the local density to the star formation density threshold, n_*, meant to represent the limit beyond which the simulation fails to resolve the multiphase ISM. The exponent β is a free parameter which we take to have a value of 2 (see next section). Equation (7) is then compared to the Eddington rate, $\dot{M}_{edd}(M)$, given the SMBH's mass at time t such that $\dot{M}_{BH,final}(t) = \min(\ \dot{M}(t),\ \dot{M}_{edd}(M_{BH}(t)\ )\ )$.

4.3 Numerical Implementation for Accretion and Feedback

In this section, I discuss the details behind the numerical implementation of the accretion rate calculation described above, as well as the transfer of feedback energy to nearby gas particles as a result of accretion onto a SMBH.

4.3.1 Accretion Rate Calculation

Standard for such simulations, we calculate the accretion rate onto a SMBH by smoothing the properties of the nearby gas particles over the SPH kernel. For the tangential velocity calculation described in the previous section, we require the velocities of gas particles at distances between 3 and 4 softening lengths. Thus, we first gather all of the particles at distances smaller than 4 softening lengths from the SMBH.

After the local tangential velocity is calculated, as described above, from the total angular momentum of gas particles between 3 and 4 softening lengths from the SMBH, we proceed with the particle smoothing step, where the accretion rate is given by the following calculation using the nearest 32 particles to the SMBH (if less than 32 particles exist within 4 softening lengths, less particles are used, but this will naturally end up being a very minor accretion event).

$$\dot{M} = \sum_{i}^{N} \omega_i m_i f(\rho_i, c_{s,i}) \tag{4.8}$$

Here ω_i is the smoothing kernel value, m_i is the mass, ρ_i is the density, and $c_{s,i}$ is the sound speed of the ith particle near the SMBH. The function, f depends on the average kinematics of the gas, as described in the pervious section.

$$f(\rho, c_s) = \alpha \times \begin{cases} (v_{\rm bulk}^2 + c_s^2)^{-3/2} & \text{if } v_{\rm bulk} > v_\theta \\ \\ c_s(v_\theta^2 + c_s^2)^{-2} & \text{if } v_{\rm bulk} < v_\theta \end{cases} ; \alpha = \begin{cases} \left(\frac{\rho}{\rho_*}\right)^\beta & \text{if } \rho \geq \rho_{th,*} \\ \\ 1 & \text{if } \rho < \rho_\star \end{cases} \tag{4.9}$$

Both v_θ and v_{bulk} are calculated as described above. Importantly, we do not attempt to calculate accretion based on individual gas particle velocities in order to avoid numerical noise.

4.3.2 Transfer of Mass and Momentum

Often accretion methods perform mass transfer stochastically, but we opt for a more deterministic approach. We weight each particle based on its accretion properties (essentially the value of $w_i f(\rho_i, c_{s,i})$ as defined above). We then take mass accordingly from particles that have contributed the most to the accretion rate until all of the mass accreted during the duration of the current timestep, Δt, has been transferred to the SMBH ($\dot{M}\Delta t$).

Momentum from the accreted mass is transferred directly to the SMBH particle. However, particles that are on longer time steps that have not yet completed will fail to properly conserve this momentum. Through some initial tests we found that this failure can have important consequences for SMBH dynamics if the timestep difference is extreme enough. To overcome this we do not allow SMBHs to consume gas particles that, at the completion of the SMBH time step, have not yet completed their own. Because SMBHs are always placed on the lowest global time step of the simulation, this can be a very common occurrence that

may prevent the SMBH from accreting anything at all. To prevent this from happening, we keep track of 'un-accreted' gas that the SMBH still requires and 'snow ball' this with the mass, $\dot{M}\Delta t$, accreted from subsequent time steps. Eventually, enough gas nearby will have finished their time step at the same time as the SMBH and it will be able to grow as it should.

This, however, may present a problem on its own, creating an artificially more bursty accretion (and therefore feedback) history for the SMBH. Here we utilize a feature of ChaNGa that allows the adjustment of particle time steps on the fly. We require that all gas particles nearby a SMBH have a time step no more than twice that of the SMBH. This allows accretion of gas to occur, in the worse case scenario, every other SMBH time step. Because these time steps are small by design, accretion onto the SMBH can still be resolved with very good time resolution. In the testing phase of this code, we made made sure that this accumulation of mass was not extreme so as to create large bursts of accretion and feedback.

Another issue to account for, given that SMBHs accreted onto a galaxy will not immediately sink to the center, is multiple SMBHs attempting to eat gas from the same particle. When this occurs, it is possible to 'over eat' a particle, resulting in a failure of conservation of mass. To avoid this, we do not allow any particle to consume mass from a particle already being consumed by another SMBH.

4.3.3 Feedback from SMBHs

Energy from accretion is isotropically imparted to particles within the smoothing kernel. Once again, only particles within 4 softening lengths are allowed to receive this energy. If more than 32 particles exist within this distance, the 32 nearest particles receive the energy. Note that the choice of 32 particles for both feedback and accretion calculations is consistent with other calculations done by the simulation, all of which use 32 particles as the fiducial number to calculate smoothed quantities (except for dynamical friction, which uses 64 particles in order to decrease the effect of noisy particle dynamics).

To ensure that the feedback energy is realistically dissipated, gas particles that receive

energy from a SMBH are not allowed to cool for a time equal to the timestep of the SMBH (typically 10^3 to 10^4 yrs), which is meant to represent the continuous transfer of energy during each SMBH timestep. This is a similar technique that is used in the Blastwave supernova feedback prescription, though here we utilize a different cooling shutoff time meant to approximate the continuous accretion and subsequent feedback that should occur during a timestep. This technique is meant to avoid the over-cooling problem inherent in lower resolution simulations. The instantaneous transfer of energy to high density gas will be radiated away in artificially fast timescales.

The amount of energy coupled to surrounding gas particles is given by

$$E = \epsilon_r \epsilon_f \dot{M} c^2 \Delta t, \tag{4.10}$$

where the radiative efficiency, ϵ_r, is assumed to be 10% and the efficiency that energy couples to gas, ϵ_f is set to 2% (see below for discussion on free parameter calibration). The accretion rate is assumed to be constant throughout one black hole timestep, Δt.

4.4 Summary and Discussion

Bondi-Hoyle accretion has become the standard algorithm for SMBH accretion in cosmological simulations with a large amount of success. However, the approach has severe issues. Limited resolution in large scale simulations means that the properties of gas nearby SMBHs will be unresolved, causing the Bondi-Hoyle rate to be underestimated. In the regime of angular momentum supported gas, e.g. when SMBHs feed from a gaseous galactic disk, the assumption of symmetries inherent in Bondi-Hoyle accretion break down.

The new model I have implemented into ChaNGa for SMBH accretion uniquely accounts for the angular momentum support of gas in a way that fits naturally into the Bondi-Hoyle formalism, requiring no new assumptions beyond those already inherent to Bondi-Hoyle accretion. In the regime where rotational motion dominates over bulk motion and the local sound speed of the gas, the accretion rate onto the SMBH will be determined by how efficiently angular momentum will be transferred through torques at larger scales.

Chapter 5

THE ROMULUS SIMULATIONS

In this chapter, I describe the ROMULUS Simulations, a set of large-scale cosmological simulations that incorporates the SMBH physics implementation I have developed (see chapters 2, 3, and 4). Table 5.1 shows all of the simulations discussed in this chapter, including a series of smaller simulations used to explore the effects of different physics as well as the ROMULUSC simulation that will be discussed further in Chapter 7.

First I describe the details of the simulation code, CHANGA, sub-grid physics, and how I constrained the free parameters inherent in these sub-grid models. I will then present results from the flagship simulation, ROMULUS25, a $(25\ \mathrm{Mpc})^3$ uniform volume simulation, showing that it reproduces observed galaxy and SMBH properties. I will then explore a series of smaller $(8\ \mathrm{Mpc})^3$ simulations that highlight the role of SMBH feedback compared to SN in shaping galaxy evolution as well as the differences resulting from my SMBH implementation compared to more common approaches. Finally, I will present an example of how, utilizing both the dynamics and accretion algorithms for SMBHs I have developed, we can track the evolution of SMBH pairs that eventually coalesce into a binary system following a galaxy merger.

Material from this chapter has been previously published in collaboration with Michael Karcher, Fabio Governato, Marta Volonteri, Tom Quinn, Andrew Pontzen, Lauren Anderson, and Jillian Bellovary in the September 2017 edition of Monthly Notices of the Royal Astronomical Society (Tremmel et al., 2017), and has been reproduced here with permission of the Royal Astronomical Society.

Table 5.1: Physics implementations in different simulations presented in this Paper.

Name	Box Size (Mpc)	Accretion[a]	SMBH Dynamics[b]	ϵ_{SN}^{c}	Run to z =
Romulus8	8	Bondi+AM	Dyn. Frict.	0.75	0.5
Romulus25	25	Bondi+AM	Dyn. Frict.	0.75	0
RomulusC	N/A	Bondi+AM	Dyn. Frict.	0.75	0
Advect	8	Bondi+AM	Advection	0.75	0.5
Bondi	8	Bondi	Dyn. Frict.	0.75	0.5
highSN	8	N/A	N/A	2.0	0.5

a Bondi+AM denotes the implementation described in this work

b 'Advection' denotes method utilized in Sijacki et al. (2007) and 'Dyn. Frict' is that from Tremmel et al. (2015)

c how much energy per SN is coupled to gas (in units of 10^{51}ergs) All the runs have identical particle mass, force resolution and numerical parameters.

5.1 Simulation Properties

5.1.1 *The* ChaNGa *N-Body+SPH Code*

The simulations are run using the new Tree + SPH code ChaNGa (Menon et al., 2015), which includes standard physics modules previously used in GASOLINE (Wadsley et al., 2004, 2008; Stinson et al., 2006; Shen et al., 2010) such as a cosmic UV background, star formation,'blastwave' SN feedback and low temperature metal cooling. The 'blastwave' implementation of SN feedback is a well tested approach that has been shown to reliably reproduce observable properties of galaxies, including cored dark matter profiles in dwarf galaxies (Governato et al., 2010). This is distinct from 'super bubbles' (Keller et al., 2014), a newer approach to SN feedback that will be implemented in future simulations.. The SPH implementation includes thermal diffusion (Shen et al., 2010) and eliminates artificial gas surface tension through the use of a geometric mean density in the SPH force expression (Ritchie & Thomas, 2001; Menon et al., 2015; Governato et al., 2015). This update accurately simulates shearing flows with Kelvin-Helmholtz instabilities. ChaNGa (Menon et al., 2015) is part of the AGORA (Kim et al., 2014) code comparison collaboration.

The main advantage with using ChaNGa is its ability to scale up to a large number of cores. Cosmological simulations such as Romulus include many particles and therefore requires the ability to run efficiently on thousands of cpus. However, the more cores a simulation uses, the more overhead exists, as each processor must communicate with all of the others to properly integrate the equations of motion of all the particles, all of which are experiencing both gravitational and hydrodynamical interactions. ChaNGa uses Charm++, which includes libraries specifically designed to allow efficient communication between processors. Combining this with a load balancer that is able to account for the clustered nature of these simulations due to the growth of structure through cosmic time, ChaNGa is able to efficiently scale to 100,000s of cpus (Menon et al., 2015). This allows large, high resolution simulations like the ones I run to finish in a more reasonable amount of time.

5.1.2 Cosmology and Resolution

All of the simulations I present are run assuming a ΛCDM cosmology following the most recent results from Planck ($\Omega_0 = 0.3086$, $\Lambda = 0.6914$, h= 0.67, $\sigma_8 = 0.77$; Planck Collaboration et al., 2016) and at the same resolution, with a spline force softening of 300 pc (Plummer equivalent force softening of 250 pc). Unlike many similar cosmological runs, the dark matter distribution is *oversampled*, such that we simulate 3.375 times more dark matter particles than gas particles, resulting in a dark matter particle mass of 3.39×10^5 $M_\odot$ and gas particle mass of 2.12×10^5 $M_\odot$. This is an important shift from the standard approach of simulating the same number of gas and dark matter particles, as it allows us to decrease numerical noise and allow for more accurate black hole dynamics (Tremmel et al., 2015). Our mass resolution is better than recent large volume simulations (Sijacki et al., 2015; Volonteri et al., 2016b) and our force resolution is comparable to the highest resolution runs of the EAGLES series (Schaye et al., 2015). Spline force softening converges to a Newtonian force at scales twice the gravitational softening, ϵ_g.

5.1.3 Sub-Grid Parameter Optimization

In ChaNGa, SF and SMBH physics are regulated through a series of sub-grid prescriptions that parameterize unresolved physics into several free parameters. In order to set these parameters to their optimal values we employ a quantitative optimization technique to map out the suitability of the parameter space and near-converge on the 'best' parameters. The idea of this approach is similar to that of Bower et al. (2010), but tailored specifically for more complicated simulations where only a few galaxies can be run with 10s of different parameter combinations. A summary of the procedure is the following (see Appendix A for a more detailed description):

1. We simulate a large number of sets of 4 'zoomed-in' galaxies (Governato et al., 2007, 2009) at the same resolution as Romulus, with halo masses ranging from $10^{10.5}$ to 10^{12} $M_\odot$, with dozens of different sub-grid parameter realizations.

2. We compare the properties of the resulting galaxies to local empirical scaling relations, grading each parameter set accordingly based on the logarithmic distance of each galaxy from the relation.The score of each parameter realization is then the sum of the distance (in log space) of each halo from each empirical relation.

3. The procedure is repeated, each time sampling in more detail around the best graded models until a best set of parameters is converged upon. The Kriging algorithm (see Appendix A) is used to efficiently explore parameter space and determine convergence.

A first set of simulations was run with only SF physics and with higher weight placed on reproducing the observed properties of lower mass galaxies, where the effect of SMBH physics should be less important. The parameters searched were the local SF efficiency, the density threshold for SF, and the fraction of SN energy coupled to the surrounding gas (see §4). Once the best SF parameters were identified (with the SN efficiency being the most important overall), a second set of galaxies was run including SMBHs physics, leaving the SF parameters unchanged but varying 1) the SMBH accretion and 2) energy coupling efficiencies (see §5.3). For results from the SF parameter search, we point the reader to Appendix A and Anderson et al. (2017).

The z=0 relations used to grade the galaxy sets were: 1) The stellar mass - halo mass relation, 2) The HI gas fraction as a function of stellar mass[1], 3) The galaxy specific angular momentum vs stellar mass, and 4) The SMBH mass vs stellar mass (SMBHs only). The first two scaling relations (Moster et al., 2013; Cannon et al., 2011; Haynes et al., 2011) allow us to respectively constrain the SF efficiency over the whole Hubble time, and the low redshift gas depletion time (i.e the recent SF rates). Our simulations follow the HI abundance of gas so M_{HI} is derived explicitly from the total gas content of each halo. The relationship between stellar mass, angular momentum, and morphology (Obreschkow & Glazebrook, 2014) is a useful proxy of galaxy sizes as well as the removal of low angular momentum gas through

[1]ALFALFA data from private correspondence with Jessica Rosenberg.

feedback processes. The M_{BH}-$M_{\star}$ relation (Schramm & Silverman, 2013) is a final test specific for SMBH physics. These four scaling relations control several fundamental aspects of galaxy formation connected to the regulation of SF, angular momentum evolution, and the growth of SMBHs. Taken together they provide useful, low-z constraints to our model without *unconsciously* biasing our effort to reproduce one specific scaling relation. For the sake of simplicity and to avoid biasing the analysis, we use just the raw logarithmic distance from each relation to determine the plausibility of each parameter set, implementing no weighting between different relations. However, we do exclude the dwarf galaxy from the morphological and SMBH relations, as explained in Appendix A.

When applied to setting three star formation parameters, the technique was able to converge with little user input after 27 realizations (a total of 80 simulations; see Appendix A). For two SMBH parameters, we were able to find a suitable parameter set after 12 realizations (a total of 48 simulations; see §5.5).

This 'zoomed-in' approach to parameter optimization allows us to efficiently explore the parameter space without having to simulate as many parameter realizations as would be required for a standard random-walk Markov-chain. It presents several advantages over shutting off or including individual physics modules (Genel et al., 2014) or to running a small cosmological volume multiple times (Schaye et al., 2015, 2010), the main issue being that running large simulations, particularly those at high resolution, is computationally expensive and will result in only a very limited parameter space exploration. Using this approach, the non linear effect of changing more than one parameter at a time can now be followed and the search for best parameters can cover the mass range of the final, large scale simulation (which tend to have more massive halos than small test volumes). Finally the set of zoomed-in runs provides a useful post main run framework to understand significant deviations from observed properties of galaxies or SMBHs should they emerge from the production runs.

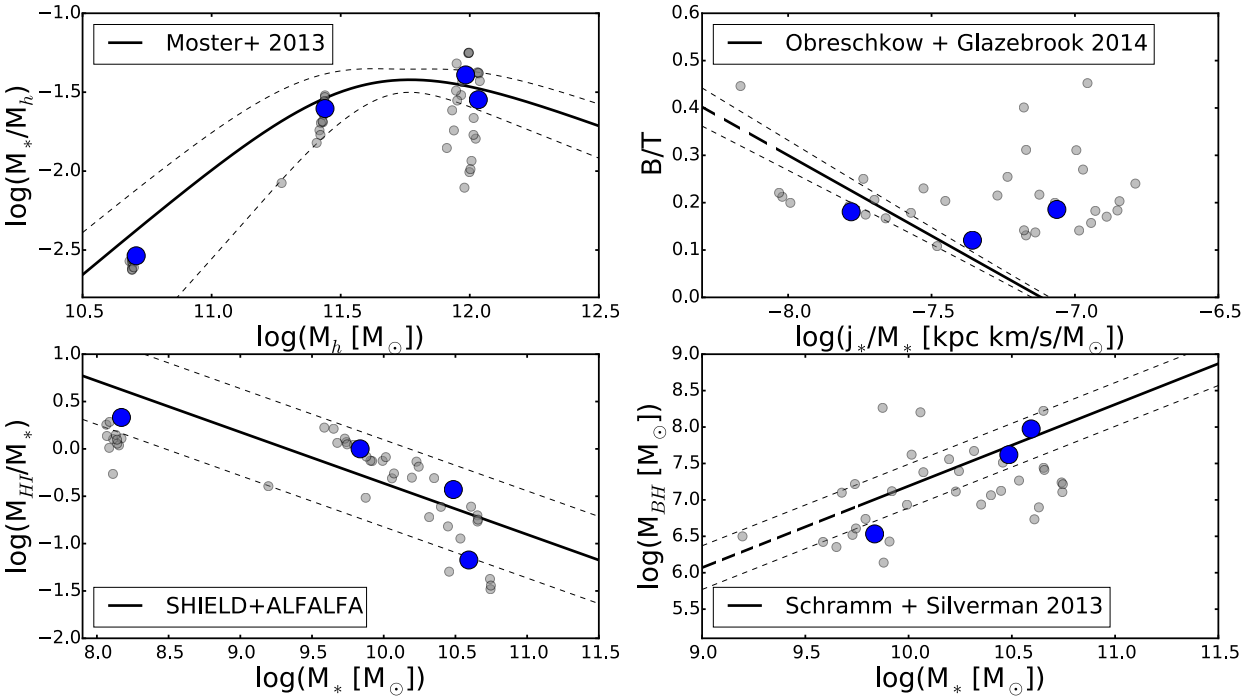

Figure 5.1: SMBH Parameter Optimization. Results from the search for optimal free parameters related to SMBH accretion and feedback. 12 realizations of accretion boost factor (β) and feedback efficiency (ϵ_f) for SMBHs were run, each with four zoomed in runs of galaxies. All of the models are shown in light grey points and the best fitting model (the one that best matches overall to the four relations shown) is in blue. Each model is compared to different empirical relations governing star formation efficiency (upper left, Moster et al., 2013), angular momentum (upper right, Obreschkow & Glazebrook, 2014), HI content (lower left, derived from SHIELD and ALFALFA data, see Cannon et al., 2011; Haynes et al., 2011) and black hole growth (lower left, Schramm & Silverman, 2013). The thin dashed lines represent $1-\sigma$ errors. The thick dashed lines represent where each relation has been extrapolated beyond observations. The blue points have the parameters, $\beta = 2, \epsilon_f = 0.02$, which are what we implement in the Romulus models as well as the other simulations listed in Table 1. Note that for the angular momentum and SMBH mass tests, the dwarf galaxy was excluded. The former is due to the fact that angular momentum decomposition is difficult for a galaxy of this size. The latter is because observed SMBH masses are uncertain for dwarf galaxies and in our simulations, including in these parameter search runs, not every dwarf galaxy forms a SMBH. Figure from Tremmel et al. (2017), ©RAS. Reproduced with permission.

5.1.4 Star Formation Physics

As in our standard implementation (Stinson et al., 2006) for runs at this resolution, star formation (SF) is regulated by:

1. the normalization of the SF efficiency, $c_\star$, used to calculate the probability of creating a star particle from gas with dynamical time t_{dyn} and characteristic star formation time, Δt, assumed to be 10^6 yr

$$p = \frac{m_{gas}}{m_{star}}(1 - e^{-c_\star \Delta t / t_{dyn}}), \tag{5.1}$$

2. The fraction of SNe energy that is coupled to the ISM

3. the minimum density ($n_\star$) and maximum temperature ($T_\star$) thresholds beyond which cold gas is allowed to form stars.

The final values adopted for these three sub-grid parameters are:

- SF efficiency $c_\star = 0.15$
- Gas temperature threshold, $T_\star = 10^4$ K
- Gas density threshold, $n_\star = 0.2$ m_p/cc)
- SNe energy coupling efficiency, ϵ_{SN}, of 75%

SN feedback adopts the 'blastwave' implementation (Stinson et al., 2006). Gas cooling is regulated by metal abundance as in Guedes et al. (2011) and SPH hydrodynamics and thermal and metal diffusion are described in Shen et al. (2010) and Governato et al. (2015). Our simulations do not include H_2 cooling as their resolution is not sufficient to model individual star forming regions. We use a Kroupa IMF (Kroupa, 2001), with the associated metal yields.

It is important to note that without SMBH feedback, parameters that work the best for dwarf galaxies based on our grading criteria (see §3) are different from those that work best for higher mass galaxies. The parameters used here represent those that grade the highest when dwarf galaxy results are more heavily weighted. The idea is to start with a SF model that performs very well at low masses and allow SMBH physics to create better results for high mass galaxies.

5.1.5 SMBH Physics

The sub-grid model for SMBHs used in my simulations is described in detail in chapters 2, 3, and 4. SMBHs are formed in the fastest growing, highest density regions in the early Universe (Chapter 3). They grow via a modified Bondi-Hoyle accretion algorithm that accounts for both the limited resolution of the simulation as well as the local kinematics of the gas (Chapter 4). SMBHs are not tethered to the centers of galaxies. Rather, SMBHs can become perturbed away from halo center or be accreted by other galaxies and then sink (or not) back to the center due to dynamical friction (Chapter 2).

SMBHs are allowed to merge based on the same criteria as Bellovary et al. (2011). Once SMBHs become closer than two softening lengths in relative distance, they merge if they have low enough relative velocities such that they would be considered gravitationally bound to one another, i.e. $\frac{1}{2}\Delta\mathbf{v} < \Delta\mathbf{a}\cdot\Delta\mathbf{r}$, where $\Delta\mathbf{v}$, $\Delta\mathbf{a}$, and $\Delta\mathbf{r}$ are the relative velocity, acceleration, and distance vectors between two SMBH particles. In reality, this is should be considered the time at which two SMBHs form a bound binary system. However, for the practical purpose within the simulation and analysis, the SMBHs are considered a single object. In terms of observations, such close binaries are challenging to observe and would often be considered a single object as well. In Chapter 6 we will examine in detail the formation of these SMBH binaries and how the timescale for format depends on the morphology and masses of the merging galaxy pairs.

5.1.6 Halo and Galaxy Extraction

For all simulations referred to in this work, we use the Amiga Halo Finder (Knollmann & Knebe, 2009) to extract individual halos. We calculate galaxy properties based on all of the particles within a given halo. However, for a better 'apples-to-apples' comparison with observational results, we utilize the corrections from Munshi et al. (2013) to account for the mass of stars missed in observations and the baryonic effects on halo mass not accounted for in dark matter only (DMO) simulations. These corrections have been calibrated for halos with virial mass $10^8 - 10^{12}$M$_\odot$ and are shown to be roughly constant across this range. Specifically, M$_{\star,obs}$ = 0.6 M$_{\star,sim}$ and M$_{vir,sim}$ =0.8 M$_{vir,\mathrm{DMO}}$. We apply these corrections to halos with M$_{vir}$ as large as 10^{13}M$_\odot$. In these halos, such corrections are particularly necessary, as $\sim$40% of stars exist far from halo center, either in an extended stellar halo or in satellite galaxies, and would not be included in observational estimates for stellar mass.

5.2 First Results from ROMULUS25*: The Build-up of Stars and Black Holes*

In this section we present initial results from our flagship ROMULUS25 uniform volume simulation, run to $z = 0$. It should be noted that such a small volume will miss some of the effects of large-scale structure and will not include the population of satellite galaxies in large halos. We see this effect most strongly in regards to downsizing of both star formation and SMBH accretion (see below). In future work, we will include the cluster simulations in our analysis as well. Within the scope of this paper, we find the ROMULUS25 simulation to be sufficient as a proof of concept that our method produces realistic galaxies and SMBHs at $z = 0$.

Figure 5.2 shows the stellar mass halo mass (SMHM) relationship in ROMULUS25 at z = 0 after removing all satellite galaxies from the sample. Our results are consistent with results from Moster et al. (2013), which our model has been calibrated to reproduce, as well as Kravtsov et al. (2014) for halos spanning more than three decades in mass. It should be noted that while these results are in part due to our parameter calibration, the results for

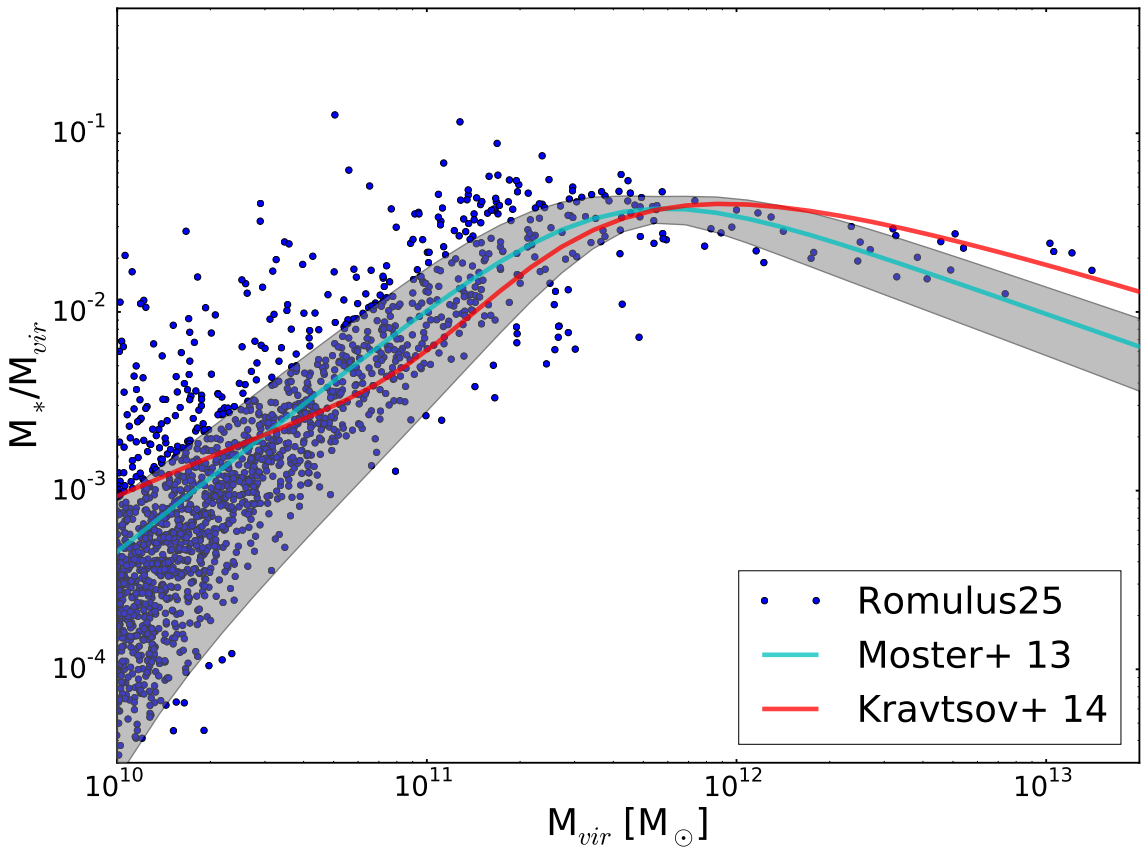

Figure 5.2: Stellar Mass Halo Mass (SMHM) Relation. Data from Romulus25 at z = 0.25 is shown in blue, plotted against two abundance matching relations from Moster et al. (2013) and Kravtsov et al. (2014). Any halo at least partially within the virial radius of a larger halo is not counted in this analysis in order to exclude satellites and interacting systems. The grey region shows the error in the Moster et al. (2013) relation, calculated from the errors reported for the best fit parameters. The stellar and virial masses for each halo are corrected to make them more directly comparable to observations following Munshi et al. (2013) (see §2.3). Our results match well with those from abundance matching. Of particular interest are the high mass galaxies ($M_{vir} > 10^{12} M_\odot$), which indicate that SMBH feedback is correctly regulating their growth. Figure from Tremmel et al. (2017), © RAS. Reproduced with permission.

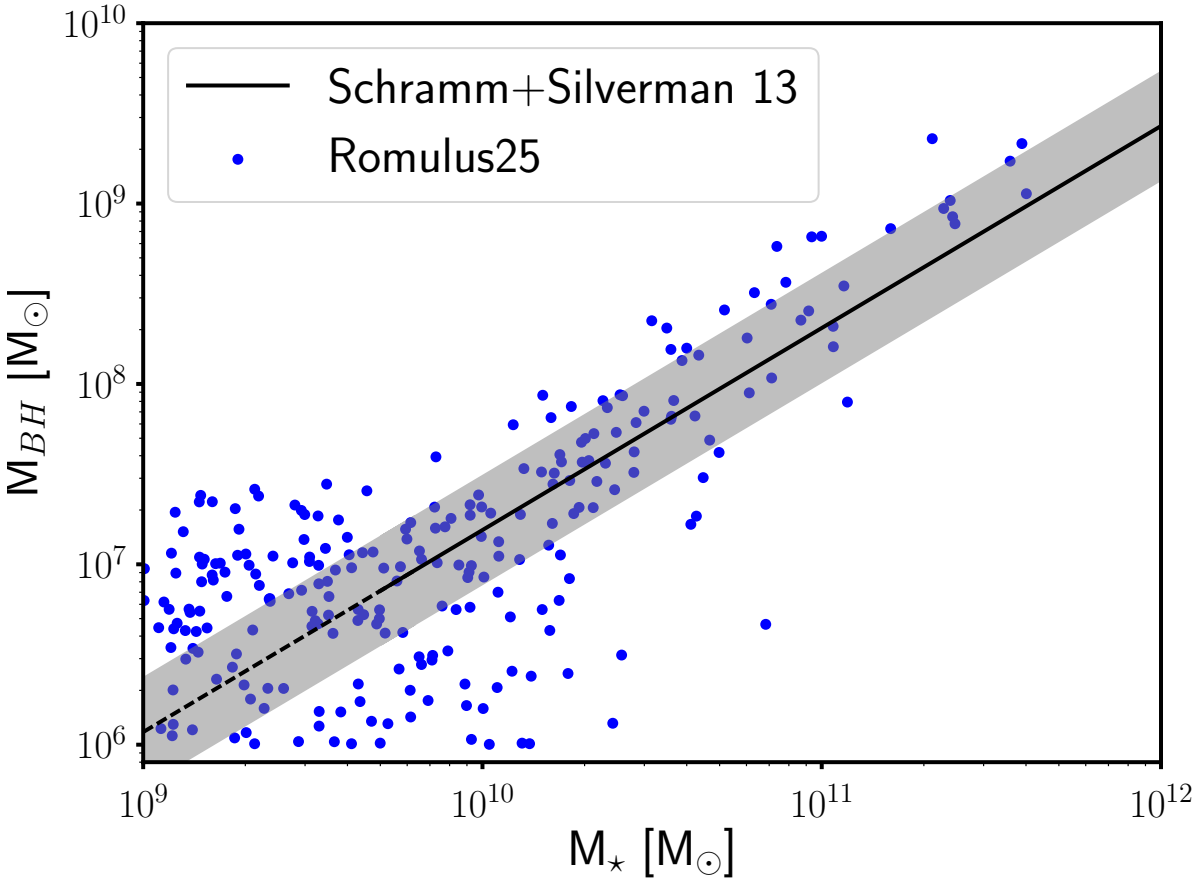

Figure 5.3: The SMBH Mass Stellar Mass Relation. Each point plots the mass of the largest black hole in each galaxy against each galaxy's stellar mass, corrected by a factor of 0.6 from the total stellar mass in each halo (see §2.3). Also shown is the empirical relation from Schramm & Silverman (2013), where the grey region represents the $1-\sigma$ scatter and the dashed part of the line is where the relation has been extrapolated past observations. The overall match to the data is good, particularly at higher masses. High mass galaxies tend to exhibit less scatter and lie near the relation, though slightly biased toward higher mass SMBHs. Less massive systems show a broader scatter in black hole mass. The relation from Schramm & Silverman (2013) was derived from higher mass galaxies and there is evidence that smaller, star forming galaxies lie on different relations (Reines & Volonteri, 2015; Savorgnan et al., 2016). Figure from Tremmel et al. (2017), ©RAS. Reproduced with permission.

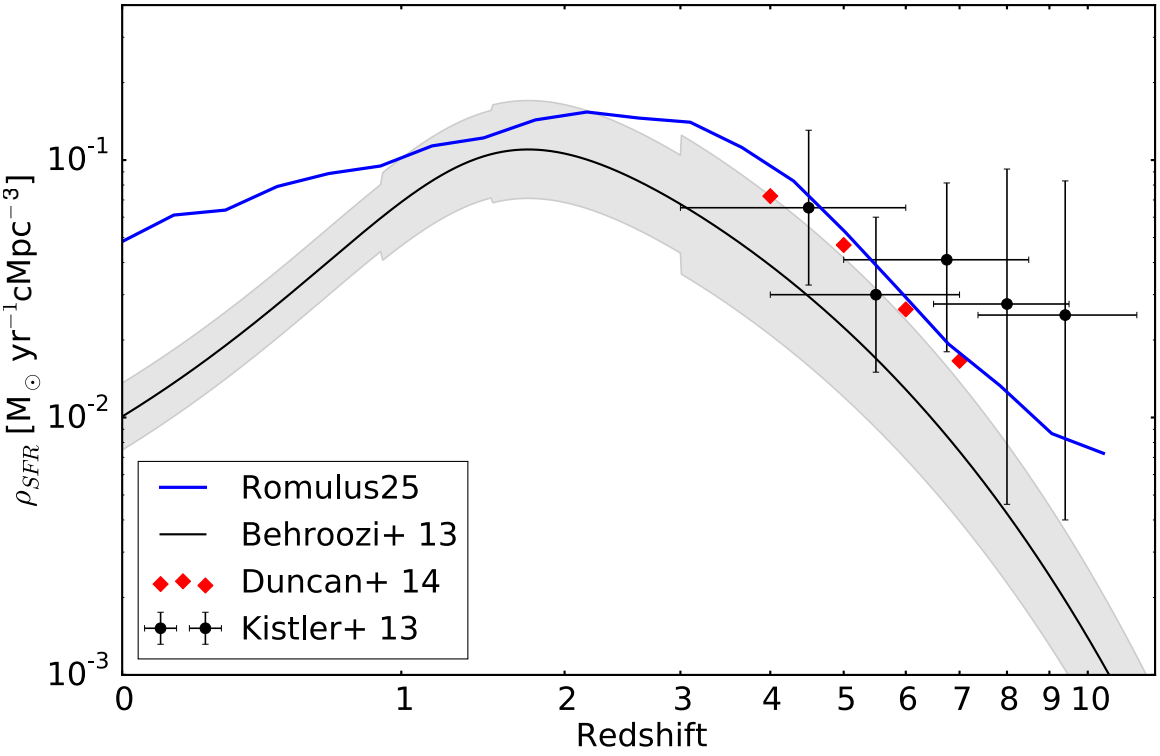

Figure 5.4: Cosmic Star Formation History. The solid blue line shows the total cosmic star formation history in Romulus25 plotted against a fit to observation data from (Behroozi et al., 2013a) as well as recent high redshift observations (Kistler et al., 2013; Duncan et al., 2014). The grey region represents the spread in observational data for different redshift bins, as reported by Behroozi et al. (2013a). Romulus25 accurately reproduces the evolution of the cosmic star formation rate density at high redshift, reaching a maximum at z = 2 and declining toward lower redshift. The overproduction of stars at low redshift, which is in stark contrast with observations, is due to only a handful of high SFR systems, a result of our relatively small volume. A 25 Mpc volume lacks larger systems that would better sample the effect of cosmic downsizing at late times. At $z > 5$ a significant portion (50%-90%) of star formation in Romulus25 occurs galaxies with stellar masses less than 10^8 M$_\odot$, a regime where the observed luminosity function is not well constrained (Anderson et al., 2017). Figure from Tremmel et al. (2017), ©RAS. Reproduced with permission.

high mass halos ($M_{vir} > 10^{12}$ $M_{\odot}$) have not been calibrated and can be considered predictions of our model. At $M_{vir} > 10^{12.5}$, the ROMULUS25 halos match better to the Kravtsov et al. (2014) results. As discussed in §2.3, we utilize the corrections from Munshi et al. (2013) for the stellar and virial masses to attain a more 'apples-to-apples' comparison. The correction, particularly when applied to larger group-size halos, accounts for the mass that exists in extended stellar halos and satellites.

Figure 5.3 plots the mass of SMBHs in ROMULUS25 against the stellar masses of their host galaxies, again applying the correction from Munshi et al. (2013). Satellite galaxies have also been removed from this sample. This is another empirical relation that we had used to constrain our sub-grid model, so the fact that the simulation data matches the relation from Schramm & Silverman (2013) is a success of our parameter search technique. High mass galaxies show less scatter than low mass galaxies, but are slightly biased to higher SMBH mass compared to the empirical relation. At low mass, we see a lot of scatter, both above and below the relation. While it is beyond the scope of this paper to examine in detail the nature of this scatter, it follows from recent observations that low mass, star forming galaxies have significantly more scatter in SMBH mass than higher mass galaxies, indicative that not all galaxies should lie on the same relation (Reines & Volonteri, 2015; Savorgnan et al., 2016). The significant scatter above the relation could be explained by tidal stripping (Volonteri et al., 2008a, 2016b; Barber et al., 2016), but we have removed satellite galaxies, making this connection less obvious. Likely it is due to stochastic SMBH growth in smaller galaxies. We will explore this further in future work.

The parameter search was meant to ensure that stars and SMBHs form and grow in the correct places. This is achieved in ROMULUS out to mass scales beyond those that the parameter search probed. Of particular interest are the high mass halos ($M_{vir} > 10^{12}$ $M_{\odot}$) that were not explicitly constrained with our parameter search and represent the regime in which feedback from SMBHs dominates stellar feedback in regulating star formation (Croton et al., 2006; Keller et al., 2016). The fact that these halos produce galaxies with stellar masses very similar to abundance matching results as well as SMBH masses that are consistent with

empirical scaling relations is a very promising result. How and when the growth of stars and SMBHs occur in ROMULUS25 is also a testable prediction of the model.

Figure 5.4 shows the cosmic star formation history in ROMULUS25, which matches nicely with observations at high (z ¿ 2) redshift, reaching a maximum just before $z = 2$ and then dropping off accordingly toward $z = 0$. At high redshift (z ¿ 5), we find the bulk of star formation is occurring in small galaxies ($M_\star < 10^8$ $M_\odot$), likely missed by high redshift observations (Anderson et al., 2017). This explains why ROMULSU25 lies above the derived star formation history from Behroozi et al. (2013a) but is more similar to estimates using more recent data that are more sensitive to lower mass galaxies. At low redshift (z $<$ 2) ROMULUS25 lies far above the observed star formation rates. This overproduction of stars at low redshift is due to only a handful of high SFR systems, a result of our relatively small volume which does not properly sample the higher density environments needed to recover the behavior of cosmic downsizing at late times.

Figure 5.5 plots the cumulative mass density accumulated in luminous SMBH accretion events across time. We only include data from SMBHs with mass greater than 110% of their initial seed mass (see §5.1). We verify that excluding these systems does not substantially change our results. The cuts in luminosity are meant to not only show the contribution of different varieties of active SMBHs, but also ensure that we only sample the portion of the luminosity function that can be accurately constrained by observations. We verify that for each luminosity cut, the contribution from low Eddington ratio SMBHs, where accretion is thought to become radiatively inefficient ($\lambda_{fedd} < 0.01$) is negligible. At early times, the black hole population grows more rapidly, slowing as it gets to lower redshifts. At all times the overall growth is dominated ($\sim 50 - 80\%$) by the more luminous SMBHs ($L_{bol} > 10^{44}$ ergs/s). Below z = 1, a significant fraction of this growth is taking place in a small number (1-5) of very luminous SMBHs ($L_{bol} > 10^{45}$ ergs/s). This is similar to the effect we see with star formation, where our small volume is unable to appropriately sample AGN downsizing.

The overall growth of the black hole population in ROMULUS25 is consistent with observations. The grey region is from Lacy et al. (2015) and is obtained from integrating the

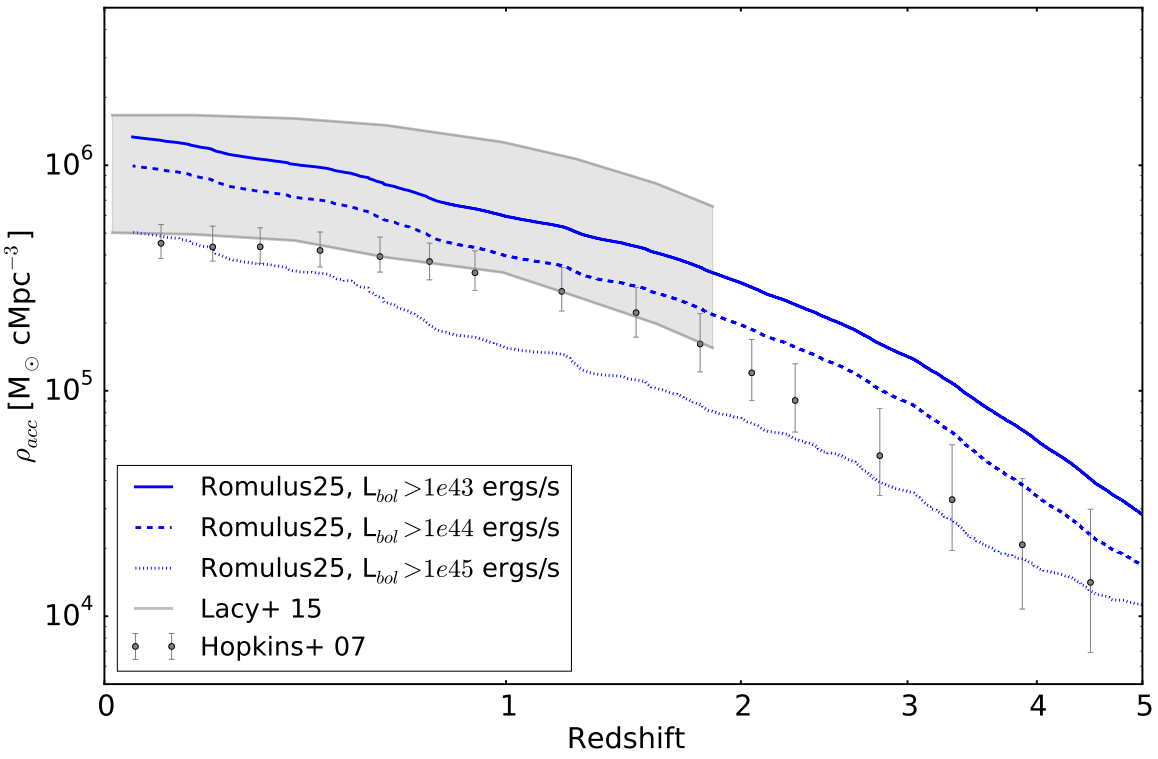

Figure 5.5: SMBH Accretion History. The cumulative mass density accumulated in luminous SMBH accretion events in Romulus25 across cosmic time. SMBH growth is faster at high redshift and slows down at later times. Higher luminosity systems ($L_{bol} > 10^{44}$ ergs/s) account for 50-80% of the accreted mass density at all times. The late time evolution at z ¡ 1 is driven by a small number ($\sim 1-5$) of systems with $L_{bol} > 10^{45}$ ergs/s. These results are consistent with the integration of AGN luminosity functions out to high redshift (Lacy et al., 2015, shown as the grey region for a range of different values of radiative efficiency). Also shown are the results from Hopkins et al. (2007), which are the result of different assumptions regarding absorption and bolometric corrections. Figure from Tremmel et al. (2017), ©RAS. Reproduced with permission.

observed AGN luminosity function between z = 0 and z = 5 assuming a radiative efficiency, ϵ_r between 0.06 (upper limit) and 0.18 (lower limit) and the data points with error bars are from Hopkins et al. (2007). The data from Lacy et al. (2015) were obtained from Spitzer observations in the mid-infrared. This makes them less sensitive to absorption, which can significantly impact optical and X-ray observations across all redshifts (Treister et al., 2010; Lansbury et al., 2015; Buchner et al., 2015; Lacy et al., 2015). However, the data from Lacy et al. (2015) are poorly constrained at redshifts higher than ~ 2, which is why we limit this region to $z < 2$. The higher luminosity data from ROMULUS25 ($L_{bol} > 10^{44}$ ergs/s) fits well with both observational data sets shown. The divergence away from the Hopkins et al. (2007) data at $z < 1$ is due to a small number of bright SMBHs, a consequence of our relatively small volume. Bolometric luminosities less than 10^{44} ergs/s represent a regime in which the observed luminosity functions are poorly constrained, particularly at high redshift, and sensitive to assumptions regarding the redshift and luminosity dependencies of absorption and bolometric correction (Merloni, 2016).

These initial results show that ROMULUS25 1) produces galaxies with stellar and black hole masses that are consistent with observations at low redshift (Figures 5.2 and 5.3) and 2) produces high redshift star formation and SMBH accretion histories that are consistent with observations, where differences arising at low redshift (z ¡ 2) are due to our small volume not being able to properly capture downsizing for high mass galaxies. These results show the strength of both our SMBH sub-grid model and our method for free parameter calibration. We leave the analysis of gas content and kinematics in ROMULUS for future work.

5.3 Black Hole Feedback Compared to Stellar Feedback

In this section, we wish to explore the differences in SMBH and supernovae (SN) feedback mechanisms. It is often possible to tune parameters in order to reproduce observations of galaxies of a certain mass. During our parameter search (see §3 and Appendix A) we found that the models for star formation and SN feedback without SMBHs that produced the most realistic galaxies in MW-mass halos did not work well in reproducing realistic smaller

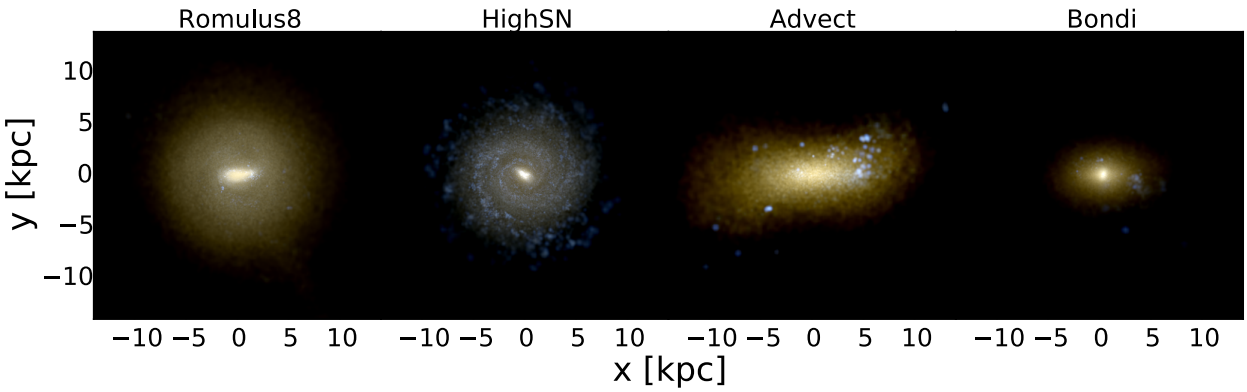

Figure 5.6: Mock Images of Stars in the largest galaxy from the Romulus8, HighSN, Bondi, and Advect simulations at z = 0.5. The virial mass of the host halo is $\sim 2 \times 10^{12}$ $M_{\odot}$. On average, galaxies of this size should be quenched by this time (Papovich et al., 2015). Colors are based on the contribution of different bands within each pixel using U (blue), V (green), J (red) assuming a Kroupa IMF, so young stars look blue and older stars look yellow. These images are indicative of the importance of physically motivated SMBH physics implementations on the evolution of large galaxies. It is clear that the inclusion of only SN feedback (HighSN) is not enough to quench the galaxy. SMBH feedback is able to quench in all cases, but the morphology and star formation history (see figure 5.8) are noticeably affected by the details of the implementation. Figure from Tremmel et al. (2017), ©RAS. Reproduced with permission.

galaxies. However, in this section we go beyond this to show that SMBH feedback is not only a crucial ingredient for reproducing scaling relations across all mass scales, it also has important consequences for reproducing the evolution of galaxies. In this case, we focus on MW-mass halos ($M_{vir} \sim 10^{12}$ $M_{\odot}$).

We compare two 8 Mpc uniform volume simulations, Romulus8 and HighSN (see Table 1), in order to gain insight into how the addition of extra feedback in the form of black holes compares to simply increasing the efficiency of SN feedback. The feedback efficiency in HighSN was chosen based off of the value we found to best reproduce scaling relations for galaxies in 10^{12} $M_{\odot}$ halos. The simulations are run to z = 0.5 to avoid some of the biases such a small volume will introduce into the evolution at later times.

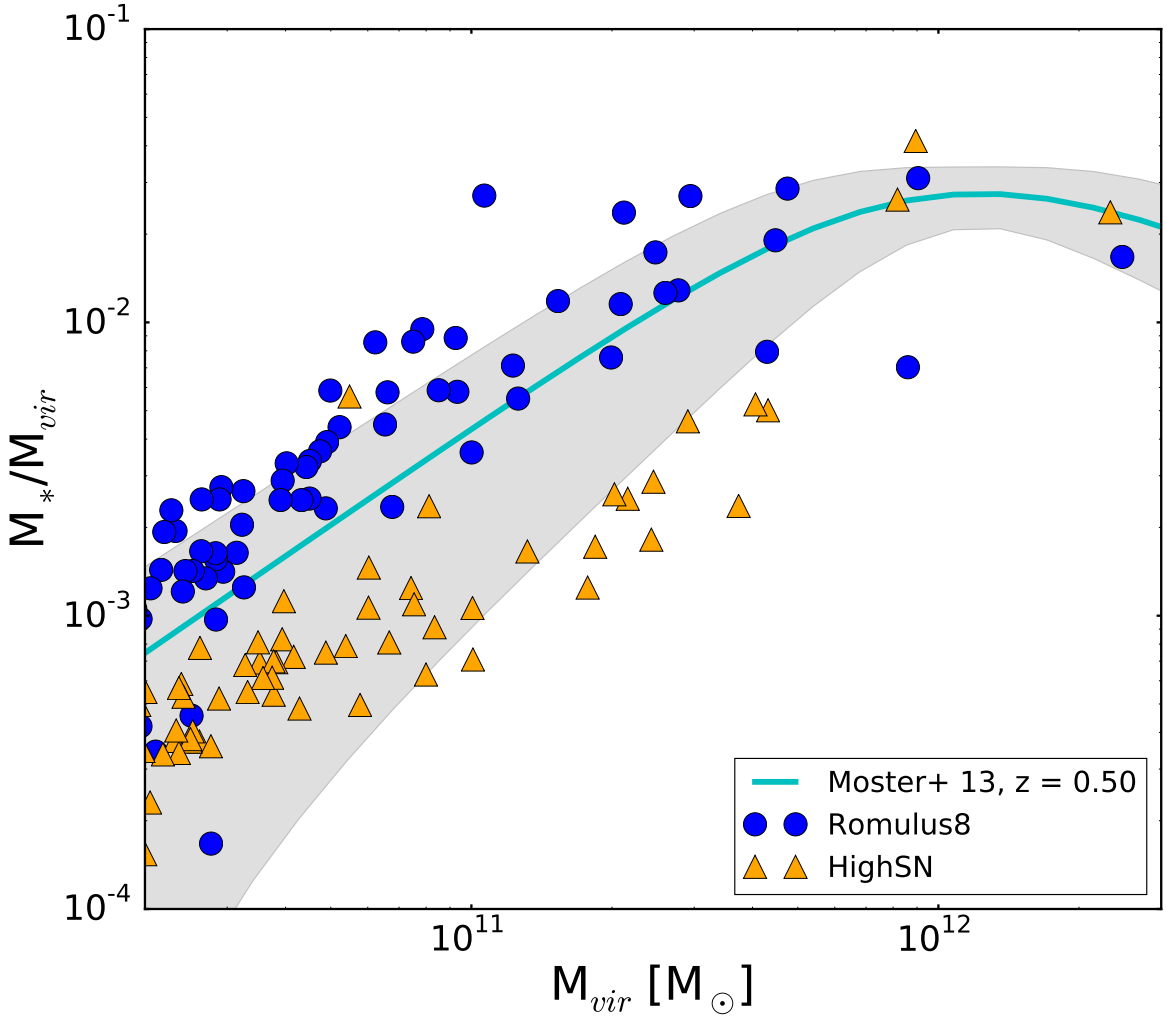

Figure 5.7: How Feedback from SMBHs and SN Affect SF Efficiency. The SMHM relation for the Romulus8 (blue) and HighSN (orange) simulations. Increasing the efficiency of stellar feedback to produce stellar masses that match observations for higher mass galaxies (HighSN) causes and underproduction of stars in low mass systems. The high mass galaxies match the observed relations well in the HighSN simulation, but this success is misleading, as the galaxies maintain significant star formation through the end of the simulation (see figures 5.6 and 5.8). The inclusion of black hole feedback combined with a lower stellar feedback efficiency (see table 1) produces realistic stellar masses in halos ranging from dwarfs to MW-mass. Figure from Tremmel et al. (2017), ©RAS. Reproduced with permission.

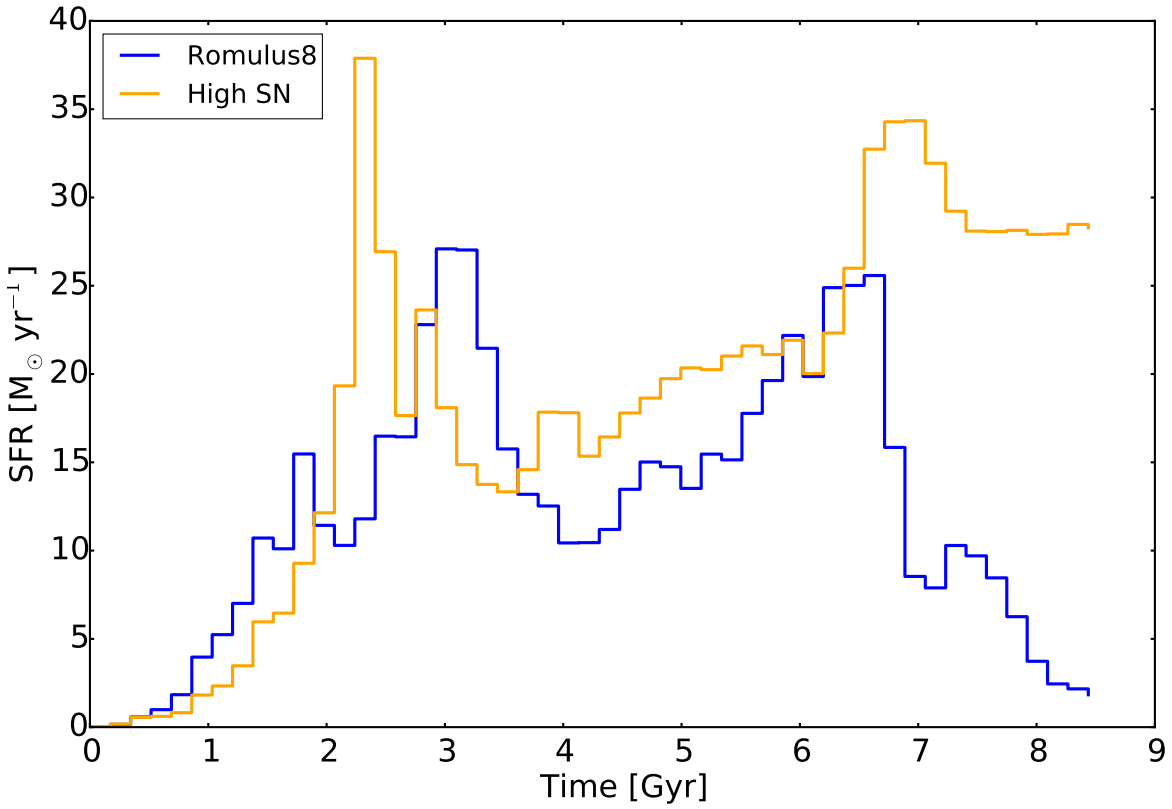

Figure 5.8: SMBHs and Galaxy Quenching. The star formation rate as a function of time for the most massive halo in the 8 Mpc volume, run with both the Romulus8 and HighSN models. The halo mass is consistent with being a Milky Way progenitor. The star formation histories are similar up until about 2 Gyr prior to the end of the simulation. While the enhanced SN feedback is able to make stellar masses consistent with observations (see Figure 5.7) the feedback from stars alone is unable to turn off star formation at late times, which is expected for systems of this mass (Papovich et al., 2015). With lower SN feedback but the inclusion of black hole accretion and feedback (Romulus8), the galaxy is able to attain both a realistic stellar mass and have star formation quench before z = 0.5. Figure from Tremmel et al. (2017), ©RAS. Reproduced with permission.

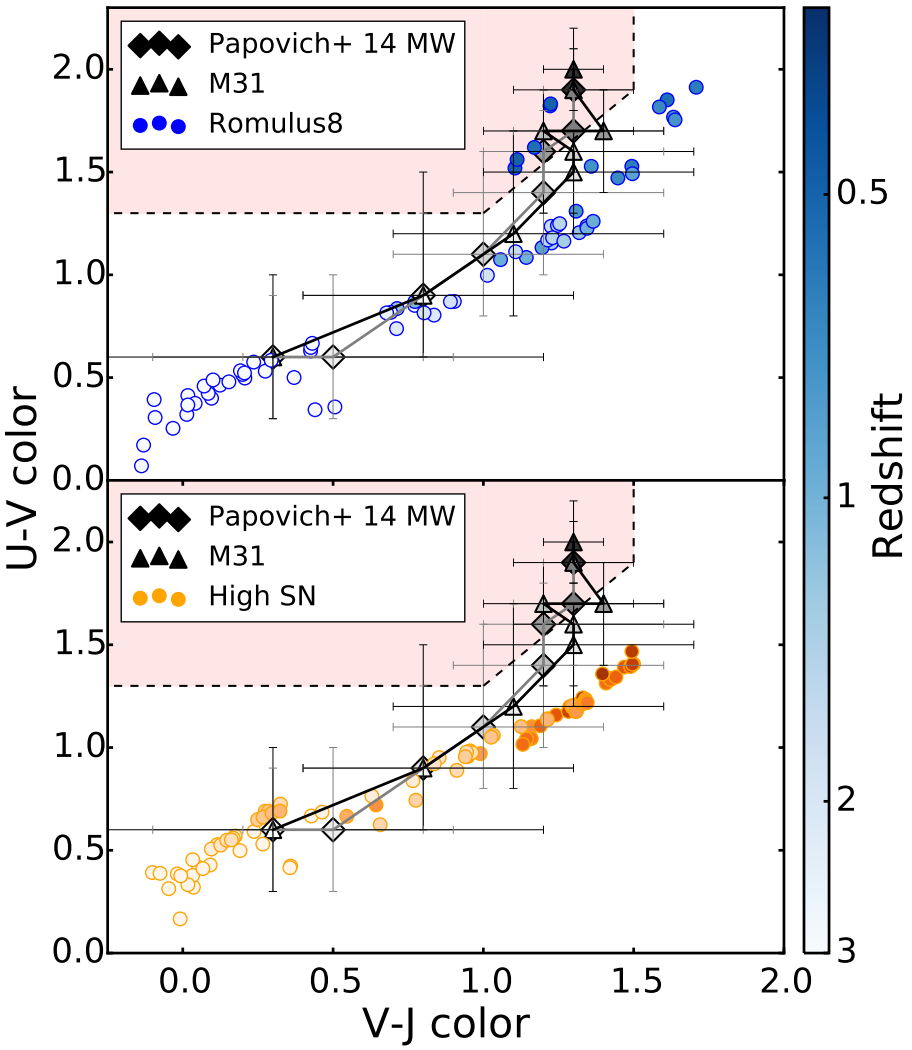

Figure 5.9: A Color-Color History of MW halos in the Romulus8 and HighSN simulations with a simple prescription for the average dust attenuation (see Appendix B). Darker points represent lower redshifts. The observed data points (black) are from CANDELS and ZFOURGE, using abundance matching techniques to define Milky Way and M31 progenitors across cosmic time (Papovich et al., 2015). In Romulus8 (blue), the two Milky Way progenitors follow closely the average observed evolution, becoming quenched by z = 0.5. In the HighSN simulation (orange), the galaxy remains in the realm where color is dominated by dust attenuation and ultimately fails to quench by z = 0.5. Without black hole feedback, Milky Way mass halos remain very gaseous and dusty, with star formation continuing at high levels. Figure from Tremmel et al. (2017), ©RAS. Reproduced with permission.

Figure 5.7 shows the stellar mass halo mass relationship for the two simulations, plotted against the $z = 0.5$ best fit relationship from Moster et al. (2013), applying the correction to stellar and halo masses from Munshi et al. (2013). The Romulus8 model fits the data well. The highSN model drastically under-produces stars in intermediate mass halos. This is, of course, due to the fact that SN feedback is much more efficient in lower mass halos that exhibit a shallower potential well (Governato et al., 2010; Brook et al., 2011). Such high efficiencies are necessary, however, to reproduce observed stellar masses in higher mass halos without SMBH feedback. Because SMBH growth naturally depends on the host galaxy mass, SMBH feedback is able to preferentially limit the growth of higher mass galaxies, while not quenching the star formation in low mass halos.

Figure 5.8 shows the star formation history of the most massive halo ($M_{vir}(z = 0) \sim 2 \times 10^{12} M_{\odot}$) in the volume for each simulation. While the final stellar masses are within realistic bounds in both simulations, the galaxy in Romulus8 has very low star formation by the end of the simulation while the same galaxy in highSN fails to quench. The majority of galaxies (70-80%) in this mass range should be quenched by $z = 0.5$ (Papovich et al., 2015).

Figure 5.9 shows the color evolution of the two most massive galaxies in the simulations run with SMBH physics (Romulus8) compared to that run only with enhanced SN feedback (HighSN). The galaxies show different color evolution, with Romulus8 following much more closely the results from the CANDELS and ZFOURGE data (Papovich et al., 2015). Colors from stellar emission are calculated using tables generated from population synthesis models using http://stev.oapd.inaf.it/cgi-bin/cmd (Marigo et al., 2008; Girardi et al., 2010). Dust is accounted for using a simple approach based on metallicity and cold gas content of a galaxy (see Appendix B). In the highSN simulation, the colors of the galaxies remain dominated by dust at late times, never falling into the 'quenched' regime. The color evolution also fails to follow the evolutionary path seen in the multi-epoch observations.

SMBH feedback, because it is more concentrated than SN feedback, is able to drive more powerful winds, which can disrupt inflowing material and lead to galaxy quenching (Volonteri et al., 2016c; Pontzen et al., 2017). Here we have shown that this effect is important for

reproducing the observed evolution of MW-mass progenitor galaxies. One of the failures of simulations without SMBH feedback is the inability to quench galaxies in MW-mass halos, something that our SMBH model is able to produce. Quenching galaxies in halos of $\sim 10^{12}$ $M_{\odot}$ has generally been challenging for modern cosmological simulations (e.g. Bluck et al., 2016).

5.4 Results from Different Black Hole Physics Implementations

In this section we compare our implementation for SMBH dynamics and accretion (model Romulus8) against more common implementations found in large cosmological simulations (models Bondi and Advect). It is instructive to note that our parameter optimization was done using our SMBH implementation. While it may be possible to find a combination of parameters that create galaxies that fall on various empirical relations using these other models, the point of this section is to explore the effects that the additional physics our implementation includes have on galaxy evolution.

We are again using a smaller 8 Mpc uniform volume realizations of our main simulation suite. Figure 5.10 shows the SMHM relationship of the three simulations. The high mass end of the relationship is the only part noticeably affected by the different models, indicating that a lack of SMBH growth in low mass galaxies is a natural consequence of the environment and not greatly affected by choice of sub-grid SMBH physics. Both aspects of our implementation (described in section 3) work to soften the effect of SMBHs on their host galaxy, as both Advect and Bondi have lower stellar masses at a given halo mass.

Synthetic images of the stars in the central galaxy of the most massive halo in the volume are shown in Figure 5.6, where a clear distinction between the three models can be seen. In Figure 5.11, we plot the star formation history of the most massive halo in the volume and the luminosity of the brightest black hole in that halo throughout time, averaged over 50 Myr intervals. While the star formation histories are quite different between models, the accretion history of black holes in the halo are not strikingly different and at later times the Romulus8 model is the most active of the three.

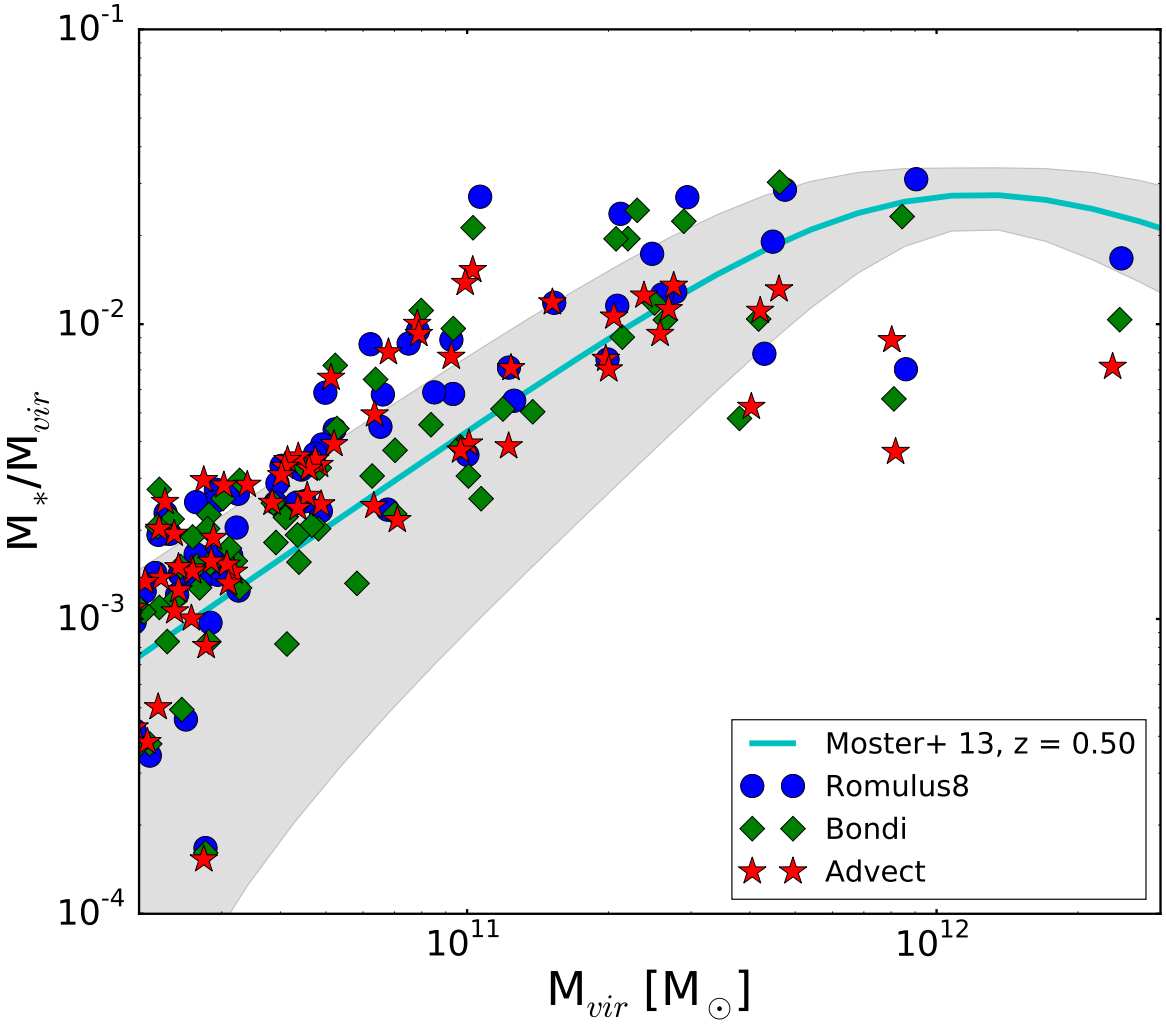

Figure 5.10: The Effect of SMBH Implementation on SF Efficiency. Same as Figure 5.7 but for the Romulus8, Advect, and Bondi simulations. The stellar mass halo mass relation changes little between the simulations for low mass halos, but noticeable differences can be seen for halos with virial masses above $\sim 2 \times 10^{11} M_\odot$. SMBHs do exist in smaller halos in this simulation (see section 3.1) but, regardless of the SMBH physics implemented, small galaxies will not experience much black hole growth or feedback. For higher mass galaxies, artificial advection and Bondi accretion not limited by gas dynamics work to increase the effect of SMBHs on star formation compared to our implementation utilized in the Romulus8 simulation. Figure from Tremmel et al. (2017), ©RAS. Reproduced with permission.

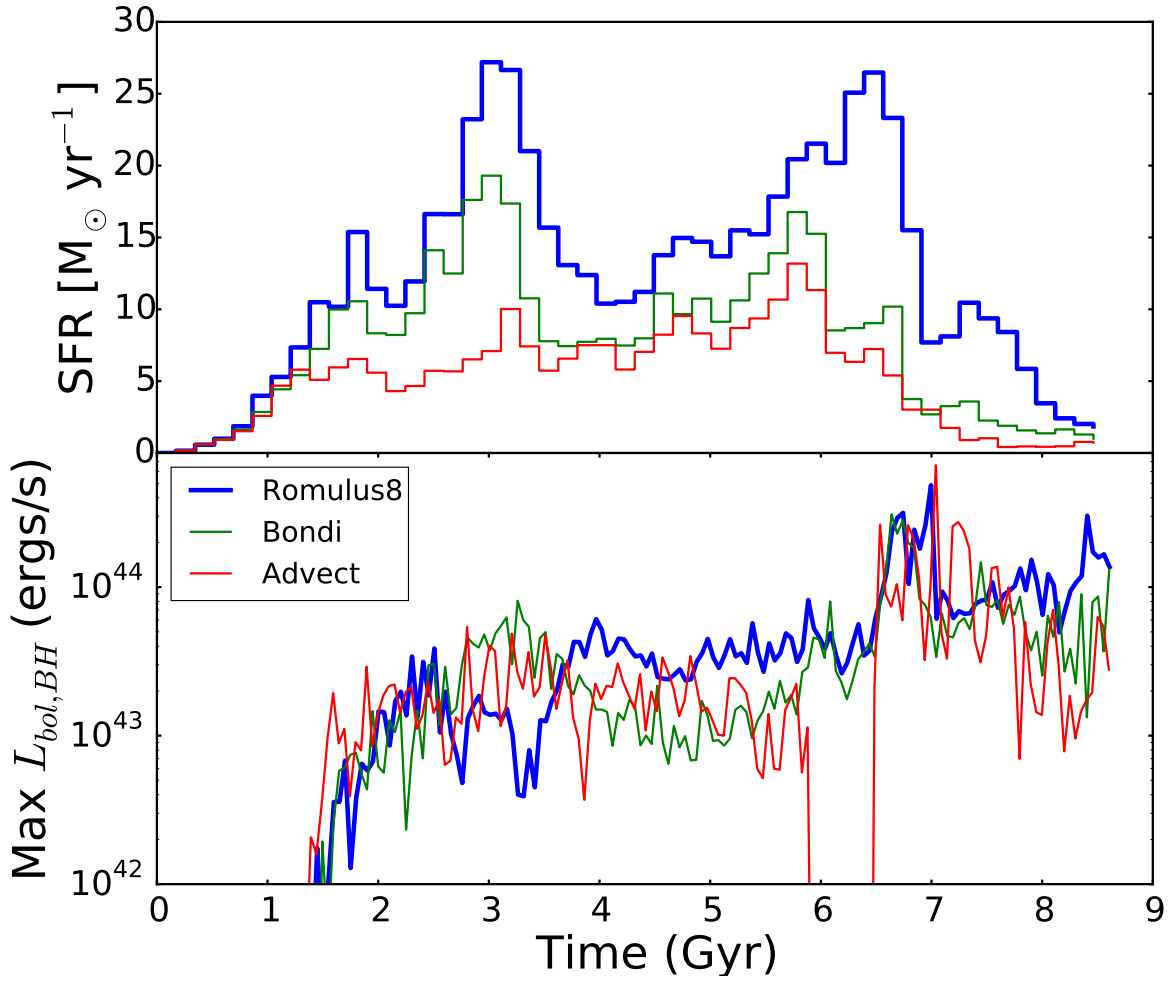

Figure 5.11: The Effect of SMBH Implementation on the SF History of Massive Galaxies (Top) The star formation history of the most massive halo in the 8 Mpc simulations, taken from the total stellar population of the galaxy at z = 0.5. A clear difference can be seen between Romulus8 (blue), Advect (red) and Bondi (green). (Bottom) For the same galaxy, the luminosity of the most luminous black hole across time within the galaxy's main progenitor branch. At later times Romulus8 has more active black holes. The values of luminosity are averaged over 50 Myr intervals. The strong dip in the red curve is due to the active black hole instantaneously transferring between two halos during a major merger. Figure from Tremmel et al. (2017), ©RAS. Reproduced with permission.

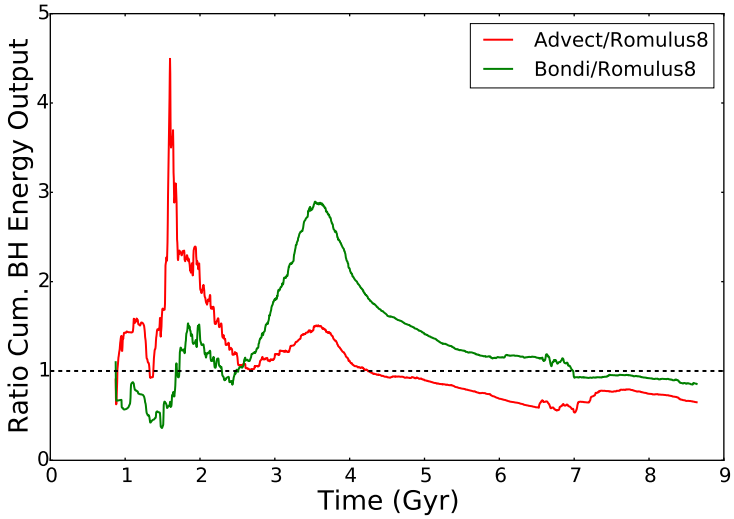

Figure 5.12: The Cumulative Energy Output from SMBHs within the most massive halo in the 8 Mpc simulations. The Advect (red) and Bondi (green) models compared with Romulus8 across cosmic time. During the first 4 Gyr of the simulation, the Romulus8 halo experiences less feedback from SMBHs. Figure from Tremmel et al. (2017), ©RAS. Reproduced with permission.

The important difference in how black holes regulate the star formation of their host galaxies occurs at high redshift. Figure 5.12 plots the cumulative energy output of black holes within the central galaxy, tracking the halo backward in time along its main progenitor branch. The energies are reported relative to that in the Romulus8 model. We find that both Bondi and Advect experience more activity during the first several billion years of the simulation. The implications from this are 1) early black hole activity can have important consequences for later galaxy evolution and 2) black hole dynamics and angular momentum limited accretion play an important role in determining accretion in the early Universe. It makes sense that the former is true, as the environment in which the black holes are active is different, namely the host halo is smaller, which would allow feedback from black holes to play a more drastic role in shaping the host galaxy. At early times, the black holes will exist in smaller galaxies that are undergoing more interactions, thus the black holes are more likely to become perturbed away from the galaxy center if they are allowed. In addition, at

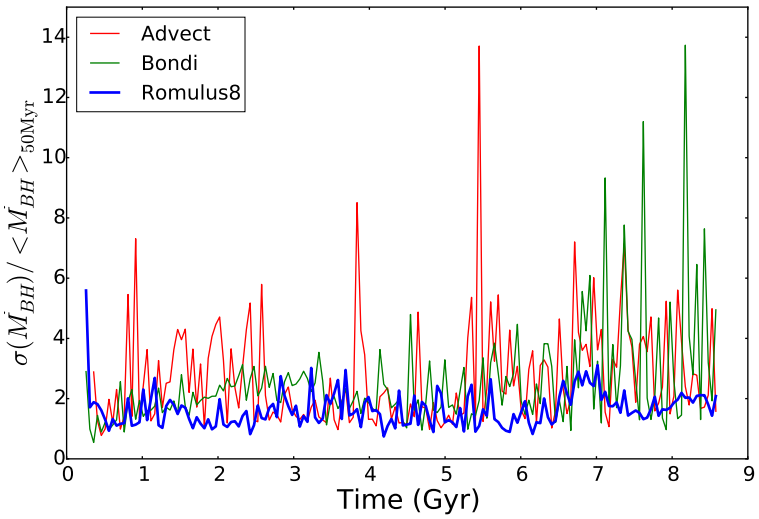

Figure 5.13: The 'Burstiness' of SMBH Accretion for the most massive black hole in the most massive halo in the three 8 Mpc simulations: Romulus8 (blue), Advect(red), and Bondi (green), defined to be the ratio of the standard deviation to the mean accretion rate over 50 Myr timescales. In both Advect and Bondi we see that the black hole experiences a much more bursty accretion history. Figure from Tremmel et al. (2017), ©RAS. Reproduced with permission.

earlier times, when star formation is climbing toward its peak, one would expect to see more cold, disk dominated galaxies.

The black hole model not only affects where and when accretion takes place, but also how the accretion rate varies on smaller timescales. Figure 5.13 plots the standard deviation of the accretion rate for the most massive black hole in the most massive halo of the simulation, taken over intervals of 50 Myr and normalized by the average accretion rate throughout that time. For the entire simulation, both Advect and Bondi experience a significantly more bursty accretion history. So, while the smoothed accretion rate may look relatively similar between the models (see figure 5.11) there is a more bursty process occurring on smaller timescales. For Advect, the cause is numerical, as repositioning each timestep can cause the black hole to feel numerical noise, as the location of the potential minimum fluctuates (Wurster & Thacker, 2013; Tremmel et al., 2015). In the Bondi simulation, the reason for such bursty accretion is that, without regulation, the accretion rate will rise quickly with gas density, which in turn will create a stronger feedback event that will drive gas back temporarily. The black hole then waits for the gas to relax again and the process continues. Including the gas dynamics in the accretion calculation softens this process because dense gas tends to also be in a disk, which will feel rotational support.

A future paper is planned to look in more detail of the relative effects of angular momentum limited accretion and stellar feedback on the evolution of Milky Way and sub-Milky-Way mass galaxies. Within the scope of this paper, the important result is that both black hole dynamics and angular momentum regulated accretion have an appreciable effect on galaxy evolution for galaxies in higher mass halos ($M_{vir} > 10^{11.5}$).

5.5 Application: Understanding Dual AGN in a Larger Context

Dual AGN, systems with multiple active black holes, are beginning to be observed in the local Universe (Comerford et al., 2011, 2013, 2015) and represent an important regime for studies of SMBH-galaxy co-evolution, as they are a transient state possibly connected to a recent or on-going galaxy merger. Being able to reproduce such systems in simulations is

necessary in order to gain a theoretical understanding of their place in the broader context of SMBH-galaxy co-evolution. Some important work has already been done to that end (Van Wassenhove et al., 2012; Hirschmann et al., 2014; Steinborn et al., 2016) and the methods presented in this paper represent the logical next step.

Our approach to black hole physics is particularly well suited for realistically modeling dual AGN because we are able to accurately follow the dynamics of black holes within their host galaxies as they get perturbed away from center or fall into a new host following a galaxy merger event. We are able to track the black hole orbits to an accuracy of the simulation's resolution limit (250 pc) and without making assumptions regarding the larger scale structure of the galaxy or halo in which the black hole resides. We are therefore not only able to create dual AGN down to a separation of < 1 kpc, we can follow the evolution of the system accurately throughout the parent system's evolution.

An example of dual AGN created using our approach, taken from the Romulus8 simulation during the last major merger of the most massive halo in the volume, is shown in Figure 5.14 (the same halo used for analysis in the previous two sections; see Figures 5.6, 5.8, and others in §7 and §8). We show 5 snapshots in time of a single galaxy merger that results in three instances of a dual AGN with separations of ~ 50 kpc, ~ 12 kpc, and ~ 1.5 kpc. These are progenitor events leading up to a black hole merger and the quenching of the host galaxy, which by the end of the simulation has halo and stellar masses similar to the Milky Way. By looking at each snapshot, we gain insight into how the simulation is evolving. The entire process takes less than 1.5 Gyr from the initial dual AGN event until black hole merger. Two of these dual AGN events (snapshots 2 and 3 on the plot) look analogous to systems found by Comerford et al. (2015). When searching for these events, we defined 'active' to mean a bolometric luminosity of more than 10^{43} ergs/s.

To give the events more context, we plot the black hole luminosity as a function of star formation rate for the merging galaxies in each snapshot (Figure 5.14). The smaller galaxy is in the process of being stripped by the larger galaxy. The original baryonic masses of the galaxies before the merger was $M_1/M_2 \sim 1.2$ and the ratio of black hole masses was

$M_{BH,1}/M_{BH,2} \sim 0.5$, where the less massive galaxy, denoted by 2, is the one that is being stripped and the one that hosts the more massive black hole.

The stripped galaxy is clearly in the process of being quenched by a combination of its environment and the active black hole within it. As the galaxies get closer, the black holes become more active. The star formation rate of the larger galaxy remains roughly constant while the stripped galaxy is further quenched. Throughout the interaction, the black hole activity and star formation rate of the more massive galaxy matches well with the relation derived from observations of z = 1-2 galaxies (Mullaney et al., 2012). The stripped galaxy always lies above the relation. After the two galaxies merge, the black hole originally in the stripped galaxy becomes even more active, with a luminosity much higher than expected given the star formation rate in its new host. After the black holes merge, the central black hole remains very active and the galaxy moves further to the left on the plot as it quenches. This merger event, over the course of $\sim$ 1.5 Gyr and resulting in different instances of dual AGN, is the progenitor to a newly quenched galaxy. The heightened black hole activity corresponds with the quick decay of the star formation rate over the next billion years.

In the example given here from the Romulus8 simulation, we show that the Dual AGN event is a direct result of a major merger taking place between the galaxies. The black hole in the smaller galaxy becomes active as its galaxy quenches, with activity increasing as it moves closer to the more massive galaxy. In this case, having multiple black holes was indicative of a future black hole merger and would result in the quenching of what originally was a gas rich, star forming galaxy.

This is only one example, but it shows the level of detail with which we can approach the problem of Dual AGN. It is also indicative that these systems are not necessarily very rare across cosmic time, as we were able to generate a relatively long lived event in a volume of only 578 Mpc^3. In a future paper we will search both the 25 Mpc volume (ROMULUS25) and the cluster (ROMULUSC) for Dual AGN events across cosmic time, giving us a much larger sample to look at and understand better the physical processes necessary to generate Dual AGN.

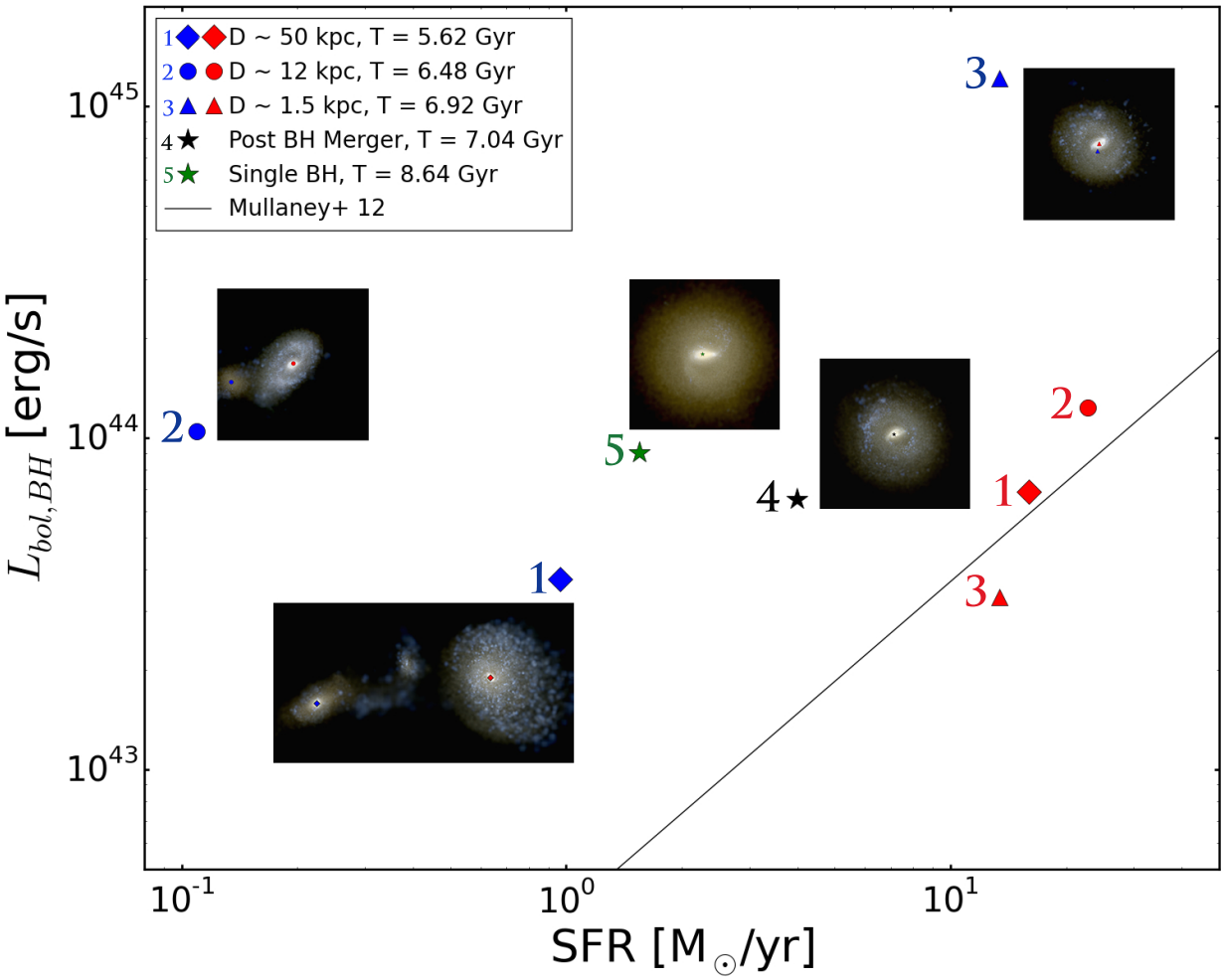

Figure 5.14: The Evolution of Dual AGN The evolution a merging galaxy pair and resulting remnant galaxy in terms of star formation rate and black hole luminosity. Thumbnails showing the stars of the galaxies are shown along with each data point set. The different colored points in each thumbnail represent the positions of the active black hole(s) at each time. The data points and thumbnails shown were chosen to encapsulate several important phases of evolution: 1) the beginning of the interaction, when the smaller galaxy has just entered the virial radius of the larger galaxy and is being stripped and environmentally quenched 2) the end of the galaxy merger phase, where there are two distinct galaxies, but the smaller one has been completely stripped. 3) the remnant resulting from the galaxy merger, still with two separate, bright black holes 4) just after the two black holes merge. 5) the merger remnant after it has been given time to relax, showing the galaxy quenching under the influence of a single, still very active black hole. Figure from Tremmel et al. (2017), ©RAS. Reproduced with permission.

5.6 Summary

We presented the initial results from our flagship simulation, ROMULUS25, showing that our model reproduces the observed SMHM and M_{BH}-$M_\star$ relations for z = 0 galaxies. We also show that both the star formation and SMBH accretion histories are consistent with observations at high redshift, though both suffer from our small volume's inability to capture cosmic downsizing. Using a set of smaller simulations, we also show how SMBH physics is a necessary component for quenching star formation in massive galaxies and reproducing the observed evolution of MW-mass galaxies. We also show that our implementation gives appreciably different results for galaxies in massive (10^{12} $M_\odot$) halos compared with more common approaches. This highlights not only the importance of including SMBH physics in cosmological simulations, but also that the details of the implementation are imprinted on the evolution of massive galaxies.

Finally, we present an illustrative example of how our implementation will result not only in realistic SMBH mergers, but also allow us to study the dual AGN that may often precede such events with unprecedented detail. This will be explored more thoroughly in future work, but represents an important proof of concept that our model will provide new data to put transient events such as dual AGN and SMBH mergers into a broader context.

The ROMULUS simulation suite, with resolution on par with the highest resolution cosmological simulations run to date, will provide a crucial dataset with which to study the evolution of galaxies with halo mass $10^9 - 10^{13}$ $M_\odot$. The inclusion of ROMULUSC will provide further insight into galaxy evolution in rarer, high density regions not sampled by ROMULUS25 alone. The high resolution of these simulations is necessary not only to study the structure of galaxies, but also to properly follow the dynamics of SMBHs (Tremmel et al., 2015). The SMBH implementation we presented in this Paper will allow SMBHs to form in the early Universe and exist in both large galaxies and dwarfs, while ensuring that they respond realistically to their changing environment. This is the first set of simulations of this size and resolution to simultaneously provide physically motivated sub-grid models

for SMBH formation (§5.1) and dynamics (§5.2 and Tremmel et al., 2015) while also accounting for resolution effects (Booth & Schaye, 2009) and dynamically supported gas (§5.3) when calculating SMBH accretion. ROMULUS represents a natural next step for cosmological simulations to provide more detailed insight into the evolving structure of galaxies, the co-evolution of galaxies and SMBHs, and transient events such as Dual AGN and SMBH mergers.

Chapter 6

SMBH BINARY FORMATION TIMESCALES IN ROMULUS

In this chapter, I present the first self-consistent prediction for the distribution of Supermassive Black Hole (SMBH) orbital decay timescales following galaxy mergers. Using ROMULUS25, the first cosmological simulation to explicitly track the orbital evolution of SMBHs within their host galaxies down to sub-kpc scales, I find that SMBHs pairs can spend several Gyrs within the same galaxy or merging pair of galaxies before forming a close pair ($D < 700$ pc), the precursor phase to a bound SMBH binary. How quickly close SMBH pairs form following a galaxy merger event depends strongly on the mass and morphology of the accreted satellite galaxy. Low stellar mass ratio mergers with galaxies that lack a dense stellar core are more likely to become tidally disrupted and deposit the SMBH at large radii without any stellar core to aid in their orbital decay. Conversely, SMBHs in galaxies that avoid disruption remain embedded within a stellar core and sink to the galactic center on significantly shorter timescales to form a close SMBH pair. This timescale is a crucial, though often ignored or very simplified, ingredient to models of SMBH mergers as well as those exploring the connection between SMBH and star formation activity.

6.1 Introduction

Future observations of gravitational waves emitted from binary and merging SMBHs via pulsar timing arrays (Sesana, 2013) and the planned LISA mission (Klein et al., 2016), combined with semi-analytic modeling, will provide unique constraints to the SMBH mass function across cosmic time as well as critical insight into their possible formation mechanisms (Volonteri et al., 2008b; Volonteri & Natarajan, 2009; Klein et al., 2016) and their growth and spin evolution (Barausse, 2012). Further, on-going observations of active SMBHs that

are offset from the center of their host galaxies, possibly in galaxies with multiple luminous SMBHs, can potentially help constrain the extent to which galaxy mergers drive SMBH growth (Comerford et al., 2015; Barrows et al., 2017).

The formation of a SMBH binary and subsequent merger of two SMBHs can be described in a number of stages. First, a dark matter halo accretes a satellite halo, which then sinks to the center via dynamical friction, its central galaxy merging with that of the main halo. Following the merger of two galaxies hosting SMBHs, dynamical friction acting on the SMBHs causes them to sink to galactic center and form a close pair with sub-kiloparsec (kpc) separation. The close pair, through dynamical interactions with gas and stars, then forms a bound SMBH binary ($D < 10$ pc), which then itself hardens to the point where gravitational wave emission causes rapid orbital decay and the two SMBHs merge ($D < 0.001$pc).

While the orbital evolution of close SMBH pairs and the bound binary systems that follow are extensively studied using numerical and analytic techniques (e.g. Armitage & Natarajan, 2002; Yu, 2002; Sesana & Khan, 2015), it is also critical to understand the evolution of SMBH pairs on larger scales, as these timescales can be quite long (e.g. Callegari et al., 2009, 2011) and present a critical bottleneck to SMBH binary formation. However, studies of SMBH orbital evolution prior to the formation of close pairs has so far been severely limited. Semi-analytic models account for this timescale using simple models for dynamical friction (e.g. Dvorkin & Barausse, 2017). Detailed simulations of isolated mergers have indicated that SMBH sinking timescales following major mergers depend on the central stellar density of both galaxies (Governato et al., 1994) and can be quite short (Mayer et al., 2007), while SMBH sinking timescales following minor mergers can be much longer and depend sensitively on the orientation of the merging galaxies (Callegari et al., 2009, 2011). However, these idealized simulations do not produce the realistic merger and gas accretion histories that real galaxies experience in a full cosmological context.

Cosmological simulations potentially provide a more self-consistent view of SMBH orbital decay timescales and are the logical next step from isolated galaxy merger simulations to better understand the timescales of close pair formation. With these simulations, the

effects of different morphology and merger dynamics are naturally accounted for without *a priori* assumptions, as each galaxy in the simulation has a cosmologically realistic accretion and merger history. However, past simulations generally had poor resolution, which required simplified assumptions such as 'advection', where SMBHs quickly sink into the deepest nearby potential well, resulting in unrealistic, nearly instantaneous SMBH orbital decay. This approximation contrasts with the above numerical results as it assumes that the orbital sinking timescale on kpc scales is effectively zero. In previous works we have shown that this technique often results in inaccurate SMBH dynamics within galaxies and a drastic underestimate of sinking timescales (Tremmel et al., 2015).

In this Paper, using the ROMULUS25 cosmological simulation (Tremmel et al., 2017) that includes an explicit description of SMBH dynamics down to sub-kpc scales (Tremmel et al., 2015), *we present the first robust estimate of SMBH sinking and subsequent close SMBH pair formation timescales over a range of cosmic epochs and galaxy properties.*

6.2 The ROMULUS *Simulations*

As described in Chapter 5, the ROMULUS simulations are a set of large-scale, high resolution cosmological simulations with emphasis on implementing a novel approach to SMBH formation, dynamics, and accretion. For this work, we focus on ROMULUS25, our flagship 25 Mpc per side volume simulation, as it provides a uniform sample of galaxies within a wide range of halo masses (3×10^9 to 2×10^{13} $M_\odot$). SMBH seeding occurs at early times as a prediction of the model, without *a priori* assumptions of halo occupation and allowing SMBHs to exist in small galaxies at all epochs. Accretion onto SMBHs accounts for the kinematics of the nearby gas, responding appropriately as those kinematics evolve, e.g. during and following galaxy merger events. Finally SMBH dynamical evolution is well resolved in the simulation down to sub-kpc scales due to the sub-grid dynamical friction model described in (Tremmel et al., 2015, see also Chapter 2).

6.3 SMBH Dynamics and the Formation of Close SMBH Pairs

Following the merger of two galaxies hosting SMBHs, the accreted SMBHs sink toward the center of the descendant galaxy through dynamical friction, the force exerted by the gravitational wake caused by a massive body moving through an extended medium (Chandrasekhar, 1943; Kazantzidis et al., 2005; Binney & Tremaine, 2008). However, the limited mass and gravitational force resolution of cosmological simulations leaves this process largely unresolved. The ROMULUS simulations include the sub-grid correction accounting for this unresolved dynamical friction described in Tremmel et al. (2015) and Chapter 2 that has been shown to produce realistically sinking SMBHs.

This is a critical improvement over standard approaches to correcting SMBH dynamics that involve repositioning or pushing SMBHs toward their local potential minima (e.g. Di Matteo et al., 2005, 2008; Genel et al., 2014; Schaye et al., 2015). Such methods force an un-physically fast sinking timescale for accreted SMBHs, leading to a nearly immediate formation of a SMBH binary that does not sample the properties or kinematics of the merging galaxies (Tremmel et al., 2015). With this technique, the dynamics and morphology of the merging galaxies are self-consistently accounted for in the SMBH sinking timescales and the subsequent formation (or not) of a close SMBH pair.

SMBHs are assumed to form a close pair when they become closer than two softening lengths (≈ 700 pc in our simulations) with relative velocities small enough such that they can be considered bound, i.e. $\frac{1}{2}\Delta\mathbf{v} < \Delta\mathbf{a} \cdot \Delta\mathbf{r}$, where $\Delta\mathbf{v}$, $\Delta\mathbf{a}$, and $\Delta\mathbf{r}$ are the relative velocity, acceleration, and distance vectors between two SMBH particles. Below this distance limit, the simulation fails to resolve the relevant stellar and gas dynamical processes involved in SMBH pair evolution and such calculations are not attempted.

In the simulation, once two SMBHs form a close pair, they are taken to act as a single SMBH with the sum of the masses. While there are still many theoretical uncertainties in the timescales to form and merge a binary SMBH system, binary hardening timescales can be relatively quick if even a small amount of gas is present (Armitage & Natarajan, 2002;

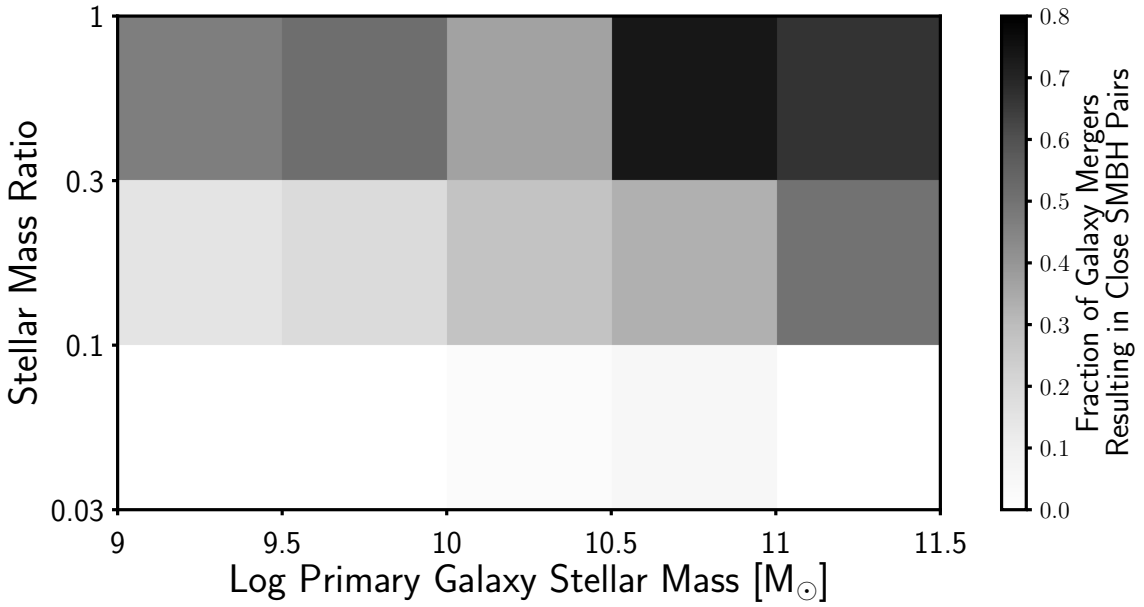

Figure 6.1: Likelihood of Close SMBH Pair Formation. The fraction of galaxy mergers that result in a close SMBH pair forming within a Hubble time as a function of the stellar mass of the primary galaxy and the stellar mass ratio at the time of first satellite in-fall. Considered are galaxy mergers resulting from initial satellite in-fall at $z < 5$. The formation of a close SMBH pair is not a common result of galaxy mergers. The likelihood of a close SMBH pair forming is sensitive to both stellar mass and mass ratio, being the most likely to occur in massive, major mergers.

Haiman et al., 2009; Colpi, 2014), and even in some cases for gas poor systems (Holley-Bockelmann & Khan, 2015). If the binary hardening timescales are significant compared to the relevant timescales of the simulation, because the smallest resolved scales are much larger than the typical binary separation, taking the pair to act as a single object with respect to accretion and feedback is still a reasonable approximation for approximating those processes. It is instructive to note that the timescales examined here can be seen as a lower limit to the timescale to form a SMBH binary, as well as a SMBH merger.

We predict that the formation of close SMBH pairs is a relatively rare occurrence, with an average formation rate per co-moving volume of 0.013 cMpc^{-3} Gyr^{-1}. Figure 6.1 shows the likelihood that galaxy mergers result in the formation of a close SMBH pair within a Hubble time, which is very sensitive to the stellar mass ratio of the merging galaxies as well as the stellar mass of the primary galaxy. Lower mass galaxies are less likely to host SMBHs with our formation scheme (§2.2). In addition, as we explore in the next section, galaxies in lower mass ratio mergers are more likely to become tidally disrupted and deposit their SMBHs on very wide orbits with larger sinking timescales. While we will focus in the following sections on close SMBH pairs that do form in the simulation, it is important to note that only a fraction of galaxy mergers result in a close SMBH pair forming within a Hubble time.

6.4 Close SMBH Pair Formation Timescales

While several different timescales are important for understanding the formation and evolution of SMBH pairs, the evolution of SMBH orbits on kpc scales is often simplified, relying on analytic approximations that do not self consistently account for the kinematics and internal properties of the merging galaxies (e.g. Dvorkin & Barausse, 2017), which previous studies have shown can have an important role in determining how the SMBHs will evolve following a galaxy merger (.e.g Governato et al., 1994; Callegari et al., 2009, 2011). With the realistic model of SMBH dynamics included in ROMULUS25, the simulation is uniquely capable of estimating this timescale for a realistic population of galaxy mergers taking place within a fully cosmological environment.

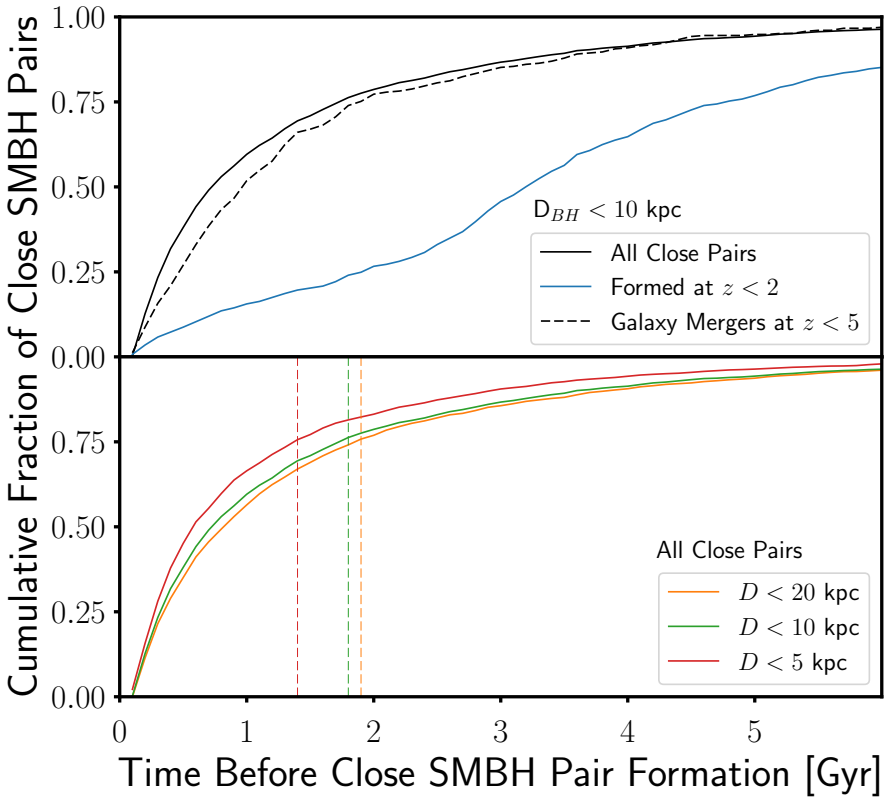

Figure 6.2: The Timescale to Form Close SMBH Pairs. *Top:* The cumulative distribution of time that SMBH pairs spend separated by less than 10 kpc prior to close pair formation for all close SMBH pairs formed in Romulus25 (black). While about half of the close pairs form relatively quickly (< 0.5 Gyr) there is a significant fraction that spend several Gyr at galaxy-scale separations. Close pairs that form at low redshift (blue) are mostly very far removed from their progenitor galaxy merger event. Also shown is the subset of close SMBH pairs resulting satellites in-falling after $z = 5$ (dashed), used in much of our analysis and which, as shown here, have timescales representative of the whole population of close SMBH pairs. *Bottom:* The cumulative distribution of timescales that SMBH pairs spent at 5, (red), 10 (green), and 20 (orange) kpc separations before forming a close pair with sub-kpc separation. As expected, closer proximity implies faster sinking timescales, as the dynamical time of the galaxy at smaller radii decreases. Overall, the distributions are quite similar, implying that our results are insensitive to the specific choice of separation scales explored. Vertical dashed lines show the 75th percentiles.

For our analysis we measure the time that each eventual close pair of SMBHs spends at 'galaxy-scale' ($\sim 1 - 10$ kpc) separations. Position information for each SMBH is recorded every 1.6 Myr and simulation snapshots are recorded every $10 - 100$ Myr, with higher time resolution at earlier epochs. In our analysis we only include close SMBH pairs formed within resolved DM halos, with at least 10,000 DM particles, resulting in a lower mass limit of $\sim 3 \times 10^9$ $M_\odot$. We also only include close pairs that form at least 100 Myr after each SMBH has been seeded, in order to avoid counting binaries that occur as a result of multiple SMBHs forming from the same cloud of gas, a rare but possible result of our formation scheme and should be considered degenerate to a single SMBH growing quickly from a particularly large, dense cloud of gas. We confirm that our results are insensitive to the specific choice of this time threshold.

The top panel of Figure 6.2 shows the cumulative distribution of time that SMBH pairs spend within 10 kpc of one another before forming a close pair. The distance is small enough that the two target SMBHs must be within the same galaxy or interacting pair of galaxies. For the overall population (black line) most of the close pairs form with less than 1 Gyr spent at these intermediate separations, consistent with many studies of isolated galaxy mergers (e.g. Mayer et al., 2007). However, there is a significant population of pairs that remain at galactic-scale separations for several Gyr. Taking only the population of close pairs that form at low redshift ($z < 2$; blue line) we see that the majority of these close pairs form several Gyr after their original galaxy merger event. We therefore predict that a significant fraction of low redshift SMBH pairs (and therefore subsequent SMBH binaries and SMBH merger events) are formed from a population of long-lived, 'wandering' SMBHs (Bellovary et al., 2010) born out of early galaxy mergers.

This result can have critical implications for gravitational wave analysis in the future, affecting how such signal is interpreted in terms of connecting SMBH mergers to galaxy evolution. It can also be important for interpreting dual and offset AGN observations, as it becomes unclear how connected they may be to actual galaxy mergers. Though beyond the scope of this paper, we will explore in more detail the implications of these results to

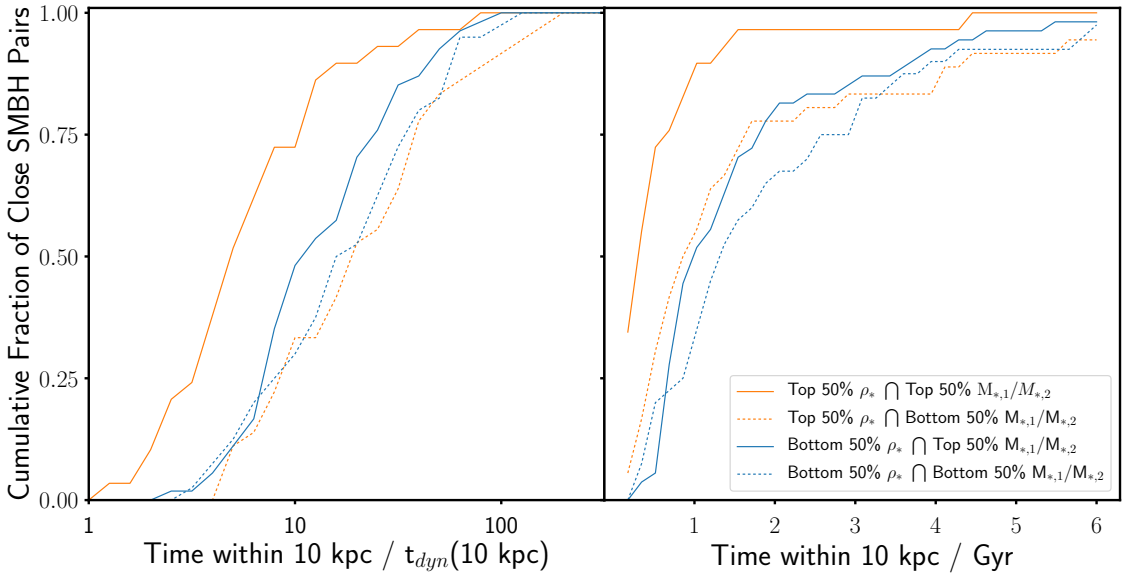

Figure 6.3: Close Pair Formation Timescales and Merging Galaxy Properties. The cumulative distribution of the number of dynamical times (left) and total time (right) that SMBH pairs spend within 10 kpc of one another before forming a close pair. The data is taken from 196 unique galaxy mergers taking place at $z < 5$, resulting in 330 close SMBH pair. Shown here are only those close pairs where the accreted SMBH is initially within the central 1 kpc of its host satellite galaxy (159 total pairs). The distributions are split up based on the 50th percentiles in central stellar density of the accreted galaxy and the stellar mass ratio calculated at the in-fall time of the satellite halo. Accreted galaxies that have both high central stellar densities and high stellar mass ratios compared to the main galaxy are significantly more likely to result in a quick formation of a close SMBH pair.

gravitational wave predictions as well as the population of offset and dual AGN in future work.

The bottom panel of Figure 6.2 shows the cumulative distribution of timescales that SMBH pairs spend at 5, 10, and 20 kpc separations. As expected, the evolution of SMBH pairs occurs on slightly shorter timescales for smaller separations. The sinking timescale due to dynamical friction depends on the local dynamical time, which decreases toward galactic center. Still, we find SMBH pairs that spend several Gyrs separated by 5 kpc or less. This shows that our results are insensitive to our specific choice of separation threshold. In the following sections, we choose 10 kpc as our galaxy-scale separation threshold, as it corresponds to the size of the Galactic disk and is a good representation of the inner region of a dark matter halo that is dominated by baryonic processes. Additionally, we have confirmed that our other conclusions are also insensitive to this chosen scale.

The distribution of timescales presented in Figure 6.2 is likely due to several variables, including the kinematics of the merging galaxies, the morphology of the galaxy merger remnant, the mass of the SMBHs, and where within that galaxy the SMBHs are deposited. Callegari et al. (2011) find that the behavior of in-falling satellite galaxies and their host SMBHs depend strongly on the angle of the interaction. How SMBHs are deposited within a galactic disk can also affect the efficiency of dynamical friction. If the host galaxy has a cored density profile, delay timescales can also be made longer (Read et al., 2006; Di Cintio et al., 2017). Similarly, a large stellar core with high velocity dispersion could also make dynamical friction less effective, as there would be more stars moving too fast to contribute. All of these merger and galaxy properties are a natural consequence of the simulation volume and are folded into the timescale distributions we predict.

Because these timescales are the result of many different variables interacting with one anther, we find little overall dependence on single parameters like SMBH mass or halo mass. However, we do find a strong dependence on the morphology of the accreted galaxy and its stellar mass relative to the primary galaxy, which we explore in the following section.

6.4.1 Galaxy Disruption and Close SMBH Pair Formation Timescales

In this section, we examine how the close SMBH pair formation timescale depends on the properties of the interacting galaxies. We take a sub-set of our close SMBH pair population that result from galaxy mergers initiated by in-falling satellites at $z < 5$, where both halos are resolved ($M_{vir} > 3 \times 10^9$ M$_\odot$) at the time of satellite in-fall. This time of satellite in-fall is taken as the time the secondary galaxy's host dark matter halo crosses the Virial radius of the main halo. For halos that cross the Virial radius multiple times, the final crossing time is used. The initial properties of each galaxy prior to the merger are taken at this final in-fall time. We focus on lower redshift mergers because galaxy interactions that occur earlier are often not fully captured by our snapshots, with halos attaining a mass that passes our strict definition of what is resolved and falling into the main halo in between snapshots. This sub-sample consists of 330 close SMBH pairs resulting from 196 unique galaxy mergers. Note that, because individual galaxies can host multiple SMBHs, it is common for single galaxy mergers to result in multiple close SMBH pairs. The dashed black line in Figure 6.2 shows the distribution of delay timescales for this subset of close SMBH pairs, showing that this population is indeed representative of the whole.

In Figure 6.3 we plot the cumulative distribution of time that eventual close SMBH pairs spend within 10 kpc of one another. We group these pairs based on the central stellar density of the in-falling galaxy and the stellar mass ratio of the two merging galaxies. The stellar density is calculated within the central kpc of each in-falling satellite galaxy. Figure 6.3 shows the results in units of both Gyr (right) and number of dynamical times (left), where the dynamical time is calculated at a radius of 10 kpc of the main galaxy at the approximate time the two SMBHs come within 10 kpc of one another. The median values for the central stellar density and stellar mass ratio are 3.4×10^6 M$_\odot$ kpc^{-3} and 0.43 respectively. Only systems where the accreted SMBH is within the central 1 kpc of its host galaxy at in-fall time are considered. Initially offset SMBHs are considered in the next section.

It is clear from this figure that accreted galaxies with high central densities and higher

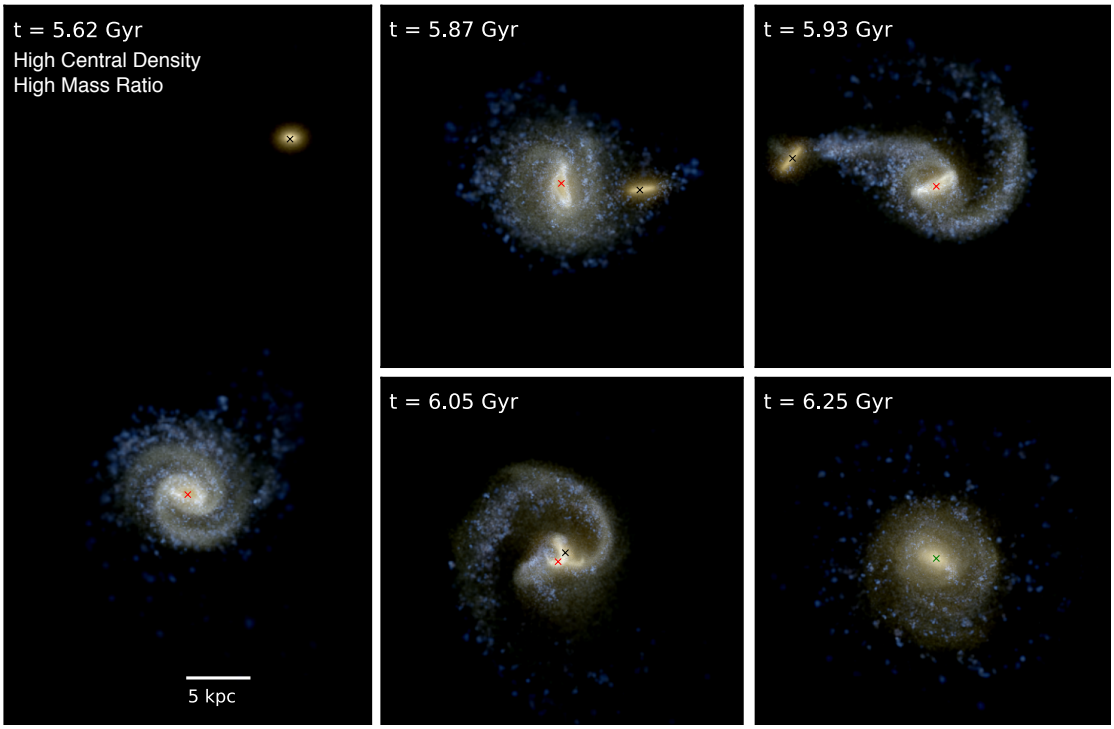

Figure 6.4: An Example of a Quickly Forming Close SMBH Pair. A time sequence showing the spatial distribution and color of stars at five different times leading up to and following the merger of the two galaxies. Colors are based on the contribution of different bands within each pixel using U (blue), V (green), J (red) assuming a Kroupa IMF, so young stars look blue and older stars look yellow. The stellar emission is calculated using tables generated from population synthesis models (http://stev.oapd.inaf.it/cgi-bin/cmd; Marigo et al., 2008; Girardi et al., 2010). Red and black crosses mark the positions of the SMBHs and the green cross in the top final frame represents a close pair of SMBHs. The initial stellar mass of the accreted and main galaxies is 1.3×10^{10} and 2.9×10^{10} $M_{\odot}$ respectively. The two SMBHs spend a total of 0.3 Gyr within 10 kpc of one another before forming a close SMBH pair, as the accreted SMBH remains within a dense stellar core throughout the interaction.

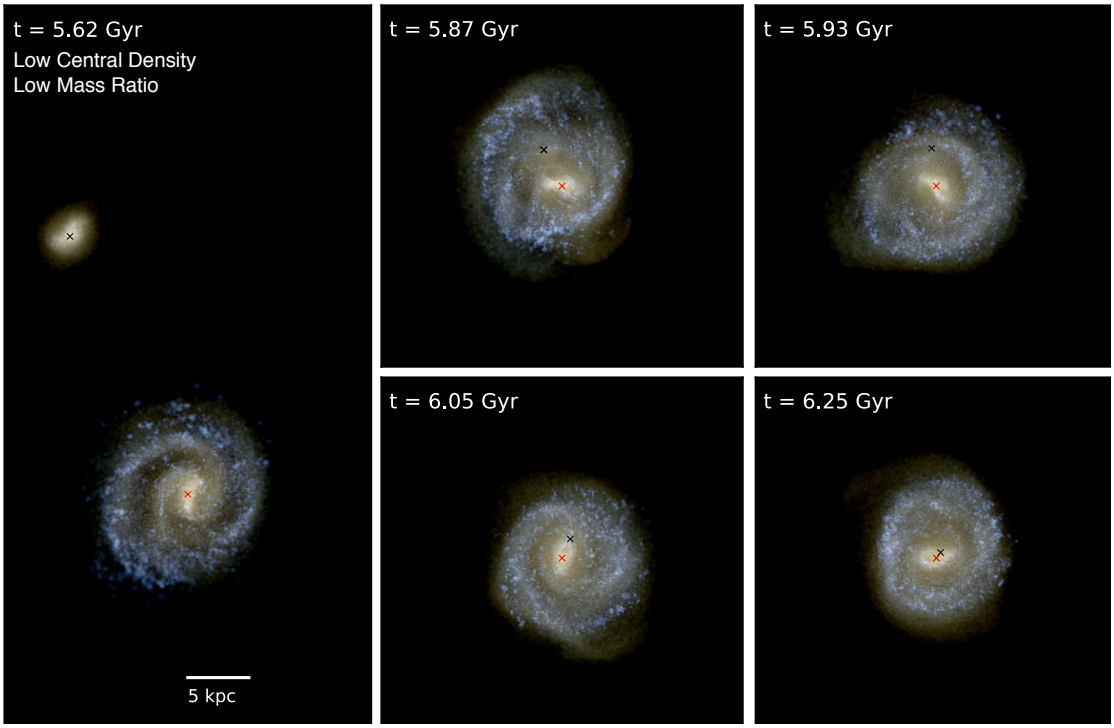

Figure 6.5: An Example of A Long Lasting 'Wandering' SMBH. Similar to Figure 6.4, but for accreted and main galaxies with initial stellar masses of 1.02×10^{10} and 4.6×10^{10} $M_{\odot}$ $M_{\odot}$ respectively. The accreted galaxy in this example had an initial stellar core that was nearly 5 times less dense than the example shown in Figure 6.4. During the interaction, the lower stellar mass ratio and central density result in the core becoming tidally heated and quickly disrupted, leaving the SMBH 'naked' within the galaxy. Despite the close passage shown in the last frame, the SMBHs will not form a close pair until $t = 7.34$ Gyr, after 1.7 Gyr, much longer than in the case shown in Figure 6.4

stellar mass ratios result in significantly shorter delay times. Galaxies with either low central densities or low stellar mass ratios experience longer times spent at galaxy-scale separations, implying that tidal disruption of the host galaxy is important for determining the timescale for close SMBH pair formation. During a galaxy interaction, ram pressure stripping can disrupt gas within galactic disks at larger radii and tidal heating can disrupt the inner core of the galaxies. Dense stellar cores within high mass ratio mergers are more likely to avoid disruption through both ram pressure stripping and tidal heating (Gnedin & Ostriker, 1999; Callegari et al., 2009; Van Wassenhove et al., 2014), so the central SMBHs remain embedded in a dense stellar core that aids in their orbital decay. In galaxies lacking a dense stellar core, or those involved in more minor mergers, tidal heating is more efficient at disrupting the inner parts of the galaxy, resulting in SMBHs deposited at large radii without any stellar core to assist in their orbital decay. This is consistent with analytical experiments showing how the orbital evolution of SMBHs is highly dependent on whether they are embedded in a stellar core or 'naked' within their new host galaxy (Yu, 2002).

Figures 6.4 and 6.5 show a series of snapshots from two example galaxy mergers taking place with both primary and secondary galaxies initially within a factor of 2 of one another in stellar mass. However, the stellar mass ratio in Figures 6.4 and 6.5 is 0.45 and 0.22 respectively. This, combined with the fact that the secondary galaxy in Figure 6.4 has an initial central stellar density nearly 5 times higher than that in the case shown in Figure 6.5, results in very different SMBH orbital evolution. In Figure 6.5, the secondary galaxy's core becomes tidally heated and eventually disrupted by the main galaxy, no longer maintaining its structure. Rather, in Figure 6.4, the denser core is able to avoid disruption and maintains its integrity up until the two cores merge, bringing the SMBHs along with them. The example of a disrupted galaxy forms a close SMBH pair only after the SMBHs spend 1.7 Gyr within 10 kpc of one another, while the case where the core avoids disruption results in a close pair after the SMBHs spend only 0.3 Gyr at galaxy-scale separations.

6.4.2 Initially Offset SMBHs

In the previous section, we focused on central SMBHs, those that are at the center of their host galaxy at the time of satellite in-fall. However, approximately half of the close SMBH pairs in our sub-sample from ROMULUS25 form from accreted SMBHs initially offset from the center of their host galaxy. As we have seen, the orbital decay of SMBHs can often take several Gyr and galaxy mergers often never result in a close SMBH pair. Massive galaxies in the ROMULUS25 simulation therefore often have several SMBHs that are offset from galactic center, gathered throughout the host galaxy's merger history. In some cases, galaxies only have offset SMBHs.

Figure 6.6 is similar to the left panel of Figure 6.3, with SMBH binaries binned based on whether the accreted host galaxy is more likely to avoid complete disruption due to a dense stellar core and high mass ratio (orange/solid), less likely to avoid disruption (blue/dashed), or whether the target SMBH is offset from the center of their host satellite galaxy by more than 1 kpc as it crosses the main halo's Virial radius (green/dotted).

The close pair formation timescale distribution for initially offset SMBHs is similar to that for more commonly disrupted satellite galaxies. When the SMBH is not central, it is likely not embedded within a dense stellar core, even if its host galaxy has one. It will therefore become accreted onto the main galaxy without a stellar core to aid in dynamical friction, just like SMBHs in galaxies whose core becomes tidally disrupted.

6.4.3 The Importance of Galaxy-Scale Orbital Evolution

The previous sections have shown that SMBH pairs can spend significant time at kpc distances before forming a close pair. However, there is another timescale to consider: the sinking time for the satellite galaxy, representing distances on the order of 10s to 100s kpc. In this section we compare this intermediate sinking timescale relevant for SMBH separations between $\sim 1 - 10$ kpc to the timescale for larger-scale evolution dominated by the orbital decay of satellite halos.

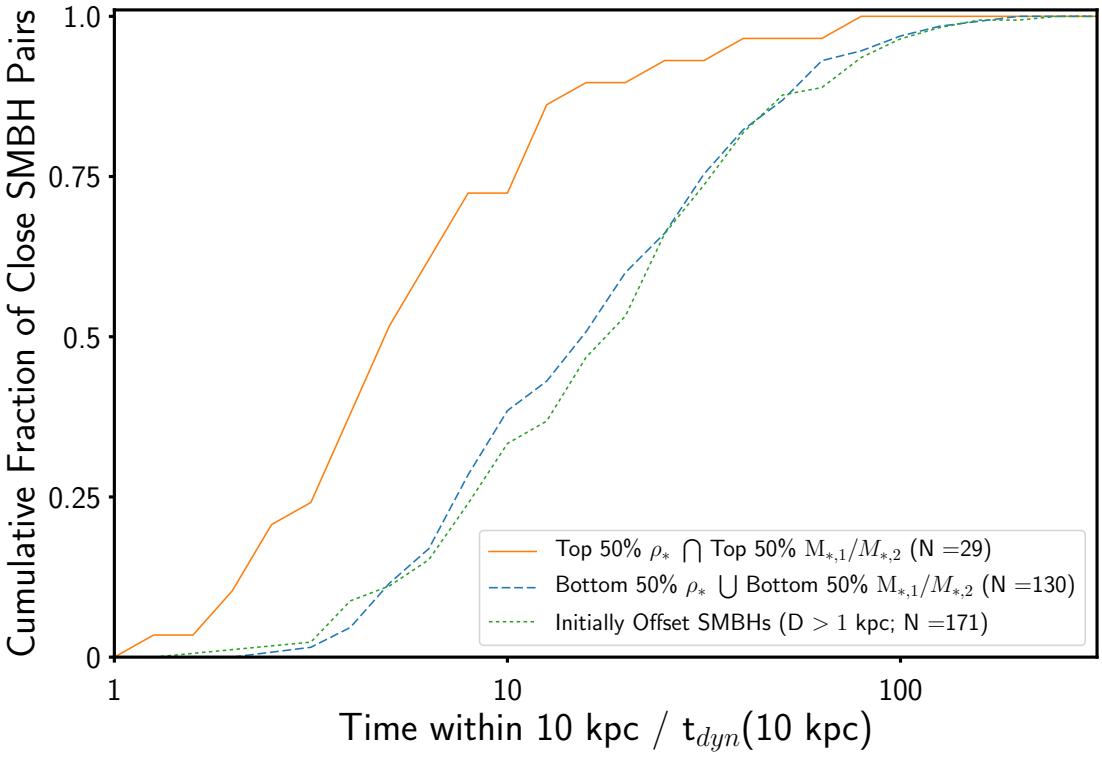

Figure 6.6: Close Pair Formation Timescales for Initially Offset SMBHs. The cumulative distribution of the number of dynamical times SMBH pairs spend within 10 kpc of one another before forming a close pair. The solid orange line represents SMBHs from galaxies that are less susceptible to disruption (same as in Figure 6.3) and the blue dashed line represents SMBHs from galaxies that are more likely to become tidally disrupted due to a lower stellar mass ratio and/or low central density. The green dotted line represents SMBHs that were initially offset from the centers of their host satellite galaxies by more than 1 kpc at the time of in-fall. The green and blue distributions are very similar, which is to be expected. In both cases, the SMBHs lack the extra support of a stellar core when making their way to the center of their new galaxy.

We find that this galaxy-scale orbital evolution is an important bottleneck to close SMBH pair formation, particularly for high redshift galaxy mergers. In Figure 6.7 we plot the close pair formation times directly from the ROMULUS25 cosmological simulation against the in-fall redshift of the parent satellite galaxy for the secondary SMBH (orange points). We compare this formation time with that which would be predicted if the orbital evolution of SMBHs on galaxy scales was ignored and close pairs were assumed to form immediately once the SMBHs come within 10 kpc of one another (blue points). We find that the orbital evolution of SMBHs from 10 kpc to sub-kpc scales is an important bottleneck to close pair formation (and the subsequent binary formation and merger) for high redshift galaxy interactions, where the dynamical timescale for satellite halos is comparatively small. At redshift less than ~ 2 we find that there is less of a clear difference between the two types of points, indicating that halo sinking timescales are more similar to or even sometimes dominant compared to galaxy-scale SMBH orbital evolution. Semi-analytic models of SMBH binary evolution find similar results, with binary evolution timescales acting as a dominant bottleneck at high redshift and increasingly less important when compared to satellite sinking timescales at low redshift (Volonteri et al., 2016a).

Examining the the halo in-fall times and the predicted close SMBH pair formation it is clear that close pairs that form at later times are often the consequence of high redshift mergers, an effect also seen in Figure 6.2. These results show that SMBH orbital evolution on galaxy scales (10 kpc down to sub-kpc separations) is a very important bottleneck for the formation of close SMBH pairs and, therefore, SMBH binaries and mergers, and must be accounted for when predicting the population of binary SMBHs and gravitational wave events across cosmic time.

6.5 Discussion and Conclusions

Using the ROMULUS25 cosmological simulation, which is able to accurately track the dynamics of SMBHs within galaxies down to sub-kpc scales, we examine the timescale for SMBHs pairs to evolve from galaxy-scale separations ($1 - 10$ kpc) to form close pairs with

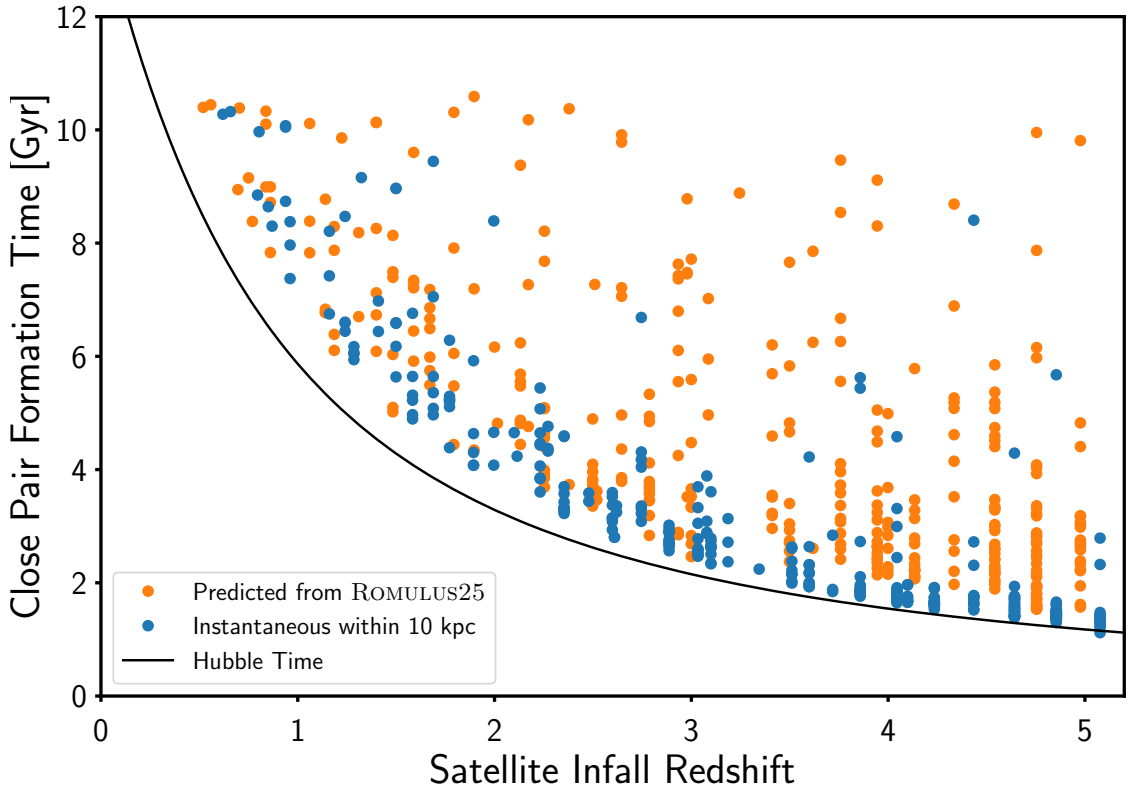

Figure 6.7: SMBH vs. Halo Sinking Timescales. The formation time of close SMBH pairs as a function of the in-fall redshift of the accreted SMBH's host satellite galaxy. The black line denotes the Hubble time as a function of redshift. The orange points plot the time of close pair formation predicted directly from the Romulus25 simulation. The blue points mark what the close pair formation time would be had it been instantaneous once the SMBHs were closer than 10 kpc. The infall redshifts are shifted slightly between the two in order to make the distinction more clear. We see that for high redshift galaxy interactions, the timescale for SMBH orbits to shrink from 10 kpc to sub-kpc scales is critical in determining when a close pair will form, representing an important bottleneck to close pair formation. At lower redshift ($z < 2$) we see that halo sinking timescales represent an increasingly important bottleneck to the formation of close SMBH pairs.

separations less than a kpc, the precursor phase to a bound SMBH binary and (possible) future SMBH merger. The formation of close SMBH pairs is a relatively rare occurrence, resulting from only a subset of galaxy mergers and becoming more common in major mergers of more massive galaxies. We find that galaxy mergers across cosmic time result in close SMBH pairs that often form several Gyr after the original galaxy merger event. SMBHs often accrete onto a new host galaxy via galaxy merger at high redshift, but only form a close SMBH pair at much lower redshift, resulting in a long lived population of 'wandering' SMBHs (Bellovary et al., 2010). This can affect how we predict and interpret future gravitational wave observations, as well as observations of dual and offset AGN.

Using a set of 330 SMBH merger events resulting from 196 unique galaxy mergers within ROMULUS25, we show that the timescales for the formation of a close SMBH pair is dependent on galaxy morphology and stellar mass ratio. Galaxy mergers with similar mass and dense stellar cores result in faster formation timescales for close SMBH pairs, as these properties make it less likely for the secondary galaxy to become tidally disrupted. SMBHs that are embedded in stellar cores that are able to avoid disruption will be aided in sinking to galactic center and forming a close SMBH pair (Yu, 2002). Galaxy mergers that are more susceptible to tidal disruption exhibit much longer SMBH sinking timescales and close SMBH pairs that form long after the galaxy merger event (if they are able to form at all). A similar situation is true for SMBHs that are initially offset from the center of in-falling satellite galaxies. These SMBHs are likely not embedded in a dense stellar core, if one exists in their host galaxy, and so are also deposited on their own and often at relatively large galactic radii.

We show that orbital evolution of SMBHs within galaxies on scales between 1-10 kpc are a major bottle neck for forming close SMBH paris, particularly for high redshift galaxy interactions. In agreement with Volonteri et al. (2016a), at lower redshifts ($z < 2$) the sinking timescale of satellite halos becomes a more dominant factor and the specific effect of galaxy-scale orbital decay is less important, though still not trivial.

It is clear that this stage of SMBH pair evolution plays a crucial role in determining

when and where close SMBH pairs occur. As these systems are the precursor to SMBH binaries and mergers, this timescale is an important ingredient when making predictions for gravitational wave observations. It is also important to understanding the time connection between AGN activity and galaxy interaction induced star formation, as the SMBH sinking timescale may be much larger than that of the typical observed starburst timescale, found to be on the order of 0.1 Gyr (Marcillac et al., 2006; Pereira-Santaella et al., 2015).

Chapter 7

SUMMARY AND FUTURE WORK

7.1 Summary and Discussion

For my Thesis I have developed a novel approach to modeling SMBH formation, dynamics, and accretion in cosmological simulations. This results in simulated SMBHs that 1) form in dense, pristine gas at early times, 2) evolve dynamically within galaxies in a realistic way, and 3) exhibit accretion rates that respond to the evolving kinematics of nearby gas. With this approach, SMBHs can be studied in more detail and in new ways.

As a cornerstone to my thesis I implemented this model into a large set of cosmological simulations, called Romulus, which consists of the flagship 25 Mpc per side uniform box simulation (ROMULUS25) and a 10^{14} $M_{\odot}$ cluster 'zoom-in' simulation (ROMULUSC). In preparation for these simulations I also lead, in collaboration with then graduate student Michael Karcher in the Statistics Department at the University of Washington, an extensive parameter search utilizing over 100 'zoomed-in' simulations in order to constrain free parameters associated with sub-grid physics.

The results from ROMULUS25 have shown that the calibrated model for star formation and SMBH physics work together to create galaxies with realistic stellar masses and SMBH masses as well as accretion and star formation histories that are consistent with high redshift observations. Using a set of smaller uniform volume simulations, I also examined how the evolution of galaxies and SMBHs is sensitive to the details of the SMBH implementation I have developed. Not accounting for the angular momentum gas during accretion or artificially tethering SMBHs to the centers of galaxies both result more bursty accretion and earlier deposition of energy into the host galaxies. The result of this is drastically different star formation histories, stellar masses, and morphologies.

As the first science case for ROMULUS25, I focus on the formation of close SMBH pairs. A major strength of my implementation is that it self-consistently models the orbital decay of SMBHs accreted onto galaxies through mergers. Using nearly 200 galaxy mergers taking place after $z = 5$, I examine the formation timescales for 330 close SMBH pairs, finding that a significant fraction of them form several Gyr after the merger of their former host galaxies. The specific timescale depends strongly on the morphology and stellar mass ratio of the merging galaxies. More specifically, if a galaxy becomes tidally disrupted it will deposit its SMBH on a relatively wide orbit with no stellar core to aid in its orbital decay. However, galaxies that are able to avoid total disruption (i.e. those with dense stellar cores in high mass ratio mergers), the SMBHs remain within their stellar core and are aided in their orbital decay (Yu, 2002). This work is the first self consistent prediction for the distribution of close SMBH pair formation timescales. I further show how this timescale for close SMBH pair formation from kpc scale distances is a critical bottleneck for the formation of close pairs, as well as any subsequent SMBH binaries and mergers.

7.2 Current and Future Work

Here I discuss several projects that I am currently developing with collaborators using both the ROMULUS Simulations and new sets of 'genetically modified' (Roth et al., 2016) zoomed-in cosmological simulations. The overarching goal of all of these endeavors is to understand how the growth of SMBHs depends on environment and halo assembly history, as well as their role in shaping the evolution of galaxies. Unless otherwise noted, the simulations described below all incorporate the physics as described in Chapters 2-5 and have the same resolution as the ROMULUS Simulations (3×10^5 DM particle mass, ~ 300 pc spline force softening).

7.2.1 Gravitational Waves

In collaboration with Marta Volonteri and Enrico Barausse at l'Institute d'Astrophysique de Paris, I am working to analyze how the delay timescale for forming SMBH binaries following galaxy mergers (see Chapter 6) can affect the predicted signal for gravitational waves that

may be detected by LISA and pulsar timing arrays. To accomplish this, we will implement a rough correction to the results of Enrico's semi-analytic models to examine the relative importance of timescales related to halo sinking, SMBH binary formation, and SMBH binary hardening in setting the predicted observed rate of detected SMBH mergers across cosmic time.

7.2.2 Galaxy Quenching and Mergers

Another of my initial research goals using the ROMULUS simulations utilizes the uniform galaxy sample present in ROMULUS25. In collaboration with Andrew Pontzen and Fabio Governato, I will build upon the work of Pontzen et al. (2017) to examine the various mechanisms that most commonly result in the quenching of star formation across cosmic time. In particular, I will focus on the role that SMBH feedback and galaxy mergers play in this process.

I am also utilizing the detailed dynamics and accretion implementation in ROMULUS to examine the activity cycles of SMBHs during and following galaxy merger events. The goal of the is to understand how merger driven growth is distinct from that driven by secular processes and how each in tandem shape the observed population of AGN and SMBHs. I am also working on examining the population of dual and/or offset active SMBHs. Because SMBH pairs can spend several Gyr within the same galaxy, it is possible that non-central SMBHs become bright due to accretion. These phenomena have been observed (Comerford et al., 2013, 2015; Barrows et al., 2016) but require input from simulations in order to say more about how these events may track merger-driven growth. If SMBH pairs exist long after galaxy mergers occur, the connection may be more tenuous than previously thought.

7.2.3 Galaxy and SMBH Evolution in Cluster Environments

The ROMULUSC simulation is a 'zoomed-in' simulation of a 10^{14} $M_{\odot}$ halo extracted from a 50 Mpc per side uniform cosmological box simulation. At this mass scale, the resolution of ROMULUSC is unprecedented, allowing us to explore in more detail the properties of not only

the brightest cluster galaxy, but also the satellite galaxies. This simulation is the logical next step from ROMULUS25, as it will allow us to explore galaxy evolution in dense environments not sampled with a small volume simulation. Analysis of ROMULUSC has already begun. We find that feedback from the central SMBH is able to eventually quench star formation in the main galaxy. We also find entropy, temperature, and stellar mass values consistent with observations of halos of similar mass.

In collaboration with Priyamvada Natarajan and Angelo Ricarta at Yale, I am examining SMBH activity within the cluster environment. Galaxies in clusters experience a unique form of 'fly-by' interaction that can affect their morphology (Moore et al., 1998). Utilizing the high resolution of ROMULUSC we are able to examine the properties of galaxies and their SMBHs as they fall into a galaxy cluster, interacting with other galaxies and the intra-cluster medium. Following SMBH accretion as their host galaxies experience such interactions we can study the luminosity and host galaxy characteristics of active SMBHs, comparing with ROMULUS25 and X-ray observations of AGN in clusters (Ehlert et al., 2015). Some preliminary results indicate that the orbits of galaxies within the cluster can greatly affect cycles of AGN activity.

With ROMULUSC, I will build further on the study of galaxy quenching. By examining the abundance, size, brightness profiles, and angular momentum distribution of quenched galaxies in ROMULUCC as a function of galaxy mass and radial position, comparing to ROMULUS25 and results from HST's Frontier Fields (Morishita et al., 2016), we can explore how galaxy clusters present new mechanisms for quenching star formation.

In addition to ROMULUSC, in collaboration with Tom Quinn two more massive cluster simulations are planned with final Virial masses of $\sim 10^{14.5}$ and $\sim 10^{15}$ $M_{\odot}$ (ROMULUSC-2,3 respectively). These represent a large computational effort and will require further optimization of SMBH physics, dealing with issues such as time stepping. It will also require some preliminary tests and a more thorough analysis of ROMULUSC to ensure realistic results The simulations will take several hundred million CPU hours.

7.2.4 Connecting SMBH and Galaxy Evolution to Halo Assembly History

The galaxy 'genetic modification' (GM) approach (Roth et al., 2016) is a powerful tool that we plan on utilizing extensively for the next set of simulations. This approach allows one to fine-tune any combination of a) halo mass, b) formation time, c) halo spin, and d) mass ratio and timing of halo mergers through careful manipulation of the initial over density field while making sure that the object remains as close as possible to its reference run. Using this, we may conduct, for the first time, controlled experiments within a cosmological environment, allowing us to quantify the effects that specific aspects of a halo's assembly history have on galaxy-SMBH co-evolution.

Currently underway, in collaboration with Andrew Pontzen and Fabio Governato, is a campaign running two large sets of 'zoomed-in' simulations for GM realizations of 10^{12} and 10^{13} $M_{\odot}$ halos. The goal of these simulations is to understand how halo assembly history is imprinted upon the evolution of galaxies and their SMBHs. The two masses are chosen to represent Milky-Way-like galaxies and massive, quenched systems respectively. Because the physics and resolution will be the same, insight can also be gained by comparing the results of these simulations to galaxies in ROMULUS.

The GM simulation suites, combined with the ROMULUS Simulations, will allow us to connect halo assembly to galaxy evolution. However, this is still a limited sample of galaxies. The next step beyond this would be to implement the results from GM and ROMULUS into semi-analytic models. Priyamvada Natarajan and Angelo Ricarte at Yale are working on new SAMs focusing on SMBH growth across cosmic time. SAMs essentially map halo merger trees to baryonic process regarding SMBH and/or galaxy evolution. The insight gathered from GM on how specific aspects of assembly history affect the evolution of SMBHs and galaxies will allow us to implement new phenomenological models into the state-of-the-art SAMs in development at Yale. Currently, the results presented in Chapter 6 on SMBH binary formation timescales is in the process of being implemented into their models, potentially an important addition to estimates of SMBH masses and accretion rates across cosmic time.

7.2.5 Double Bubble: The Next Generation of SMBH Feedback

I have begun working with Ben Keller to merge his implementation of supernovae feedback ('Superbubbles'; Keller et al., 2014) with my implementation of SMBH physics (the combination currently referred to as 'Double Bubble'). The result will be an improvement in how feedback from SMBHs is transferred to surrounding particles. The main advantage of super bubbles feedback is that it models the conduction of energy and, by splitting individual particles by 'cold' and 'hot' components, overcomes issues with over-cooling that does not require more ad-hoc approaches like shutting off cooling for gas particles. It has been shown to be an improvement over the 'blastwave' feedback currently implemented in ROMULUS. Utilizing the same approach for SMBH feedback will provide the best possible model for thermal AGN feedback. The initial implementation and the first tests are being conducted at this time. The long term goal is to run a (25 Mpc)^3 volume similar to ROMULUS with this new implementation, following another extensive parameter search, both lead by Ben.

BIBLIOGRAPHY

Agarwal B., Dalla Vecchia C., Johnson J. L., Khochfar S., Paardekooper J.-P., 2014, MNRAS, 443, 648

Anderson L., Governato F., Karcher M., Quinn T., Wadsley J., 2017, MNRAS, 468, 4077

Anglés-Alcázar D., Davé R., Faucher-Giguère C.-A., Özel F., Hopkins P. F., 2017, MNRAS, 464, 2840

Armitage P. J., Natarajan P., 2002, ApJ, 567, L9

Aykutalp A., Wise J. H., Spaans M., Meijerink R., 2014, ApJ, 797, 139

Barausse E., 2012, MNRAS, 423, 2533

Barber C., Schaye J., Bower R. G., Crain R. A., Schaller M., Theuns T., 2016, MNRAS, 460, 1147

Barrows R. S., Comerford J. M., Greene J. E., Pooley D., 2016, ArXiv e-prints

Barrows R. S., Comerford J. M., Greene J. E., Pooley D., 2017, ApJ, 838, 129

Begelman M. C., Shlosman I., 2009, ApJ, 702, L5

Begelman M. C., Volonteri M., Rees M. J., 2006a, MNRAS, 370, 289

Begelman M. C., Volonteri M., Rees M. J., 2006b, MNRAS, 370, 289

Behroozi P. S., Wechsler R. H., Conroy C., 2013a, ApJ, 770, 57

Behroozi P. S., Wechsler R. H., Wu H.-Y., Busha M. T., Klypin A. A., Primack J. R., 2013b, ApJ, 763, 18

Bellovary J., Brooks A., Volonteri M., Governato F., Quinn T., Wadsley J., 2013, ApJ, 779, 136

Bellovary J., Volonteri M., Governato F., Shen S., Quinn T., Wadsley J., 2011, ApJ, 742, 13

Bellovary J. M., Governato F., Quinn T. R., Wadsley J., Shen S., Volonteri M., 2010, ApJ, 721, L148

Benson A. J., 2014, MNRAS, 444, 2599

Binney J., 1977, ApJ, 215, 483

Binney J., Tremaine S., 2008, Galactic Dynamics: Second Edition. Princeton University Press

Bluck A. F. L. et al., 2016, MNRAS, 462, 2559

Bond J. R., Arnett W. D., Carr B. J., 1984, ApJ, 280, 825

Bondi H., 1952, MNRAS, 112, 195

Bondi H., Hoyle F., 1944, MNRAS, 104, 273

Booth C. M., Schaye J., 2009, MNRAS, 398, 53

Bower R. G., Benson A. J., Malbon R., Helly J. C., Frenk C. S., Baugh C. M., Cole S., Lacey C. G., 2006, MNRAS, 370, 645

Bower R. G., Vernon I., Goldstein M., Benson A. J., Lacey C. G., Baugh C. M., Cole S., Frenk C. S., 2010, MNRAS, 407, 2017

Bromm V., Loeb A., 2003, ApJ, 596, 34

Brook C. B. et al., 2011, MNRAS, 415, 1051

Bruce V. A., Dunlop J. S., Mortlock A., Kocevski D. D., McGrath E. J., Rosario D. J., 2016, MNRAS, 458, 2391

Buchner J. et al., 2015, ApJ, 802, 89

Bullock J. S., Kravtsov A. V., Weinberg D. H., 2000, ApJ, 539, 517

Callegari S., Kazantzidis S., Mayer L., Colpi M., Bellovary J. M., Quinn T., Wadsley J., 2011, ApJ, 729, 85

Callegari S., Mayer L., Kazantzidis S., Colpi M., Governato F., Quinn T., Wadsley J., 2009, ApJ, 696, L89

Calzetti D., 2001, PASP, 113, 1449

Calzetti D., Armus L., Bohlin R. C., Kinney A. L., Koornneef J., Storchi-Bergmann T., 2000, ApJ, 533, 682

Cannon J. M. et al., 2011, ApJ, 739, L22

Capelo P. R., Volonteri M., Dotti M., Bellovary J. M., Mayer L., Governato F., 2015, MNRAS, 447, 2123

Carr B. J., Bond J. R., Arnett W. D., 1984, ApJ, 277, 445

Chandrasekhar S., 1943, ApJ, 97, 255

Chapon D., Mayer L., Teyssier R., 2013, MNRAS, 429, 3114

Christensen C. R., Brooks A. M., Fisher D. B., Governato F., McCleary J., Quinn T. R., Shen S., Wadsley J., 2014, MNRAS, 440, L51

Colpi M., 2014, Space Sci. Rev., 183, 189

Colpi M., Mayer L., Governato F., 1999, ApJ, 525, 720

Comerford J. M., Pooley D., Barrows R. S., Greene J. E., Zakamska N. L., Madejski G. M., Cooper M. C., 2015, ApJ, 806, 219

Comerford J. M., Pooley D., Gerke B. F., Madejski G. M., 2011, ApJ, 737, L19

Comerford J. M., Schluns K., Greene J. E., Cool R. J., 2013, ApJ, 777, 64

Cowie L. L., Songaila A., Hu E. M., Cohen J. G., 1996, AJ, 112, 839

Croton D. J. et al., 2006, MNRAS, 365, 11

Debuhr J., Quataert E., Ma C.-P., 2011, MNRAS, 412, 1341

Devecchi B., Volonteri M., 2009, ApJ, 694, 302

Di Cintio A., Tremmel M., Governato F., Pontzen A., Zavala J., Bastidas Fry A., Brooks A., Vogelsberger M., 2017, ArXiv e-prints

Di Matteo T., Colberg J., Springel V., Hernquist L., Sijacki D., 2008, ApJ, 676, 33

Di Matteo T., Croft R. A. C., Springel V., Hernquist L., 2003, ApJ, 593, 56

Di Matteo T., Springel V., Hernquist L., 2005, Nature, 433, 604

Draine B. T. et al., 2007, ApJ, 663, 866

Dubois Y., Gavazzi R., Peirani S., Silk J., 2013, MNRAS, 433, 3297

Dubois Y., Peirani S., Pichon C., Devriendt J., Gavazzi R., Welker C., Volonteri M., 2016, MNRAS

Dubois Y., Volonteri M., Silk J., 2014a, MNRAS, 440, 1590

Dubois Y., Volonteri M., Silk J., Devriendt J., Slyz A., 2014b, MNRAS, 440, 2333

Duncan K. et al., 2014, MNRAS, 444, 2960

Dvorkin I., Barausse E., 2017, ArXiv e-prints

Efstathiou G., 1992, MNRAS, 256, 43P

Efstathiou G., 2000, MNRAS, 317, 697

Ehlert S. et al., 2015, MNRAS, 446, 2709

Evrard A. E., 1988, MNRAS, 235, 911

Feldmann R., Mayer L., 2015, MNRAS, 446, 1939

Fiacconi D., Mayer L., Roškar R., Colpi M., 2013, ApJ, 777, L14

Filippenko A. V., Ho L. C., 2003, ApJ, 588, L13

Gehren T., Fried J., Wehinger P. A., Wyckoff S., 1984, ApJ, 278, 11

Genel S. et al., 2014, MNRAS, 445, 175

Girardi L. et al., 2010, ApJ, 724, 1030

Gnedin O. Y., Ostriker J. P., 1999, ApJ, 513, 626

Governato F. et al., 2010, Nature, 463, 203

Governato F. et al., 2009, MNRAS, 398, 312

Governato F., Colpi M., Maraschi L., 1994, MNRAS, 271, 317

Governato F. et al., 2015, MNRAS, 448, 792

Governato F., Willman B., Mayer L., Brooks A., Stinson G., Valenzuela O., Wadsley J., Quinn T., 2007, MNRAS, 374, 1479

Governato F. et al., 2012, MNRAS, 422, 1231

Guedes J., Callegari S., Madau P., Mayer L., 2011, ApJ, 742, 76

Gültekin K., et al., 2009, ApJ, 698, 198

Guo Q., White S., Li C., Boylan-Kolchin M., 2010, MNRAS, 404, 1111

Habouzit M., Volonteri M., Dubois Y., 2017, MNRAS, 468, 3935

Haehnelt M. G., Rees M. J., 1993, MNRAS, 263, 168

Haiman Z., Kocsis B., Menou K., 2009, ApJ, 700, 1952

Häring N., Rix H.-W., 2004, ApJ, 604, L89

Haynes M. P. et al., 2011, AJ, 142, 170

Hernquist L., Barnes J. E., 1990, ApJ, 349, 562

Hirschmann M., Dolag K., Saro A., Bachmann L., Borgani S., Burkert A., 2014, MNRAS, 442, 2304

Holley-Bockelmann K., Khan F. M., 2015, ApJ, 810, 139

Hopkins P. F., Hernquist L., Cox T. J., Di Matteo T., Martini P., Robertson B., Springel V., 2005, ApJ, 630, 705

Hopkins P. F., Hernquist L., Cox T. J., Di Matteo T., Robertson B., Springel V., 2006, ApJS, 163, 1

Hopkins P. F., Kereš D., Oñorbe J., Faucher-Giguère C.-A., Quataert E., Murray N., Bullock J. S., 2014, MNRAS, 445, 581

Hopkins P. F., Quataert E., 2010, MNRAS, 407, 1529

Hopkins P. F., Quataert E., 2011a, MNRAS, 415, 1027

Hopkins P. F., Quataert E., 2011b, MNRAS, 415, 1027

Hopkins P. F., Richards G. T., Hernquist L., 2007, ApJ, 654, 731

Hosokawa T., Yorke H. W., Inayoshi K., Omukai K., Yoshida N., 2013, ApJ, 778, 178

Hoyle F., Lyttleton R. A., 1941, MNRAS, 101, 227

Ilbert O. et al., 2010, ApJ, 709, 644

Islam R. R., Taylor J. E., Silk J., 2003, MNRAS, 340, 647

Johnson J. L., Whalen D. J., Fryer C. L., Li H., 2012, ApJ, 750, 66

Kazantzidis S. et al., 2005, ApJ, 623, L67

Keller B. W., Wadsley J., Benincasa S. M., Couchman H. M. P., 2014, MNRAS, 442, 3013

Keller B. W., Wadsley J., Couchman H. M. P., 2016, MNRAS, 463, 1431

Kereš D., Vogelsberger M., Sijacki D., Springel V., Hernquist L., 2012, MNRAS, 425, 2027

Kim J.-h. et al., 2014, ApJS, 210, 14

Kistler M. D., Yuksel H., Hopkins A. M., 2013, ArXiv:1305.1630

Klein A. et al., 2016, Phys. Rev. D, 93, 024003

Knollmann S. R., Knebe A., 2009, ApJS, 182, 608

Kormendy J., Ho L. C., 2013, ARA&A, 51, 511

Kormendy J., Richstone D., 1995, 33, 581

Kravtsov A., Vikhlinin A., Meshscheryakov A., 2014, ArXiv:1401.7329

Kroupa P., 2001, MNRAS, 322, 231

Lacy M., Ridgway S. E., Sajina A., Petric A. O., Gates E. L., Urrutia T., Storrie-Lombardi L. J., 2015, ApJ, 802, 102

Lansbury G. B. et al., 2015, ApJ, 809, 115

Lodato G., Natarajan P., 2006, MNRAS, 371, 1813

Lupi A., Haardt F., Dotti M., 2015, MNRAS, 446, 1765

MacKay D. J., 1998, NATO ASI Series F Computer and Systems Sciences, 168, 133

Madau P., Quataert E., 2004, ApJ, 606, L17

Marcillac D., Elbaz D., Charlot S., Liang Y. C., Hammer F., Flores H., Cesarsky C., Pasquali A., 2006, A&A, 458, 369

Marigo P., Girardi L., Bressan A., Groenewegen M. A. T., Silva L., Granato G. L., 2008, A&A, 482, 883

Mayer L., Kazantzidis S., Madau P., Colpi M., Quinn T., Wadsley J., 2007, Science, 316, 1874

Menon H., Wesolowski L., Zheng G., Jetley P., Kale L., Quinn T., Governato F., 2015, Comp. Astrophysics and Cosmology, 2, 1

Merloni A., 2016, in Lecture Notes in Physics, Berlin Springer Verlag, Vol. 905, Lecture Notes in Physics, Berlin Springer Verlag, Haardt F., Gorini V., Moschella U., Treves A., Colpi M., eds., p. 101

Miller B. P., Gallo E., Greene J. E., Kelly B. C., Treu T., Woo J.-H., Baldassare V., 2015, ApJ, 799, 98

Monaco P., Theuns T., Taffoni G., Governato F., Quinn T., Stadel J., 2002, ApJ, 564, 8

Moore B., Lake G., Katz N., 1998, ApJ, 495, 139

Moran E. C., Shahinyan K., Sugarman H. R., Vélez D. O., Eracleous M., 2014, AJ, 148, 136

Morishita T. et al., 2016, ArXiv e-prints

Moster B. P., Naab T., White S. D. M., 2013, MNRAS, 428, 3121

Mullaney J. R. et al., 2012, ApJ, 753, L30

Munshi F. et al., 2013, ApJ, 766, 56

Natarajan P., Pacucci F., Ferrara A., Agarwal B., Ricarte A., Zackrisson E., Cappelluti N., 2017, ApJ, 838, 117

Navarro J. F., Frenk C. S., White S. D. M., 1996, ApJ, 462, 563

Nozawa T., Kozasa T., Umeda H., Maeda K., Nomoto K., 2003, ApJ, 598, 785

Obreschkow D., Glazebrook K., 2014, ApJ, 784, 26

Oh S., de Blok W. J. G., Walter F., Brinks E., Kennicutt R. C., 2008, AJ, 136, 2761

Oh S.-H., de Blok W. J. G., Brinks E., Walter F., Kennicutt, Jr. R. C., 2011, AJ, 141, 193

Okamoto T., Gao L., Theuns T., 2008, MNRAS, 390, 920

Omukai K., Nishi R., 1998, ApJ, 508, 141

Ostriker E. C., 1999, ApJ, 513, 252

Papovich C. et al., 2015, ApJ, 803, 26

Pereira-Santaella M. et al., 2015, A&A, 577, A78

Planck Collaboration et al., 2016, A&A, 594, A13

Pontzen A., Governato F., 2012, ArXiv e-prints

Pontzen A. et al., 2008, MNRAS, 390, 1349

Pontzen A., Tremmel M., Roth N., Peiris H. V., Saintonge A., Volonteri M., Quinn T., Governato F., 2017, MNRAS, 465, 547

Power C., Navarro J. F., Jenkins A., Frenk C. S., White S. D. M., Springel V., Stadel J., Quinn T., 2003, MNRAS, 338, 14

Read J. I., Goerdt T., Moore B., Pontzen A. P., Stadel J., Lake G., 2006, MNRAS, 373, 1451

Reines A. E., Comastri A., 2016, PASA, 33, e054

Reines A. E., Deller A. T., 2012, ApJ, 750, L24

Reines A. E., Greene J. E., Geha M., 2013, ApJ, 775, 116

Reines A. E., Sivakoff G. R., Johnson K. E., Brogan C. L., 2011, Nature, 470, 66

Reines A. E., Volonteri M., 2015, ApJ, 813, 82

Ritchie B. W., Thomas P. A., 2001, MNRAS, 323, 743

Rosario D. J. et al., 2015, A&A, 573, A85

Rosas-Guevara Y. M. et al., 2015, MNRAS, 454, 1038

Roth N., Pontzen A., Peiris H. V., 2016, MNRAS, 455, 974

Roškar R., Fiacconi D., Mayer L., Kazantzidis S., Quinn T. R., Wadsley J., 2015, MNRAS, 449, 494

Ruiz A. N. et al., 2015, ApJ, 801, 139

Sanchez N. N. et al., 2016, ArXiv e-prints

Savorgnan G. A. D., Graham A. W., Marconi A., Sani E., 2016, ApJ, 817, 21

Schaye J. et al., 2015, MNRAS, 446, 521

Schaye J. et al., 2010, MNRAS, 402, 1536

Schleicher D. R. G., Palla F., Ferrara A., Galli D., Latif M., 2013, A&A, 558, A59

Schneider R., Omukai K., Inoue A. K., Ferrara A., 2006, MNRAS, 369, 1437

Schramm M., Silverman J. D., 2013, ApJ, 767, 13

Sesana A., 2013, MNRAS, 433, L1

Sesana A., Khan F. M., 2015, MNRAS, 454, L66

Shen S., Madau P., Conroy C., Governato F., Mayer L., 2014, ApJ, 792, 99

Shen S., Wadsley J., Stinson G., 2010, MNRAS, 407, 1581

Shields J. C., Walcher C. J., Böker T., Ho L. C., Rix H.-W., van der Marel R. P., 2008, in IAU Symposium, Vol. 245, IAU Symposium, Bureau M., Athanassoula E., Barbuy B., eds., pp. 259–260

Shimizu I., Yoshida N., Okamoto T., 2011, MNRAS, 418, 2273

Sijacki D., Springel V., Di Matteo T., Hernquist L., 2007, MNRAS, 380, 877

Sijacki D., Springel V., Haehnelt M. G., 2009, MNRAS, 400, 100

Sijacki D., Vogelsberger M., Genel S., Springel V., Torrey P., Snyder G. F., Nelson D., Hernquist L., 2015, MNRAS, 452, 575

Somerville R. S., 2002, ApJ, 572, L23

Somerville R. S., Hopkins P. F., Cox T. J., Robertson B. E., Hernquist L., 2008, MNRAS, 391, 481

Somerville R. S., Primack J. R., 1999, MNRAS, 310, 1087

Spaans M., Silk J., 2006, ApJ, 652, 902

Springel V., Di Matteo T., Hernquist L., 2005, MNRAS, 361, 776

Steinborn L. K., Dolag K., Comerford J. M., Hirschmann M., Remus R.-S., Teklu A. F., 2016, MNRAS, 458, 1013

Stinson G., Seth A., Katz N., Wadsley J., Governato F., Quinn T., 2006, MNRAS, 373, 1074

Taffoni G., Mayer L., Colpi M., Governato F., 2003, MNRAS, 341, 434

Tan J. C., McKee C. F., 2004, ApJ, 603, 383

Teyssier R., Pontzen A., Dubois Y., Read J. I., 2013, MNRAS, 429, 3068

Todini P., Ferrara A., 2001, MNRAS, 325, 726

Treister E., Urry C. M., Schawinski K., Cardamone C. N., Sanders D. B., 2010, ApJ, 722, L238

Tremmel M., Governato F., Volonteri M., Quinn T. R., 2015, MNRAS, 451, 1868

Tremmel M., Karcher M., Governato F., Volonteri M., Quinn T. R., Pontzen A., Anderson L., Bellovary J., 2017, MNRAS, 470, 1121

Treu T., Ellis R. S., Liao T. X., van Dokkum P. G., 2005, ApJ, 622, L5

Turk M. J., Abel T., O'Shea B., 2009, Science, 325, 601

Ueda Y., Akiyama M., Ohta K., Miyaji T., 2003, ApJ, 598, 886

Van Wassenhove S., Capelo P. R., Volonteri M., Dotti M., Bellovary J. M., Mayer L., Governato F., 2014, MNRAS, 439, 474

Van Wassenhove S., Volonteri M., Mayer L., Dotti M., Bellovary J., Callegari S., 2012, ApJ, 748, L7

Volonteri M., 2010a, A&A Rev., 18, 279

Volonteri M., 2010b, A&A Rev., 18, 279

Volonteri M., 2012, Science, 337, 544

Volonteri M., Bellovary J., 2012, Reports on Progress in Physics, 75, 124901

Volonteri M., Bogdanović T., Dotti M., Colpi M., 2016a, IAU Focus Meeting, 29, 285

Volonteri M., Dubois Y., Pichon C., Devriendt J., 2016b, MNRAS, 460, 2979

Volonteri M., Gnedin N. Y., 2009, ApJ, 703, 2113

Volonteri M., Haardt F., Gültekin K., 2008a, MNRAS, 384, 1387

Volonteri M., Habouzit M., Pacucci F., Tremmel M., 2016c, in IAU Symposium, Vol. 319, Galaxies at High Redshift and Their Evolution Over Cosmic Time, Kaviraj S., ed., pp. 72–79

Volonteri M., Lodato G., Natarajan P., 2008b, MNRAS, 383, 1079

Volonteri M., Natarajan P., 2009, MNRAS, 400, 1911

Volonteri M., Perna R., 2005, MNRAS, 358, 913

Volonteri M., Reines A., Atek H., Stark D. P., Trebitsch M., 2017, ArXiv e-prints

Volonteri M., Reines A. E., 2016, ApJ, 820, L6

Wadsley J. W., Stadel J., Quinn T., 2004, New Astronomy, 9, 137

Wadsley J. W., Veeravalli G., Couchman H. M. P., 2008, MNRAS, 387, 427

Werk J. K. et al., 2016, ApJ, 833, 54

Werk J. K. et al., 2014, ApJ, 792, 8

Wurster J., Thacker R. J., 2013, MNRAS, 431, 2513

Wylezalek D. et al., 2017, MNRAS, 467, 2612

Yang G. et al., 2017, ArXiv e-prints

Yu Q., 2002, MNRAS, 331, 935

Appendix A

QUANTITATIVE PARAMETER SEARCH FOR STELLAR AND SMBH PHYSICS

Material from this chapter has been previously published in collaboration with Michael Karcher, Fabio Governato, Marta Volonteri, Tom Quinn, Andrew Pontzen, Lauren Anderson, and Jillian Bellovary in the September 2017 edition of Monthly Notices of the Royal Astronomical Society (Tremmel et al., 2017), and has been reproduced here with permission of the Royal Astronomical Society.

Large simulations require proportionally vast computational resources and face two main problems: limited force and mass resolution and the extensive need for sub- grid physics, as the modeling of physical processes happening below the resolved scales. Examples for such sub-grid physics parameters are the density at which SF should form, the fraction of energy form SNe and SMBHs that couples to the surrounding gas the speed at which metals diffuse in the Intergalactic medium (IGM). Note that the same points hold even in simulations that claim no free parameters, for numerical parameters such as the precision of the step integration, the value of the force softening or the adopted IMF.

A common problem in simulations has been how to design an efficient strategy to *quantitatively* optimize, in a statistically controlled way these physical, but poorly constrained parameters, hence optimizing the results for the chosen physical model (Governato et al., 2007). A similar problem is faced by the so-called semi analytical models (Monaco et al., 2002; Somerville et al., 2008). However parameter searches for SAM are computationally cheaper and can be performed using different statistical approaches such as emulation (Bower et al., 2010), Monte Carlo Markov Chain (MCMC) (Benson, 2014) or Particle Swarm Optimization (Ruiz et al., 2015).

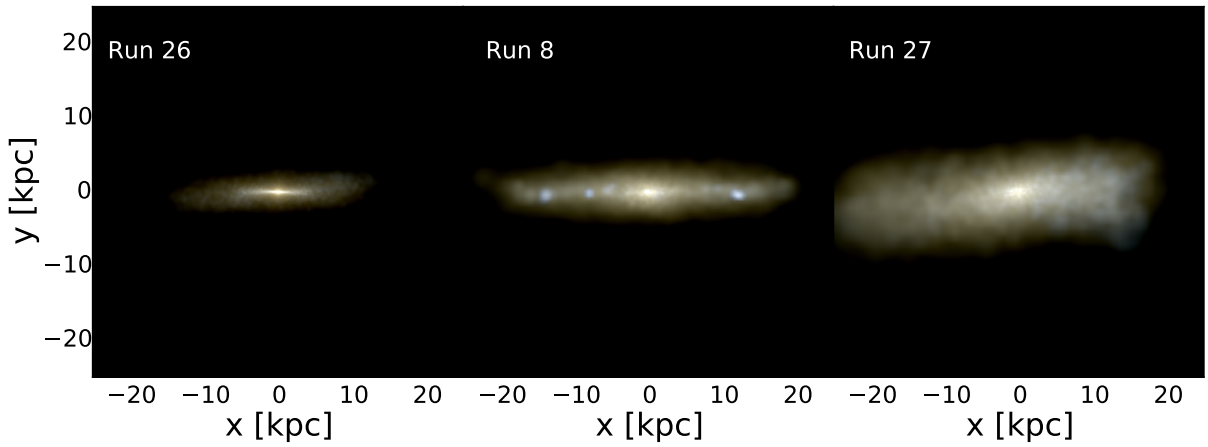

Figure A.1: Kriging Parameter Search in Practice. Here we show three realizations of our zoomed-in run of a $10^{11.5}$ $M_\odot$ halo at z = 0. From left to right we show the best parameter set, a poor set, and the worst set based on our grading criteria. See Table 1 for the parameters for each of these simulations. This illustrates that the parameters we chose and the way we varied them throughout our search has a clear effect on galaxy properties. In this case, run 26 has a clear thin disk, run 8 has a more diffuse disk and run 27 fails to form a thin disk at all. Our approach is able to thoroughly and efficiently search through the allowed parameter space and arrive at a set of parameters that results in realistic galaxies. Figure from Tremmel et al. (2017), ©RAS. Reproduced with permission.

As described in §3, in this work we have implemented a novel optimization technique to optimally choose sub-grid parameters associated with the implementations of 1) SF and SNe feedback and then 2) SMBHs accretion and feedback. To optimize the SF and SNe feedback parameters we proceeded in the way described in §2.2. Here we describe in a more detail some of the choices we made and the so–called Kriging techniques (see below) that we used to map out the suitability of the parameter space explored. The kriging algorithm penalizes parameter values that lead to simulations that deviate from the properties of real galaxies and then searches for parameter values that instead minimize this deviation. Runs are repeated with the same galaxies set, but with the updated parameters until the desired 'convergence' to the SF values listed in §4.

To summarize, our approach introduces a number of desirable qualities compared when only a limited number of experiments, as typical of numerical simulations, can be carried out. It presents several advantages over shutting off or including individual physics modules (Genel et al., 2014) or to running a small cosmological volume multiple times (Schaye et al., 2015, 2010). Namely the non linear effect of changing more than one parameter at the time can now be followed (Schaye et al., 2015) and the search for best parameters can cover a mass range similar to that of the final, large scale simulation (which tend to have more massive halos than small test volumes).

- 1) Minimal resources are wasted in 'bad' regions of parameter space.

- 2) There is no need to wait for convergence, every simulation is useful immediately (unlike Markov chain Monte Carlo and many optimization techniques) and

- 3) Kriging is robust to changes in model choice and penalization/weighting methods as suitability values can easily be recalculated.

Figure A.1 illustrates the results of this process, showing images of the stars of a disk galaxy at z=0 using the best, poor, and worst star formation parameters.

A.1 Grading Parameter Realizations

Each parameter set realization is graded against a set of z = 0 empirical scaling relations that govern star formation efficiency (Moster et al., 2013), the gas depletion time (Cannon et al., 2011; Haynes et al., 2011), galaxy size and angular momentum (Obreschkow & Glazebrook, 2014), and SMBH growth (Schramm & Silverman, 2013). The stellar mass fraction for our simulated galaxies is obtained following (Munshi et al., 2013), a procedure that includes the effects of a fixed aperture and the under-weighting of older, redder stellar populations. The HI fractions are measured directly from the simulations, which track the HI content of each gas particle. To calculate the bulge to disk ratio, galaxies are decomposed into their different dynamical components based on the energy and angular momentum of each particle. Then the total angular momentum is calculated from every star particle not considered to be dynamically a part of the halo. Black hole masses are taken directly from the most massive black hole in each halo.

The SMHM relation constrains the SF efficiency over the whole Hubble time. SF efficiency also affects many other structural relations such as the $M_\star$-V_{peak}, and the stellar mass - metallicity relation. The $J_{star}/M_\star$ relation and the HI/stellar mass relation were included as good proxies of the effect of feedback processes on low redshift SF and the angular momentum distribution and size of a galaxy. Finally the M_{BH}-$M_\star$ is an important constraint on SMBHs processes, in particular the coeval growth of stars and SMBHs within galaxies. These grading choices are by no means unique, but allow us to be confident in the success of a given parameter set in creating galaxies that match what is observed in the local Universe, while still leaving room to make predictions for the evolution of various galaxy properties over cosmic time.

A.2 Finding the Optimal Parameters

In order to avoid a 5-dimensional parameter space calculation, we first performed the full analysis, using the Kriging technique, on galaxies with no SMBH physics. This allowed us

Run	$n_\star$	$c_\star$	ϵ_{SN}
1	1.000	0.2000	2.000
2	0.100	0.1000	1.000
3	0.100	0.1000	4.000
4	0.100	0.4000	1.000
5	0.100	0.4000	4.000
6	4.000	0.1000	1.000
7	4.000	0.1000	4.000
8	4.000	0.4000	1.000
9	4.000	0.4000	4.000
10	0.1	0.1	1.5
11	0.1	0.1	2.0
12	0.1	0.2	1.0
13	0.1	0.2	1.5
14	0.1	0.2	2.0
15	1.0	0.1	1.0
16	1.0	0.1	1.5
17	1.0	0.1	2.0
18	1.0	0.2	1.0
19	1.0	0.2	1.5
20	0.05	0.05	0.5
21	0.05	0.05	1.5
22	0.05	0.15	0.5
23	0.05	0.15	1.5
24	0.2	0.05	0.5
25	0.2	0.05	1.5
26*	0.2	0.15	0.5
27	0.2	0.15	1.5

Table A.1: Example set of parameter space realizations. The free parameters tested are the SN efficiency, ϵ_{SN}, the threshold density for star formation, $n_\star$, and the star formation efficiency, $c_\star$. Different sets of parameters chosen based on the Kriging technique until a 'best' set of parameters is converged upon (run 26 here). Note that these runs were done with lower DM mass resolution compared to Romulus.

to converge upon the set of SF parameters that created the most realistic galaxies possible without the inclusion of SMBHs. A series of 27 parameter realizations (see Table 1) was run for sets of 3 halos with z = 0 virial masses of $10^{10.5}$, $10^{11.5}$, and 10^{12} $M_{\odot}$. Each set was graded by summing up the logarithmic distance of each galaxy from each scaling relation, though the angular momentum of the dwarf galaxy was excluded due to the fact that the dynamical decomposition technique becomes unreliable at low masses. Each galaxy is weighted evenly in the final grade for each parameter realization. The best model converged upon by this approach is marked with a star in Table 1.

Once the SF parameters were chosen, another set of 12 simulations were run with SMBH physics to find the best parameters for accretion and feedback strength (see §5.4). The same general approach was used, though a more hands-on approach was used to dictate how we traversed the available parameter space (see below). Because SMBH physics is thought to preferentially affect more massive galaxies, we include a fourth halo, with virial mass 10^{12} $M_{\odot}$, in each set of simulations. When grading each parameter set, the average deviation of these two halos is used instead of their individual deviations. Again, each galaxy is weighted evenly though the dwarf galaxy is again excluded from the SMBH relation due to the fact that the fraction of dwarfs hosting a central SMBH is not well known (see Volonteri (2010b) for theoretical arguments and (Reines & Comastri, 2016) for an observational review). Furthermore, as noted in section 5.5, the inclusion of a SMBH does not have a significant impact on the scaling relationships.

A.3 The Kriging Approach to Parameter Search

The Kriging Approach allows us to efficiently traverse parameter space and know when we have converged on the 'best' set of parameters without the use of a large number of simulations as would be required of other techniques such as MCMC.

MCMC requires 1) a joint prior distribution on the parameter space, from which initial points can be drawn, 2) a likelihood function describing the distribution of the observables given a particular parameter set, and 3) a proposal distribution that generates the next

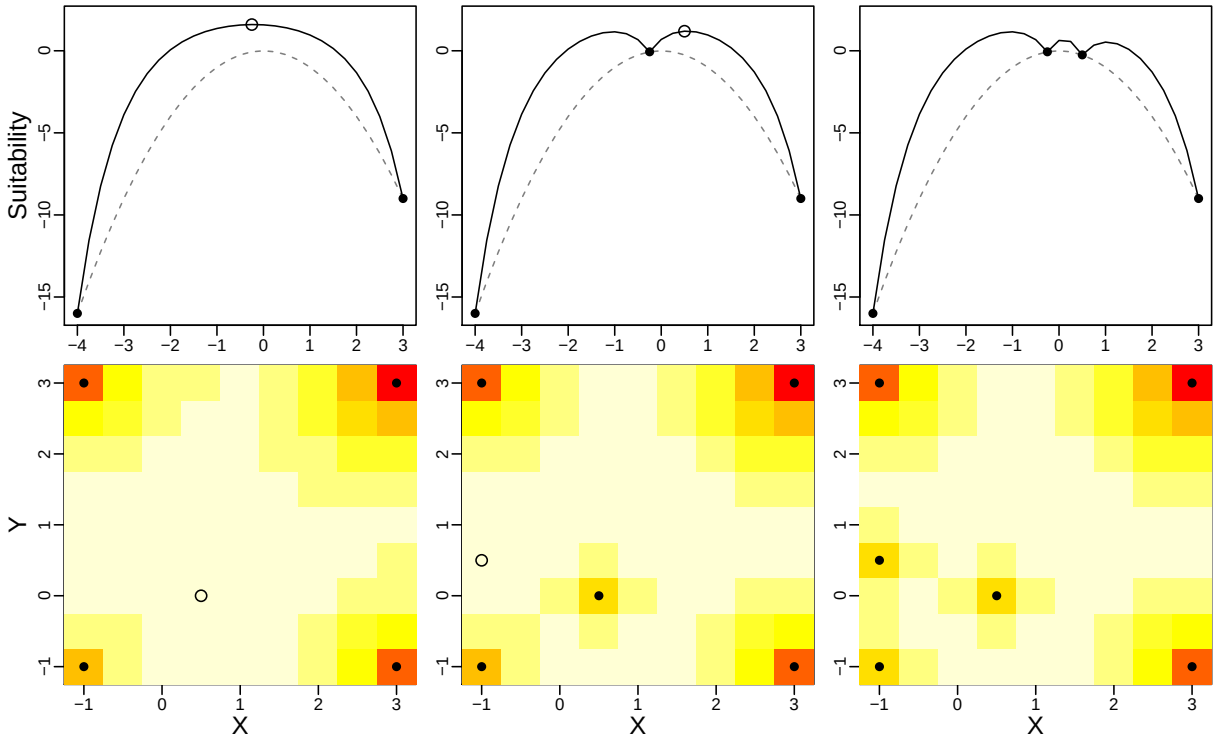

Figure A.2: Kriging parameter optimization technique example. Two iterations of the Kriging search algorithm on a 1-dimensional example (first row) and a 2-dimensional example (second row). In the 1-dimensional scenario, we are attempting to optimize the suitability function $-x^2$, shown as the dashed gray line. The algorithm starts by interpolating a pseudo-confidence manifold from two known points (filled points), and finding the greatest value (unfilled point). The algorithm then calculates the true suitability value for that point, and repeats the process. The 2-dimensional scenario is similar—we attempt to optimize the suitability function $-\mathbf{x}^2$. Here, the pseudo-confidence manifold is shown as a heatmap, with red/darker representing lower suitability and white/brighter representing higher suitability. The point selection and evaluation process (filled and unfilled points) is identical to the 1-dimensional scenario. Figure from Tremmel et al. (2017), ©RAS. Reproduced with permission.

parameter values to examine, given the current values. MCMC then uses these functions to iterate over the parameter space, deciding whether or not to jump to the next point depending on how likely the next point is to explain the data relative to the current values. After a very large number of iterations (sometimes millions), the accepted points become a sample from the posterior distribution of parameter values given the observables, and useful inferences can thereby be derived, including point estimates of the best parameter values, and 95% credible regions for where the best parameter values may lie.

Because cosmological simulations consume a large amount of computing resources, simulating so many iterations is not possible. Our approach trades the unattainable statistical properties of MCMC for the ability to make direct use of human expertise and intuition, the flexibility to adapt to changing measures of fitness, and keeping the certainty of knowing that every iteration makes a distinguishable contribution to our knowledge of the parameter space. While we lose access to the posterior distribution (i.e. a full sampling and ranking of parameter space), that is not really necessary. Instead, we gain an efficient means of finding the region of the parameter space that produces the most realistic galaxies, which is our goal.

We achieve all this by adapting Gaussian process Kriging techniques into a more intelligent and efficient grid search algorithm (see Figure A.2). We start by constructing a suitability function—a function that takes in a simulation and compares it to observed relationships and returns a score describing how realistic the simulation is (see above).

Using the following formula (MacKay, 1998), we then interpolate the suitability function between all of our simulated points and put pseudo-confidence bounds around where the suitability function will actually fall. We see,

$$\mathbf{f}_*|X_*, X, \mathbf{f} \sim N(K(X_*, X)K(X, X)^{-1}\mathbf{f}, \\ K(X_*, X_*) - K(X_*, X)K(X, X)^{-1}K(X, X_*)),$$

where X is the matrix of already-simulated parameter values, $\mathbf{f}$ is the corresponding vector of known suitability values, X_* is a matrix of new parameter values that we wish to examine, $\mathbf{f}_*$

is the corresponding as yet unknown suitabilities, and $K(\cdot,\cdot)$ is a covariance matrix derived from a pre-specified covariance function $k(x_1, x_2)$.

Since we aren't seeking statistical properties, only utilitarian properties, we don't estimate the covariance scale so much as choose one that spreads the first few suggested points away from the initial points, in our case a 99% 'pseudo confidence surface' with covariance scale of 1, meant to ensure parameter space is widely sampled. Since it is a suggestion algorithm rather than a statistical method, the covariance scale can even be adjusted freely before or after points have been selected and tested.

If we wish to take a hands-off approach, we would then examine the upper pseudo-confidence manifold, and instruct the algorithm to find the point with the highest potential suitability (at a fixed confidence level), and then numerically simulate that point. This is the approach we used for the initial search where we optimized the SF parameters (see above). However, if human intuition can be sufficient, we may also examine the pseudo-confidence manifold manually and select the next point ourselves without concern over losing statistical rigor. This is the approach we used for tuning the SMBHs parameters. One complication is that in regions of the parameter space where the Kriging process is extrapolating rather than interpolating, the confidence regions become extraordinarily wide, leading a naive algorithm to always select an extrapolated point. This has at least two solutions. One is to restrict any automation to the convex hull of already simulated points and use manual intervention to select points outside the convex hull if it becomes clear that such a point would make a good candidate. The second is to only calculate the Kriging bounds for a predefined, *a priori* reasonable region of the parameter space. The algorithm will quickly explore the outer boundary and then turn inward. From experience we learned that a good approach is to start the parameter exploration from a coarse grid of parameters values, including a range over which simulations will provide 'bad' results (e.g testing SN efficiency ranging from 0 to 4, values that will surely over and under produce stars). An option for future work would be to include higher-z constraints from the progenitors of massive present day halos, this would allow to constraint the high end of the present day galaxy stellar mass function using

a limited amount of computational resources.

A sample result of this process is in Table 1. By starting with a coarse grid of values for each of our 3 parameters, we utilize Kriging to traverse parameter space. After each iteration, Kriging sees both the current 'best' point and the algorithm will then run a simulation in a region not yet well enough constrained. With time, each parameter space realization gets closer to the 'best' values until Kriging tells us it has sufficiently converged. Regions of parameter space that behave the worst are then sampled much less often while regions nearby the 'best' parameter set are sampled in more detail. The results presented in Table 1 are from simulations that do not oversample DM particles and therefore have lower mass resolution for DM than the ROMULUS simulations. We find that this increased resolution results in higher star formation in dwarf galaxies. Thus, the ROMULUS simulations use the values from run 26, but with a higher SN efficiency of 0.75, a combination we find results in final properties very similar to run 26 in Table 1.

Appendix B

DUST EXTINCTION APPROXIMATION

Material from this chapter has been previously published in collaboration with Michael Karcher, Fabio Governato, Marta Volonteri, Tom Quinn, Andrew Pontzen, Lauren Anderson, and Jillian Bellovary in the September 2017 edition of Monthly Notices of the Royal Astronomical Society (Tremmel et al., 2017), and has been reproduced here with permission of the Royal Astronomical Society.

When comparing the colors of simulated galaxies to observations, it is important to account for dust attenuation. Because we only care about the average attenuation across all lines of sight integrated over all stars in a given galaxy, we utilize a simple 'spherical cow' approach similar to Shimizu et al. (2011).

For a given dust distribution, the amount of attenuation can be calculated at any wavelength using the Calzetti Law (Calzetti et al., 2000), but first it must be properly normalized. For this, it is convenient to use far UV light, since the extinction cross section is roughly equal to the dust grain size. We choose 1600 Angstroms as our normalizing far UV wavelength. We then make the assumption that the dust is uniformly distributed in a sheet around the stars, which allows us to relate the dust extinction by a simple function of the dust optical depth (Calzetti, 2001).

$$A_\lambda \sim \frac{\tau_\lambda}{0.921} \tag{B.1}$$

This is obviously not true in reality, but is not a bad assumption if we think of this calculation as an average over all lines of sight. Assuming spherical symmetry also makes the optical depth a simple function of average dust properties.

$$\tau\lambda = \int \sigma_d(\lambda) n(r) r \sim \frac{\sigma_d(\lambda)\Sigma_d}{m_p} \tag{B.2}$$

In the above equation σ_d is the dust cross section, Σ_d is the column density, and m_p is the mass per dust grain. When dealing with far UV light, the cross section is just the cross sectional area of the average dust particle. Because we are not accounting for structure within the gas, we can use instead estimate the average column density using the total mass, M_d of dust within the galaxy and the half mass radius, $\mathrm{R}_{1/2,d}$ of the dust.

$$\Sigma_d \sim \frac{(1/2)\mathrm{M}_d}{\pi \mathrm{R}_{1/2,d}^2} \tag{B.3}$$

The total mass in dust for a halo is given by the following relation from Draine et al. (2007) summed over the HI mass, $m_{HI,i}$ of every gas particle in a halo. We follow Shimizu et al. (2011) and normalize instead to the solar metallicity, rather than galactic O/H values as in the original paper.

$$\mathrm{M}_d \sim \sum_{i=1}^{N_{gas}} 0.01 \frac{Z}{Z_\odot} m_{HI,i} \tag{B.4}$$

These equations, put together with the physical properties of dust grains and applied to 1600 Angstroms, gives us A_{1600}, which we can use to set the normalization of the Calzetti Law. We take the dust particle size to be 0.1μm and density to be $2.5 g/cc$ (Todini & Ferrara, 2001; Nozawa et al., 2003). We cap A_{1600} at a value of 2, given that more advanced dust models show that attenuation deviates significantly from its linear relationship with optical depth as column densities increase due to the fact that dustier systems will tend to be clumpier (Calzetti, 2001). This normalization, combined with our adopted value of $R_v = 4.0$, gives us the ability to estimate the dust attenuation at any wavelength. When dealing with bands of wavelengths, we calculate attenuation using the central wavelength of the band.